FABRICATION OF NANOFILTRATION HOLLOW FIBER MEMBRANES FOR SUSTAINABLE PHARMACEUTICAL MANUFACTURE

SUN SHIPENG
(B. Eng., Tianjin University)

A THESIS SUBMITTED

FOR THE DEGREE OF DOCTOR OF PHYLOSOPHY

IN CHEMICAL AND PHARMACEUTICAL ENGINEERING

SINGAPORE-MIT ALLIANCE

NATIONAL UNIVERSITY OF SINGAPORE

2011

ACKNOWLEDGEMENT

TABLE OF CONTENTS

SUMMARY

The molecular design of nanoporous membranes with desired morphology and selectivity has attracted significant interests over the past decades. A major problem in their applications is the trade-off between sieving property and permeability. A novel elongation-induced nano-pore evolution was discovered. The method can synergistically decrease the pore size and increase the pure water permeability of a novel Torlon® polyamide-imide (PAI) nanofiltration (NF) hollow fiber membrane with the aid of external stretching in a dry-jet wet-spinning process. The molecular weight cutoff (MWCO) and pore size distribution of the membranes were finely tuned by this approach.

Zeta-potential and salt rejection tests verify that the PAI NF membrane has an isoelectric point at about 3.2, above which the membrane is negatively charged. As a result, the resultant PAI NF membranes exhibit highly effective fractionation of the divalent and monovalent ions of NaCl/Na$_2$SO$_4$ salt solutions. Furthermore, more than 99.5% glutathione can be rejected by the PAI NF membranes at neutral pH, offering the feasibility to recover this tripeptide.

A dual-layer NF hollow fiber membrane was fabricated by the simultaneous co-extrusion of polyamide-imide and cellulose acetate dopes through a triple-orifice spinneret in a dry-jet wet phase inversion process. The nanopores of dual-layer hollow fiber membranes were molecularly designed by controlling the phase inversion process with the aid of various non-solvent additives into the polymer solutions.

Compared to ethanol and 2-propanol, the addition of methanol into the dope led to a significantly decreased pore size but dramatically increased pure water permeability. The improved NF performance may be attributed to (1) a controllable thin selective outer layer; (2) a less resistant interface between the outer and inner layers; and (3) a fully porous substructure with reduced transport resistance.

A positively charged NF membrane was fabricated by hyperbranched polyethyleneimine (PEI) induced cross-linking on a PAI hollow fiber. It is found that after PEI induced cross-linking, the membrane pore size is significantly reduced. The membrane surface becomes more hydrophilic and positively charged. As a result of these synergic effects, the rejection of ciprofloxacin is substantially enhanced. The NF membrane modified by a high molecular weight PEI_60K exhibits the highest rejection, the lowest fouling tendency and keeps a constant flux over the whole pH range.

A thin-film composite NF membrane was fabricated by interfacial polymerization of hyperbranched polyethyleneimine and isophthaloyl chloride. After interfacial polymerization, the NF membrane possesses a negatively charged substrate and a positively charged selective layer with a mean pore radius of 0.36 nm, MWCO of 489 Da, and pure water permeability of 4.85 $lm^{-2}bar^{-1}h^{-1}$. Due to this double-repulsion effect, together with the steric-hindrance and the solute electro-neutrality effects, the newly developed NF membrane shows superior rejections (over 99%) for both positively and negatively charged dye molecules. By adjusting the pH of cephalexin aqueous solution to modify the ionization states of this zwitterionic molecule, the NF membrane shows high rejections over a wide pH range. The NF membrane may

potentially be useful to reduce waste, recycle valuable products and reuse water for pharmaceutical, textile and other industries.

LIST OF TABLES

LIST OF FIGURES

LIST OF SYMBOLS

A	effective filtration area of membrane (m^2)
$A_k/\Delta x$	ratio of membrane porosity over thickness (m^{-1})
C_f	solute concentration in the feed solution ($mol\ m^{-3}$)
C_m	concentration at the membrane surface ($mol\ m^{-3}$)
C_p	solute concentration in the permeate ($mol\ m^{-3}$)
CA	cellulose acetate
D_i	diffusivity of ion i in free solution ($m^2\ s^{-1}$)
D_s	diffusivity of solute in the solution ($m^2\ s^{-1}$)
EG	ethylene glycol
J_s	solute or ion flux ($mol\ m^{-2}\ s^{-1}$)
J_v	permeate flux ($m^3\ m^{-2}\ s^{-1}$)
MW	molecular weight (Da)
MWCO	molecular weight cut off (Da)
NMP	n-methyl-2-pyrrolidinone
OD	outer diameter (μm)
ID	inner diameter (μm)
IPC	isophthaloyl chloride
P	solute permeability ($m\ s^{-1}$)
ΔP	trans-membrane pressure drop (bar)
PAI	polyamide-imide
PEI	polyethyleneiminne
pK_a	ionization equilibrium constant (-)
IPA	2-propanol
PSf	polysulfone
PWP	pure water permeability ($liter\ m^{-2}\ bar^{-1}\ hr^{-1}$)
Q	water permeate flux ($m^3\ h^{-1}$)
r_s	solute Stokes radius (nm)
r_p	effective pore radius (nm)

R_T	solute rejection (-)
SPES	sulfonated polyethersulfone
TFC	thin film composite
α	transport number of cations in free solution defined as $\alpha = D_1/(D_1 + D_2)$
ε	overall porosity (-)
μ_p	mean effective pore radius (nm)
μ_s	geometric mean radius of solute at $R_T = 50\%$ (nm)
ξ	ratio of effective volume charge density (φX) of membrane to the electrolyte concentration (C_m) at the membrane surface
$\Delta\pi$	osmotic pressure difference (bar)
σ	reflection coefficient (-)
σ_g	geometric standard deviation about μ_s, (-)
σ_p	geometric standard deviation about μ_p, (-)
$\varPhi X$	effective membrane charge (mol m^{-3})

CHAPTER ONE

INTRODUCTION

1.1 Membrane technology

In the 21st century, the sustainable development of the human society faces three major problems: water, energy and health. These challenges have prompted the search of new technologies for more efficient production of clean water and renewable energy and for more effective protection of human health and the environment [1-3]. In terms of the chemical industry, many ongoing research thrusts attempt to explore innovative green technologies to reduce waste, recycle valuable products and reuse water at lower expenditure with less energy consumption [4, 5]. Membrane technology has gained enormous importance over the past decades by replacing conventional separation methods or integrating with them. This is because membrane technology has the advantages including selective permeation, reduced energy consumption and non-thermal processing of sensitive compounds [5].

The driving force for membrane separations is the difference of chemical potential between two separated phases. This potential difference can result in pressure difference, concentration difference, and electrical potential difference or any combination of these variables [6]. Membrane processes for liquid based separation that utilize pressure difference as the driving force can be divided in to microfiltration (MF), ultrafiltration (UF), nanofiltration (NF) and reverse osmosis (RO), as shown in Figure 1.1. Their general characteristics, including pore size range, separation mechanism, pressure range and flux range, are listed in Table 1.1. Among these types of membranes, MF membranes have the

largest pore size, which is only suitable to reject large particles such as suspended solids. For UF membranes, macromolecules such as proteins can be rejected while small molecules such as ions and amino acids can pass through. RO membranes are considered as non-porous or have pores only allow water to pass through.
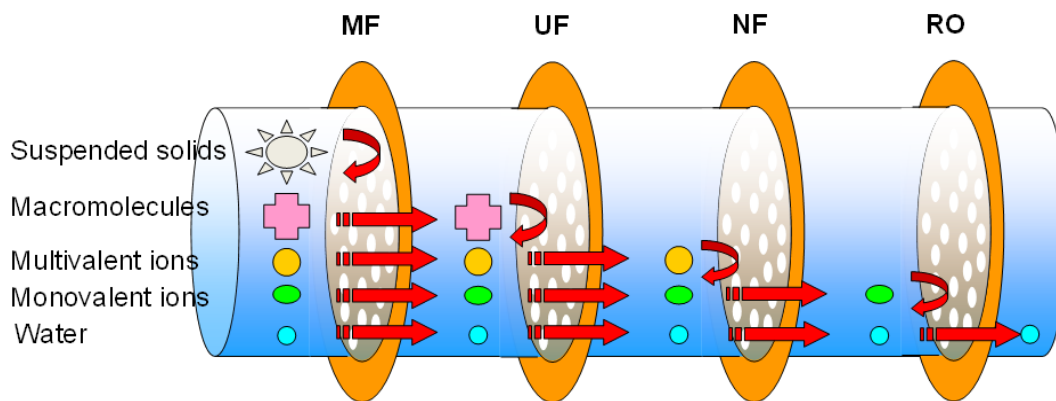
Figure 1.1 Application ranges of MF, UF, NF and RO membranes.

Table 1.1 Pressure driven processes and characteristics [6, 7].

	MF	UF	NF	RO
Pore size (nm)	50-5000	1-100	0.5-2	<0.5
Separation mechanism	Size exclusion	Size exclusion	Size exclusion and Donnan exclusion	Solution diffusion and size exclusion
Pressure (bar)	<2	1-5	5-20	10-100
Flux range ($Lm^{-2}hr^{-1}bar^{-1}$)	>50	10-50	1.4-12	0.05-1.4

1.2 Nanofiltration

NF membranes received their name because they have a nominal molecular weight cutoff (MWCO, molecular weight of solute that is 90% rejected by the membrane) ranging from 200 to 1000 Dalton and pore sizes of about 0.5 - 2.0 nm [7, 8]. Unlike the other membrane types, a unique property of NF membranes is that the separation mechanism involves not only steric (size exclusion) effect, but also an electrostatic partitioning interaction (Donnan

2

exclusion) between membrane and external solution. As a result, NF membranes can reject small organic molecules and divalent ions but let monovalent ions to pass through. In addition, it offers advantages of higher retention than UF and lower pressure requirement than RO [9]. Therefore, fabrication, characterization and application of NF membranes have received more and more attentions by researchers from both of academy and industry.

1.3 Applications of nanofiltration membranes

1.3.1 General applications

Since its inception in the early 1970s, nanofiltration (NF) has grown rapidly and become very important for liquid based separation processes through its unique ability to separate and fractionate ionic and low molecular weight organic species. In the last few decades, NF has found extensive applications as a separation and purification technique in not only aqueous separations such as desalination [1, 10], wastewater treatment [11], pharmaceutical purification [12, 13] and biomedical applications [14], but also organic solvent based separations emerging in the chemical [15], petrochemical [16] and other industries. More specific examples can be found in Table 1.2.

Table 1.2 General overview of NF applications.

Industry	Application	Reference
Water	Water softening	[17]
	Removal of natural organic matters (NOM) from water	[18]
	Removal of heavy metals from water	[19]
	Desalination in forward osmosis (FO) process	[10]
Pharmaceutical	Removal of pharmaceutical active compounds	[20]
	Recovery and concentration of antibiotics	[13]
	Enantiomer separation	[21]
	Recover organic solvents with solvent resistant NF membranes	[22]
Textile	Removal of dye, color, turbidity in waste water	[23]
Food	Concentration and demineralization of whey	[24, 25]
Pulp and paper	Treatment of effluents to reuse water	[26]
Diverse	Lube dewaxing with solvent resistant NF membranes	[27]
	Recovery of catalyst with solvent resistant NF membranes	[28]
	Concentration of proteins through FO process	[29]

1.3.2 NF membranes for sustainable pharmaceutical manufacture

Pharmaceuticals have been making significant contributions to the healthcare of human beings over the past number of decades. However, recently there is a growing concern over trace amounts of pharmaceuticals detected in the aquatic environment [30]. These pharmaceuticals are released into surface water in many ways including insufficient metabolism in the human or animal body, inappropriate treatment in the pharmaceutical industry or in hospitals and inefficient removal in wastewater treatment plants [31-33]. These pharmaceutical active compounds present in water may potentially risk human health and pollute environment. In order to produce pharmaceuticals in a sustainable way, it is important to develop novel technologies to (1) recycle valuable pharmaceutical products, and (2) eliminate waste disposal, thus prevent these compounds from entering the drinking water system.

Because the molecular weights of most pharmaceuticals range from 300 to 1000 Da, NF is a suitable candidate to purify, concentrate and remove these pharmaceuticals from aqueous solutions. If the target compound can be ionized in an aqueous solution, Donnan exclusion would be a suitable approach to increase rejection by properly choosing the membrane material and solution pH [2, 34]. For example, glutathione (L-γ-glutamyl-L-cysteinylglycine), a tripeptide, is the most abundant low-molecular-weight thiol compound in living organisms. It has already been widely used as a therapeutic drug because of its multiple biological functions as antioxidant, immunity booster, and detoxifier [35]. Currently, this tripeptide is produced by yeast fermentation, chemical and enzymatic methods [36]. Because glutathione molecule consists of the amino group ($–NH_2$), the carboxyl group ($–COOH$) and thiol group ($-SH$), its ionization states vary with pH in the aqueous solution, as shown in Figure 1.2. The molecule is negatively charged when the pH is above 3.59. Therefore, if the membrane surface is negatively charged, based on the interaction between the ionized glutathione molecules and the negatively charged membrane, NF could become a promising candidate to concentrate, recover and purify the glutathione aqueous solution by adjusting pH values [37].
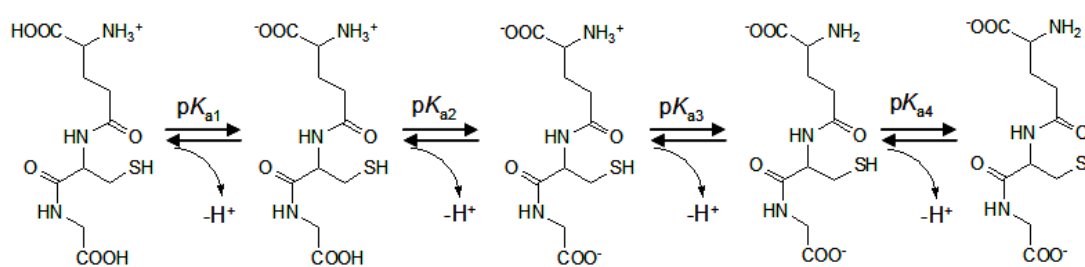
Figure 1.2 Ionization states of glutathione at different pH values.
pKa1=2.12, pKa2=3.59, pKa3=8.75, pKa4=9.65

NF is also a good candidate to remove pharmaceutical active compounds from discharge streams to the environment. For instance, ciprofloxacin (Figure 1.3) [38, 39], a representative

of fluoroquinolone antibiotics, utilized widely as human and veterinary medicines in antibacterial treatments, has been detected worldwide within the concentration range of micrograms per liter [30, 40]. Recent studies have shown that inefficient removal of this compound from discharge streams before their release into aquatic environments may not only contaminate drinking water, thus posing a risk to public health, but also inhibit photosynthesis of plants and promote the growth of antibiotic-resistant bacteria, resulting in severe ecological issues [41, 42]. Therefore, effective removal of the compound from discharge streams to the environment becomes an important issue. As shown in Figure 1.3, the molecule is positively charged below pH 8.70 and neutral within the range of 8.70 < pH < 10.58. It becomes negatively charged above pH 10.58, which is an extremely basic condition. In order to obtain the optimum rejection of ciprofloxacin under mild conditions, a positively charged NF membrane is necessary.
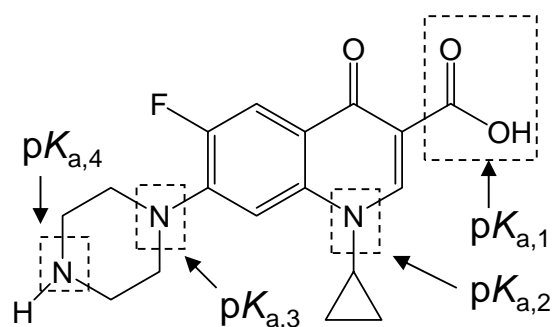
Figure 1.3 Chemical structure and ionization groups of ciprofloxacin.
p$K_{a,1}$: 3.01, p$K_{a,2}$: 6.14, p$K_{a,3}$: 8.70, p$K_{a,4}$: 10.58. MW=331.3, Log K_{ow}=0.28.

1.4 Fabrication of NF membranes

At present, most NF membranes are fabricated in two types. One type is the wholly integrated asymmetric membrane which is generally formed by phase inversion of cellulose acetate or other common polymers [6, 43]. The advantages of this kind of membrane include

easy fabrication and low cost while the disadvantages are the limited flux and limited rejection. The other type is the thin film composite (TFC) membrane which consists of a thick, porous, nonselective support layer covered by an ultrathin barrier layer, and is prepared by interfacial polymerization, coating or chemical modification [44-46]. By adjusting various processing parameters, a tailor-made membrane is possible that provides a higher flux and rejection compared to the asymmetric membrane. However, the production of high flux TFC membranes for NF applications is not trivial.

1.5 Module types for NF membrane fabrication

Table 1.3 lists the comparison of different module types. Currently, most NF modules are still made in the spiral-wound configuration by using flat-sheet membranes wound around a central tube. Compared to the flat-sheet membrane, the hollow fiber has the following advantages: (1) a much larger membrane area per unit volume of membrane modules, thus resulting in a higher productivity; (2) self-mechanical support, which can be back-flushed for liquid separation; and (3) good flexibility and easy handling during module fabrication and system operation. The relatively low manufacture cost of hollow fiber membranes raises significant interests toward its development. Nevertheless, the applications of hollow fiber membranes are still limited due to their lower water permeability and higher fouling tendency compared with flat-sheet ones [19, 47]. Therefore, technological breakthroughs are urgently needed to enhance the water permeability of hollow fiber membranes while still maintaining their separation efficiency. Intensive efforts should also be made on reducing the fouling of the hollow fiber membranes.

Table 1.3 Comparison of different module types [5, 48].

Module	Packing density (m^2/m^3)	Manufacture cost $(US\$/m^2)$	NF applications
Tubular	80-450	50-200	Rare
Plate and Frame	100-400	50-200	Rare
Spiral wound	500-1000	10-50	Major
Hollow fiber	500-5000	2-10	Some

1.6 Materials for NF fabrication: Torlon® polyamide-imide

In this study, Torlon® 4000 polyamide-imide (PAI), as shown in Figure 1.4 [49], is adopted as the membrane material. It has both superior mechanical properties typically associated with polyamides, and high thermal stability and solvent resistance associated with polyimides [50]. Therefore, Torlon® has been widely used as injection molding, engine parts of racing cars, molded parts for space shuttle, and many other critical components. Until recently Torlon® had been applied in the membrane filed such as vapor permeation [51], pervaporation [50, 52, 53] and gas separation [54-56]. Although Torlon® was also utilized to fabricate NF membranes, it was only served as the supporting layer in the flat-sheet membranes [57]. As shown in Figure 1.4, polyamide-imide has great potential to be an excellent candidate to fabricate NF membranes because it has the following advantages: (1) charge characteristics introduced by the amide group in the polymer chains; (2) the carbonyl groups of imide rings in the polymer chains are able to cross-link with amines to form amide groups.
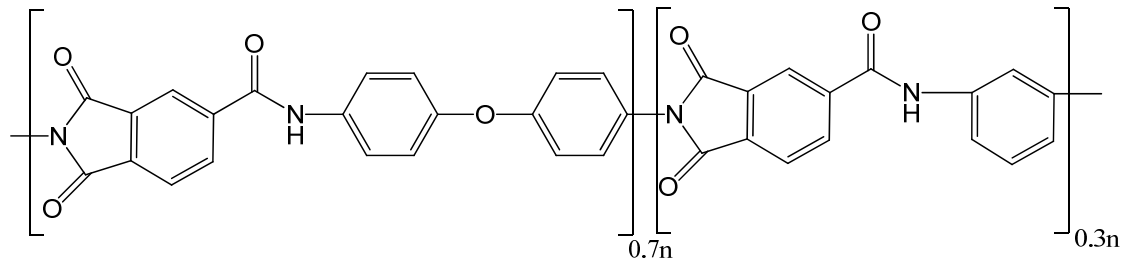
Figure 1.4 The general structure for Torlon® 4000T polyamide-imide.

1.7 Theoretical background for NF membrane characterization

1.7.1 Performance parameters

Performance parameters are usually defined in terms of pure water permeability (PWP) and solute rejections (R_T). PWP ($l\ m^{-2}\ bar^{-1}\ h^{-1}$) is calculated using the equation

$$PWP = \frac{Q}{\Delta P \cdot A} \tag{1.1}$$

where Q is the water permeation volumetric flow rate (L/h), A is the effective filtration area (m^2), and ΔP is the transmembrane pressure drop (bar).

Solute rejection is a parameter which indicates to which extent a component in the feed solution is retained. The parameter is calculated through the following equation:

$$R_T(\%) = \left(1 - \frac{c_p}{c_f} \right) \times 100 \tag{1.2}$$

where c_p and c_f are the solute concentration in the permeate and the feed solutions, respectively. Solute rejection is often used to characterize the membrane structure parameter

such as mean effective pore size, pore size distribution and molecular weight cutoff, which will be introduced in the following section.

1.7.2 Determination of mean effective pore size, pore size distribution and molecular weight cutoff (MWCO)

It has been found that the solute rejection for synthetic membranes can be expressed by a log-normal probability function of solute size, as described in the following equation [58]:

$$R_{\mathrm{T}} = erf(y) = \frac{1}{\sqrt{2\pi}} \int_{-\infty}^{y} e^{-(u^2/2)} \, du, \quad where \quad y = \frac{\ln r_{\mathrm{s}} - \ln \mu_{\mathrm{s}}}{\ln \sigma_{\mathrm{g}}} \tag{1.3}$$

where R_{T} is the solute rejection, r_{s} is the solute radius, μ_{s} is the geometric mean radius of solute at $R_{\mathrm{T}} = 50\%$, σ_{g} is the geometric standard deviation about μ_{s}, defined as the ratio of r_s at $R_{\mathrm{T}} = 84.13\%$ and $R_{\mathrm{T}} = 50\%$. When the solute rejection of a membrane is plotted against solute radius on the log-normal probability coordinates, a straight line is yielded as:

$$F(R_T) = A + B \, (\ln r_s) \tag{1.4}$$

By ignoring influences of the steric and hydrodynamic interaction between solute and pores on the solute rejection, the mean effective pore radius (μ_{p}) and the geometric standard deviation (σ_{p}) can be assumed to be the same as μ_{s} and σ_{g}, respectively. Therefore, based on μ_{p} and σ_{p}, the pore size distribution of an NF membrane can be expressed as the following probability density function [59]:

$$\frac{d R_T(r_p)}{d r_p} = \frac{1}{r_p \ln \sigma_p \sqrt{2\pi}} \exp\left[-\frac{(\ln r_p - \ln \mu_p)^2}{2(\ln \sigma_p)^2} \right] \tag{1.5}$$

where r_{p} is the effective pore radius of the membrane. The values of μ_{p} and σ_{p} determine the position and sharpness of the distribution curves, respectively.

In this study, different solutions containing single neutral solute were used to measure the solute rejection (R_T) because the relationship between Stokes radius r_s and molecular weight, *MW* of these known neutral solutes can be expressed by the following equation [60]:

$$\log r_s = -1.3238 + 0.395311 \log MW \tag{1.6}$$

where the unit of r_s is nm and that of *MW* is g mol^{-1}, respectively. From this equation the radius of a hypothetical solute at a given *MW* can be obtained. This equation can also be employed to back calculate *MW* of a hypothetical solute at a given radius.

1.7.3 Determination of reflection coefficient, σ, the solute permeability *P* and effective charge density, *ΦX*

Solute transport phenomena of the nanofiltration process can be described by the irreversible thermodynamics. Kedem and Katchalsky [61] proposed the relation of the volumetric flux J_v and the solute flux J_s through a membrane based on the following equations:

$$J_v = L_p(\Delta P - \sigma \cdot \Delta \pi) \tag{1.7}$$

$$J_s = P(c_f - c_p) + (1 - \sigma)J_v \bar{c} \tag{1.8}$$

Eqs. (1.7) and (1.8) indicate that transport across a membrane is characterized by three transport parameters, i.e. the pure water permeability L_p, the reflection coefficient σ, the solute permeability *P*. When concentration difference between the feed side and the permeate side is high, Spiegler and Kedem [62] improved this model to express it in a differential form as follows:

$$J_s = -P'(\frac{dc}{dx}) + (1 - \sigma)J_v c \tag{1.9}$$

where *P'* is the local solute permeability defined as *P' = P' Δx*.

Integrating Eq. (1.9) across the membrane thickness yields the Spiegler–Kedem equation:

$$R_T = 1 - \frac{c_p}{c_m} = \frac{\sigma(1-F)}{1-\sigma F},$$ (1.10)

where $F = \exp(-(\frac{(1-\sigma)}{p})J_v)$.

The Spiegler–Kedem equation is usually applied when there is no electrostatic interaction between the membrane and the neutral solutes. From Eq. (1.10), one can see that the reflection coefficient σ corresponds to the maximum rejection at an infinitely high permeate volume flux. The values of σ and P can be determined directly from experimental data of the real rejection R_T, as a function of J_v by any best-fitting method.

For a system of a mono-mono type electrolyte (i.e. NaCl), by combining the extended Nernst–Planck equation and the Donnan equilibrium theory, membrane parameters σ and P can be determined based on the Teorell–Meyer–Sievers (TMS) model with the following equations [63]:

$$\sigma = 1 - \frac{2}{(2\alpha-1)\xi + (\xi^2 + 4)^{0.5}}$$ (1.11)

$$P = D_S(1-\sigma)(\frac{A_k}{\Delta x})$$ (1.12)

where ξ is defined as the ratio of effective volume charge density (φX) of membrane to the electrolyte concentration (C_m) at the membrane surface, α is the transport number of cations in a free solution defined as $\alpha = D_1/(D_1 + D_2)$, where D_1 and D_2, the diffusivities of Na$^+$ and Cl$^-$, are 1.33×10^{-9} and 2.03×10^{-9} m^2 s^{-1}, respectively [64]. Therefore, the effective charge density of a membrane can be determined as a function of NaCl concentration if σ and α are

available. At a higher NaCl concentration, the membrane seems to have a larger calculated charge density. The effective charge density, ΦX, can be related to the NaCl concentration by the following empirical equation:

$$\Phi X = KC_m^n \tag{1.13}$$

1.8 Research objectives and thesis organization

The objective of this of this research is to investigate the fabrication of NF hollow fiber membranes with commercial polymeric material-Torlon$^{®}$ polyamide-imide. The resultant NF membranes are applied in recycle valuable products, reduce waste, and reuse water for a sustainable pharmaceutical manufacture.

More specifically, the present thesis addresses the following issues:

1) To explore the molecular engineering and characterization of NF hollow fiber membranes with the desired water permeability and pore size distribution via elongation-induced morphological evolution with the aid of external stretching during a hollow fiber spinning process;

2) To systematically characterize the charge properties of the PAI NF hollow fiber membranes and study the NF performance for rejection of glutathione;

3) To fabricate PAI/CA NF dual-layer hollow fiber membranes and investigate various controlling parameters such as dope additives and spinneret temperature;

4) To study the effects of hyperbranched polyethyleneimine induced cross-linking of spongy-like PAI hollow fiber membranes and to explore its applications in removal of pharmaceutical active compounds from water.

5) To further develop a novel thin-film composite NF membrane through interfacial polymerization of hyperbranched polyethyleneimine and isophthaloyl chloride on a PAI dual-layer hollow fiber membrane support.

This thesis comprises seven Chapters. Chapter One provides an introduction of this thesis including the review of nanofiltration, industrial applications of nanofiltration, especially the applications for sustainable pharmaceutical manufacture, fabrication of nanofiltration membranes, and theoretical background for NF membrane characterizations.

Chapter Two presents the molecular engineering of NF hollow fiber membranes through controlling the elongation-induced membrane pore morphology by external stretching of the fibers during the spinning process.

In Chapter Three, the charge properties of Torlon® PAI NF membranes were characterized systematically in terms of zeta-potential, reflection coefficient, effective charge density, single salts rejection and binary salts rejections. The rejection of glutathione by the NF hollow fiber membrane is also presented.

Chapter Four provides a systematic study on the molecular engineering and design of dual-layer hollow fiber membranes in terms of their pore size, pore size distribution and pure

water permeability as a function of spinning conditions. Both of non-solvent additives and spinneret temperatures will be studied.

Chapter Five presents the development of a positively charged NF hollow fiber membrane for removal of ciprofloxacin with high rejection and low fouling tendency. The effect of PEI modification on the mechanisms of ciprofloxacin removal from water is fundamentally studied.

Chapter Six delivers the fabrication of novel TFC membranes for effective removal of organic matters from the wastewater of pharmaceutical and textile industries. The effects of interfacial polymerization parameters on the NF performance will be discussed in detail.

A detailed discussion of the experimental results and conclusions are presented at the end of each respective chapter. General conclusions drawn from the whole research are summarized in the Chapter Seven. Inclusive in this ending chapter are some recommendations for future research related to this study.

CHAPTER TWO

FABRICATION OF POLYAMIDE-IMIDE NANOFILTRATION HOLLOW FIBER MEMBRANES WITH ELONGATION-INDUCED NANO-PORE EVOLUTION

2.1 Introduction

As discussed in Chapter One, hollow fibers have many advantages compared to other modules: (1) a much larger membrane area per unit membrane module volume, resulting in a higher productivity; (2) self-mechanical support, allowing the membrane to be back-flushed for liquid separation; and (3) good flexibility and ease of handling during module fabrication and system operation. Nevertheless, the applications of hollow fiber membranes are still limited due to their low water permeability relative to that of flat-sheets primarily because they are usually spun from dopes containing much higher concentrations than those used for the fabrication of flat sheet membranes in order to maintain self-supported mechanical strength and withstand high testing pressures [65]. In addition, the high shear rates and stresses during the spinning process generally enhance chain orientation and thus produce lower water permeability and higher solute rejection [19]. Clearly, technological breakthroughs are needed to enhance the water permeability of hollow fiber membranes while still retaining their separation efficiency. The objective of this study is, therefore, to explore the molecular engineering and characterization of NF hollow fiber membranes with the desired water permeability and pore size distribution. We accomplish these tasks by controlling the elongation-induced membrane pore morphology by external stretching of the fibers during the spinning process.

Molecular engineering of pore size and chain orientation in polymeric membranes has been effectively employed to control the transport properties of both gas and liquid molecules [66][13]. Several researchers have investigated the shear-induced molecular orientation and its effects on the performance of gas separation [67-69][14-16] and UF [70, 71] hollow fiber membranes. However, much less work has been done to investigate the elongation-induced morphological evolution for NF hollow fiber membranes. Perhaps Wang and Chung were the pioneers observing the interesting elongation-induced nano-pore formation when they fabricated a novel polybenzimidazole (PBI) NF hollow fiber membrane [13]. They reported that the effective mean pore size decreases, whereas the pure water permeability increases with an increase in elongational draw ratio. This phenomenon is quite different from what have been reported on the effects of elongational drawing on UF membranes and gas separation membranes [67-71]. Therefore, their work stimulated our interest to further investigate the fundamental science behind the elongation-induced nano-pore evolution in other NF membranes. To our best knowledge, no in-depth studies on this subject have been reported yet. Because the hollow fiber configuration is the most favorite choice for industry membrane systems and the employment of high take-up speeds is favorable in the spinning process [47, 72, 73], this study may have great potential in developing tailor-made high-performance NF membranes for various industrial applications.

2.2 Experimental

2.2.1 Materials

The Torlon® 4000TF polyamide-imide having a chemical structure as shown in Figure 1.1 was purchased from Solvay Advanced Polymers. N-methyl-2-pyrrolidinone (NMP) was purchased from Merck and was used as the solvent to prepare the spinning solution. Uncharged neutral solutes of glucose, saccharose, raffinose, and α-cyclodextrin (Sigma-Aldrich, USA) were utilized to characterize membrane structure parameters. Molecular weights, diffusivities and Stokes radii of neutral solutes are listed in Table 2.1 [63]. All chemicals were used as received.

Table 2.1. Diffusivities and Stokes radii of neutral solutes in aqueous solutions (at 25ºC)

Solute	MW [g·mol^{-1}]	D_s [$\times 10^{-9}$ m^2·s^{-1}]	r_s [nm]
Glucose	180	0.67	0.365
Saccharose	342	0.52	0.471
Raffinose	504	0.42	0.584
α-Cyclodextrin	972	0.35	0.701

2.2.2 Preparation of Torlon® PAI NF hollow fiber membranes

The hollow fiber membranes were prepared by the dry-jet wet-spinning process. Torlon® polymer was firstly dried in a vacuum oven at 120 °C overnight to remove the moisture, and then dissolved in NMP. The solution was stirred for 24 hours to form a homogeneous polymer solution. Then, the resultant solution was set aside for 2 days to eliminate air bubbles that may have been trapped in the solution. A Schematic diagram of a hollow fiber

spinning line is shown in Figure 2.1. The dope solution and the bore fluid were fed into the annulus of the spinneret by two ISCO pumps. After the spinning dope and the bore fluid met at the tip of the spinneret, they entered an air gap region followed by entering the coagulation (water) bath. The spinning conditions of the Torlon® PAI NF hollow fiber membranes are listed in Table 2.2.
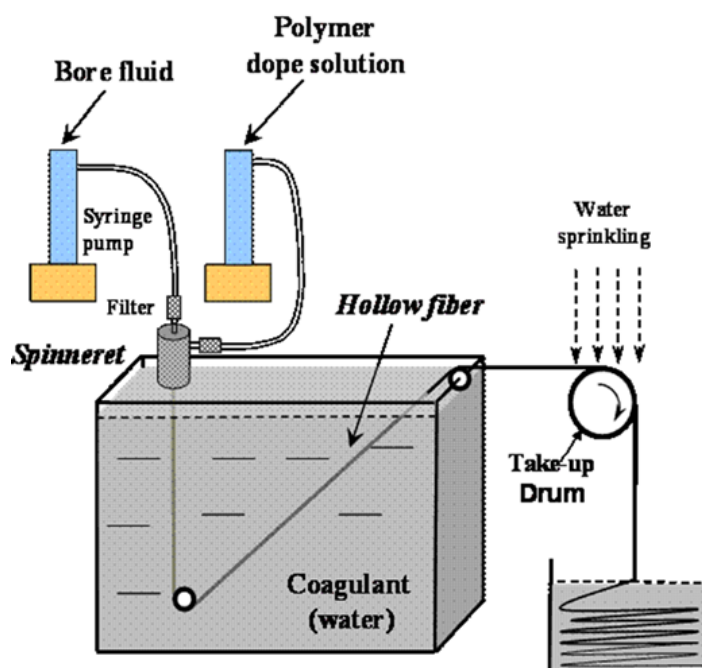
Figure 2.1 Schematic diagram of a hollow fiber spinning line

Table 2.2. Spinning conditions of Torlon® PAI NF hollow fiber membranes

Torlon® dope solution	(wt. %)	Torlon®/ NMP (26.0 : 74.0)
Dope flow rate	(ml/min)	6.0
Bore fluid composition	(wt. %)	NMP/Water (90 : 10)
Bore fluid flow rate	(ml/min)	3.0
Air gap	(cm)	5
Take-up speed	(m/min)	A: 15.0, B:32.6, C: 54.6
External coagulant		Tap water, 26 ± 1 ºC
Dope temperature	(ºC)	26 ± 1
Bore fluid temperature	(ºC)	26 ± 1
Room humidity	(%)	65 ~ 70
Dimension of spinneret	(mm)	i.d./o.d. (1.05/1.6)
Die length L of spinneret	(mm)	6.5

Elongational stretching with the aid of various take-up speeds was performed on the spinning line during dry-jet wet spinning. The elongational draw ratio φ is defined as the ratio of the cross sectional area of dope flowing channel in the spinneret to the solid cross-sectional area of the precipitated hollow fiber membrane as follows:

$$\varphi = \frac{(OD^2 - ID^2)_{Spinneret}}{(OD^2 - ID^2)_{Hollow-fiber}} \tag{2.1}$$

where OD and ID refer to the outer and inner diameters, respectively. After spinning, the as-spun hollow fiber membranes were rinsed in a clean water bath for 3 days to remove the residue solvent. The hollow fiber membranes were then divided into two groups for post-treatments. One group was dipped in a 30 wt% glycerol aqueous solution for 48 h and dried in air at ambient temperature for the use of making membrane modules. The soaking in the glycerol aqueous solution is a standard practice in the industry to prevent membrane pores from closing before use. The other group was subjected to solvent exchange by immersing membranes in methanol three times for 30 min per time and then n-hexane three times for 30 min per time under stirring. Finally, these fibers were dried in the air at the ambient temperature for further characterizations with means of SEM, AFM and polarized FTIR.

2.2.3 Characterizations

The morphologies of the hollow fiber membranes spun at different take-up speeds were observed by a scanning electron microscope (SEM JEOL JSM-5600LV) and a field emission scanning electron microscope (FESEM JEOL JSM-6700F). Before observation, the dried hollow fiber were immersed in liquid nitrogen, fractured and then coated with platinum using a JEOL JFC-1300 Platinum coater.

The membrane surface topology was examined using a Nanoscope IIIa atomic force microscope (AFM) from Digital Instruments Inc. For each membrane, an area of 500nm×500nm was scanned at a rate of 1 Hz using the tapping mode. The analysis of AFM pictures was carried out according to the previous literature [74, 75]. Various roughness parameters such as the mean roughness (R_a), root mean square of Z values (R_{ms}), and maximum vertical distance between the highest and lowest data points (R_{max}) were used to quantify the differences among various membranes. The sizes of nodule aggregates in both x- and y-directions were determined from the average of at least 10 sections of several fibers.

Polarized FTIR spectra of the hollow fiber membrane were measured by a Bio-Rad UMA 500 IR microscope attached with a Bio-Rad FTS 3500 FT-IR main bench. The system is equipped with a liquid nitrogen-cooled MCT detector and a polarizer. Measurements were carried out using a retro-reflection mode. For each sample, two types of outer surface reflectance that were parallel and perpendicular to the axis of hollow fiber were obtained respectively to study the molecular orientation near the membrane surface induced by elongational stretching.

The overall porosity ε of the hollow fiber membrane was calculated as：

$$\varepsilon = (1 - \frac{\rho_{fiber}}{\rho_{Torlon}}) \times 100\% \qquad (2.2)$$

where ρ_{Torlon} is the density of the Torlon® powder, 1.38 g/cm³ [76]. The density of the hollow fiber membrane ρ_{fiber} was determined by Eq. (2.3), where the bulk volume V was obtained by

measuring the inner and outer diameters of the membrane under a microscope. The membrane weight m was measured by a digital balance.

$$\rho_{\text{fiber}} = \frac{m}{V} \tag{2.3}$$

2.2.4. Nanofiltration experiments with Torlon® PAI NF hollow fiber membranes

Nanofiltration experiments were conducted in a lab-scale circulating filtration unit, as shown in Figure 2.2. Two modules for each hollow fiber sample were tested for nanofiltration experiments, wherein each module comprised 10 fibers with an effective length of around 17 cm. Since the outer surface of hollow fibers was the selective layer, the feed solution was pumped into the shell side, while the permeate solution exited from the lumen side of hollow fibers. A high flow rate of 1.6 L/min was applied so that the effect of concentration polarization was minimized (Re > 4000). Before testing, the hollow fiber membranes were conditioned at 12 bar for 0.5 h. Then, each membrane sample was firstly subjected to the pure water permeation experiment at 10 bar to measure the pure water permeability, PWP (l m^{-2} bar^{-1} h^{-1}) according to Eq. 1.1:

$$\text{PWP} = \frac{Q}{\Delta P \cdot A} \tag{2.4}$$

where Q is the water permeation volumetric flow rate (L/h), A is the effective filtration area (m^2), and ΔP is the transmembrane pressure drop (bar).

Subsequently, the mean effective pore size and the pore size distribution were obtained according to the protocol of solute transport experiments. Different solutions, which contain neutral solutes, inorganic salts and salt mixtures, were filtered into the membrane modules.

The apparent solute separation coefficient R_T (%) was calculated using the following equation:

$$R_T(\%) = \left(1 - \frac{c_p}{c_f}\right) \times 100 \qquad (2.5)$$

where C_p and C_f are the solute concentration in the permeate and the feed solutions, respectively.
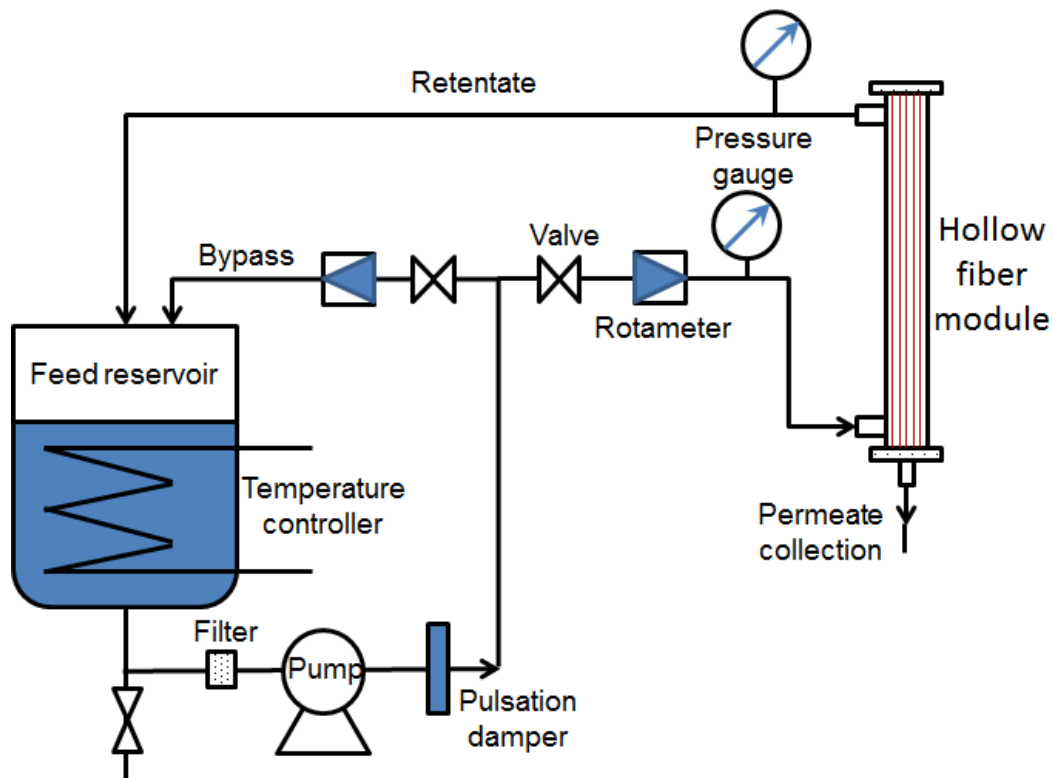
Figure 2.2. Schematic diagram of the nanofiltration system.

The following describes the procedures for nanofiltration experiments:

(1) Feed solutions were prepared by dissolving neutral solutes in deionized (DI) water at a concentration of about 200 ppm. The pressure difference across the membrane and the feed temperature were kept at 10 bar and 25°C respectively for all the experiments. The

feed solutions were circulated for about 0.5 h until the whole system reached the steady state. Both feed and permeate solutions were collected to measure the concentrations.

(2) Nanofiltration experiments were conducted with neutral organic solutes of progressively higher molecular weights. Between runs of different solutes the membrane was thoroughly flushed with DI water. The solute separation data was further used for the estimation of mean pore size and pore size distribution of the membrane.

Concentrations of the neutral solute solutions were measured with a total organic carbon analyzer (TOC ASI-5000A, Shimazu, Japan).

2.3 Results and discussion

2.3.1 Effects of take-up speed on membrane morphology, elongational draw ratio and porosity

A typical morphology of Torlon® hollow fiber membranes is shown in Figure 2.3. It is observed that the asymmetric membrane structure consists of an outer-selective skin, finger-like macrovoids, spongy-like substructure and porous inner skin. The macrovoids are all outward pointed, indicating that their origins are possibly from external water induced intrusion during the phase inversion process [77]. The dimensions of the hollow fibers were affected by the take-up speed as illustrated in Figure 2.4. The outer diameter (OD) and inner diameter (ID) decrease with an increase in take-up speed. However, the outer diameter decreases more significantly than the inner diameter, thus resulting in a decrease in wall thickness with increasing elongational draw ratio. The overall porosities of the hollow fiber membranes spun at take-up speeds of 15.0, 32.6 and 54.6 m/min were 69.3, 58.9 and 53.4%,

respectively. The reduction in overall porosities indicates the suppression of macrovoids formation with an increase in take-up speed, which was extensively discussed in our previous studies [73, 78].
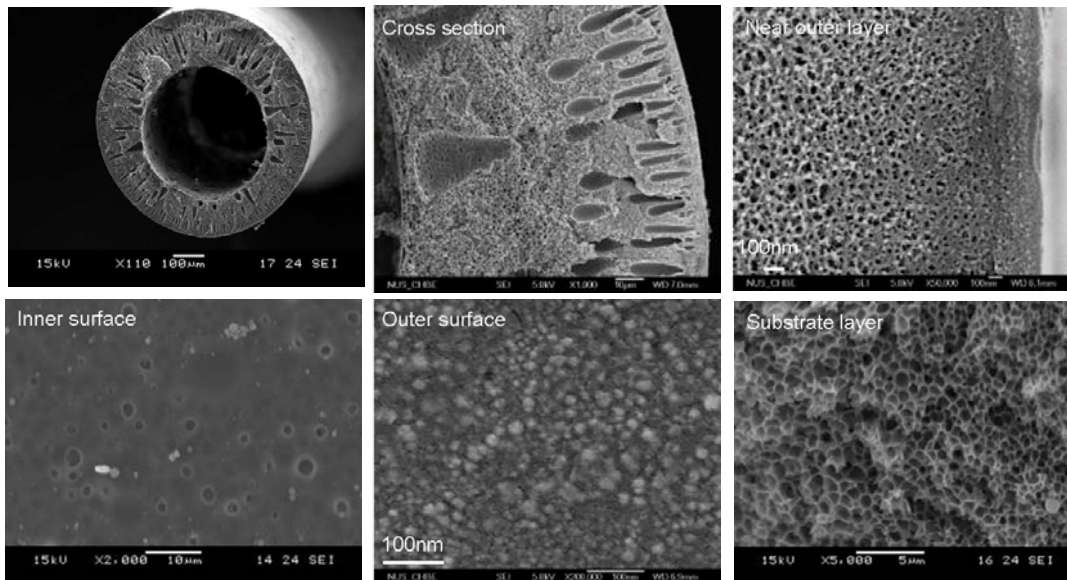
Figure 2.3. Morphology of Torlon® PAI NF hollow fiber membranes. (Take-up speed: 15 m/min)
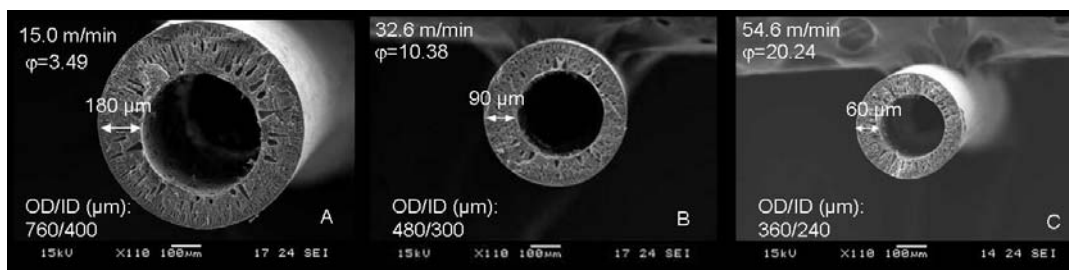
Figure 2.4. Effects of take-up speed on the membrane structure of Torlon® PAI NF hollow-fiber membranes. (The values at the left upper corner are the take-up speed and corresponding elongational draw ratio. The values at the left lower corner are the outer diameter and inner diameter of the hollow fiber membranes.)

2.3.2 Effects of take-up speed on mean pore size, pore size distribution and pure water permeability

The newly developed Torlon® PAI NF hollow fiber membranes were characterized by the solute transport method as described in Section 2.1 to obtain the mean effective pore size and

pore size distribution. The relationships of solute rejection against solute Stokes radius, obtained from the solute transport method, are plotted on the log-normal probability graph in Figure 2.5. Linear relationships are obtained with reasonable high correlation coefficients ($r^2 > 0.95$). The mean effective pore radius μ_p at $R_T = 50\%$, the molecular weight cutoff (MWCO, the molecular weight of solute at $R_T = 90\%$) and the geometric standard deviation σ_p calculated from the plots are listed in Table 2.3. The pure water permeabilities, which were obtained from Eq. (2.4), of the hollow fiber membranes spun at different take-up speeds, are also listed in Table 2.3. The cumulative pore size distribution curves and probability density function curves of the PAI hollow fiber membranes calculated from Eqs. (1.3) & (1.5) are depicted in Figures 2.6 and 2.7. It can be observed that the pore size distribution shifts towards left and becomes narrow with an increase in take-up speed.
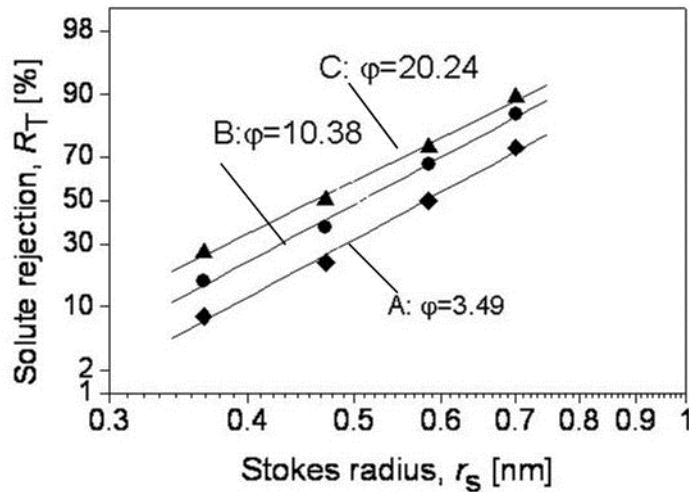
Figure 2.5. Effective rejection curves (solute rejections vs. their Stokes radii) for Torlon® PAI NF hollow fibers spun at different take-up speeds. (Plotted on the log-normal probability coordinate system)

Table 2.3. Molecular weight cut off (MWCO), mean effective pore size (r_p), geometric standard deviation (σ_p) and Pure water permeability (PWP) of Torlon® PAI NF hollow-fiber membranes spun at different take-up speeds.

Fiber	Draw ratio φ	MWCO (Da)	r_p (nm)	σ_p	PWP ($lm^{-2}bar^{-1}h^{-1}$)
A	3.49	1538	0.58	1.37	2.77
B	10.38	1126	0.51	1.38	3.52
C	20.24	976	0.46	1.42	5.39
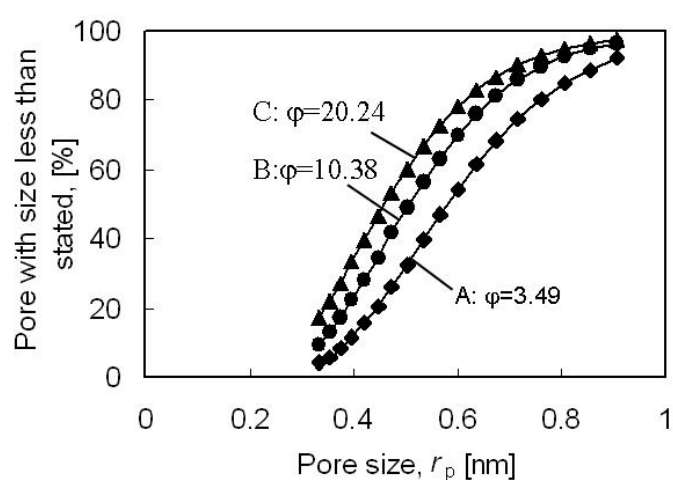
Figure 2.6. Cumulative pore size distribution curves of the Torlon® PAI NF hollow-fiber membranes spun at different take-up speeds.
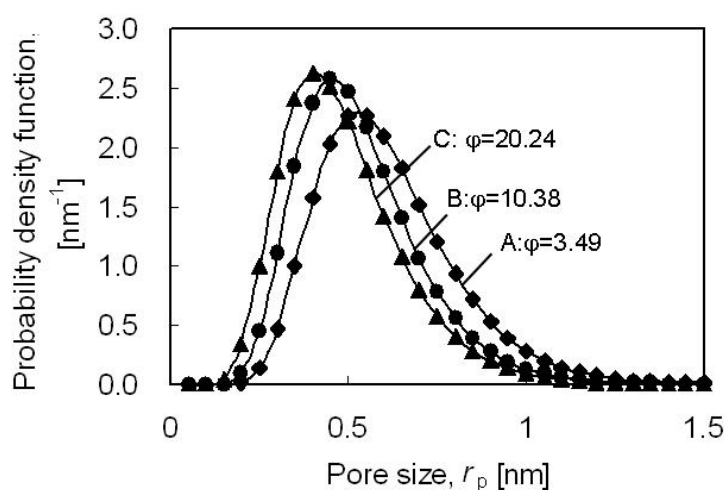
Figure 2.7. Probability density function curves of the Torlon® PAI NF hollow-fiber membranes spun at different take-up speeds.

27

Interestingly, from Table 2.3, it can be obviously found that the pure water permeability increases, whereas MWCO and the mean effective pore radius decreases, when increasing the take-up speed at the same dope flow rate, which was seldom reported previously [13]. Key membrane properties that affect the rejection of organic molecules are MWCO, pore size and membrane morphology [79]. However, the pure water permeability is dependant on pore size, surface porosity, selective layer thickness and tortuosity [80, 81]. In this section, the effects of these parameters on the sieving property and pure water permeability will be discussed.

Surface pores are considered as the interstices among nodules. As shown in the AFM phase images (the scan size is 500×500 nm) in Figure 2.8, the yellow sites represent the higher ground comprising nodules while the dark sites are the lower ground consisting of pores among nodules and those nodules with less heights. Interestingly, at the lowest take-up speed of 15.0 m/min, the phase image shows parallel strips of higher and lower grounds perpendicularly to the spinning direction. This surface morphology may be resulted from rapid solvent exchange, precipitation and solidification when the hollow fiber enters the coagulation bath, thus the membrane surface wrinkles because of severe solvent outflow. However, the strip pattern disappears and a surface fully of nodules and valleys appears at a higher take-speed of 32.6 m/min. The effects of elongational stretch become more profound at the highest take-up speed of 54.6 m/min. Smaller pores intertwined with woven/fiber-like structure were formed in the surface layer, implying the severe segregation and stretch of nodules under elongational drawing. A similar structure induced by gravity at a higher air gap distance can be found in our previous work [82].
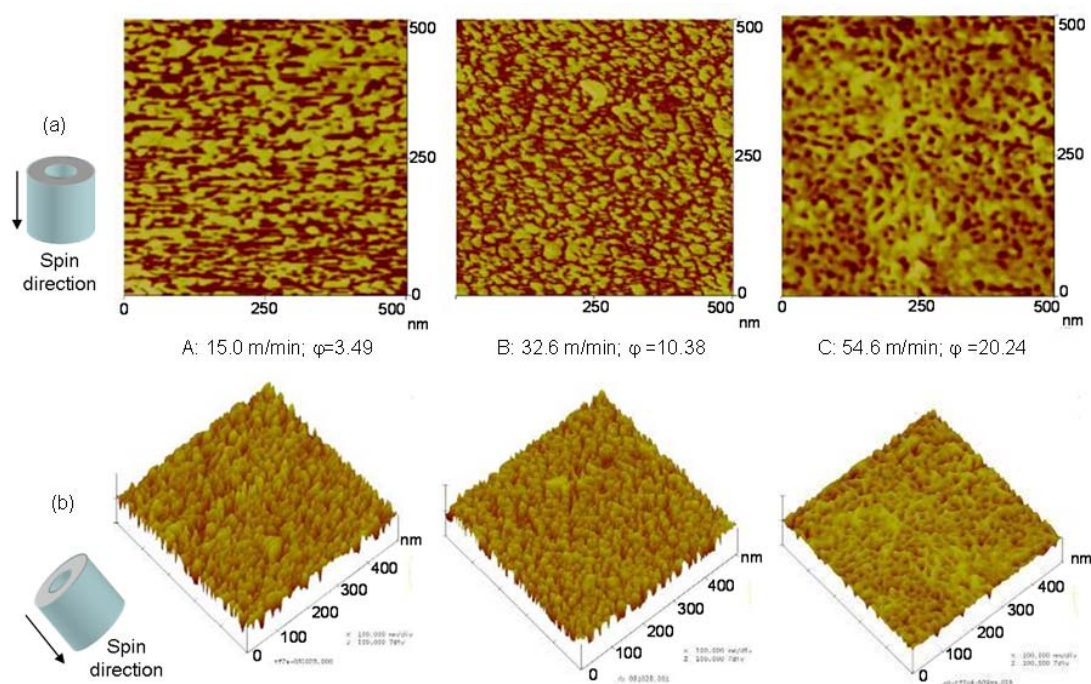
Figure 2.8. AFM images of the outer surface of Torlon® PAI NF hollow fiber spun at different take-up speeds. (a) phase image, (b) 3D image

Two possible mechanisms can be employed to explain the nano-pore morphological evolution. The first one is the "nucleation and growth" and "spinodal phase separation", which is described in Figure 2.9. At low take-up speeds, the flux ratio of in-flow coagulant to out-flow solvent is low. As a result, the state of the nascent fiber undergoes path (a) where "nucleation and growth" is the prevailing mechanism. The resultant fiber surface has a nodule-like surface layer, which can be observed in Figure 2.8 A and B. A similar structure induced by shear rate within the spinneret can be found in our previous study [75]. When the take-up speed is further increased, path (b) becomes dominant. With the aid of a higher flux ratio of in-flow coagulant to out-flow solvent, the state of the nascent hollow fiber rapidly traverses the binodal curve and enters the unstable region where "spinodal phase separation" takes place [83], leading to a woven/fiber-like porous structure shown in Figure 2.8 C. Both "nucleation and growth" and "spinodal phase separation" take place in path (b), but a high

29

take-up speed or draw ratio facilitate the spinodal decomposition and form the woven/fiber-like porous structure [82].
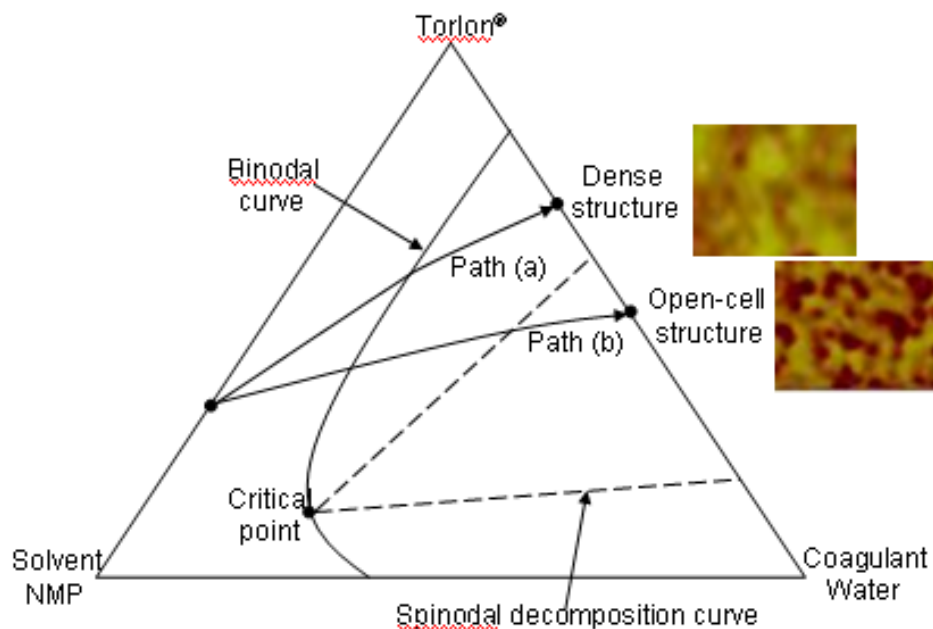
Figure 2.9. Phase diagram for a ternary system and the coagulation path during the precipitation of a Torlon® PAI hollow fiber at a constant temperature. Path (a): nucleation and growth; Path (b): spinodal decomposition

The second mechanism is due to chain disentanglement and energy dissipation. To further elaborate these phenomena, the membrane morphology were analyzed by the roughness parameters such as R_a, R_{ms}, R_{max} and dimensions of nodule size in both x and y directions. As shown in Table 2.4, the nodule sizes in both directions decrease while the roughness parameters increase when the take-up speed was increased. It is believed that the nodular structure arises from rapid demixing of the polymer solution, followed by rapid vitrification [75, 82, 83]. Since the rheology of Torlon®/NMP spinning solutions shows shear-thinning and strain-thinning characteristics [56], Torlon® molecular chains will be stretched, disentangled and sliding over one another during spinning with high elongational draw ratios. The disentangled and aligned polymer chains may result in smaller nodule sizes because of

shorter-range interactions with surrounding molecules compared to those un-stretched and entangled chains. The smaller nodule size tends to have a smaller surface pore size due to easier and higher nodules packing (see Figure 2.8), whereas the shorter-range interaction reduces the skin selective-layer thickness (see Figure 2.10) due to less chain entanglement with surrounding molecules. The former keeps a high rejection while the latter enhances flux with reduced transport resistance. In addition, the high draw ratio may not only stretch the nascent nodules as elongated fibers but also deform and elongate pores (underneath the skin surface) with narrower open windows. The surface morphology shown in Figure 2.8C is a combined result of rapid phase inversion and high elongational drawing, the nano-size pores for separation may be located immediately underneath the skin surface.

A: φ =3.49   B: φ =10.38   C: φ =20.24
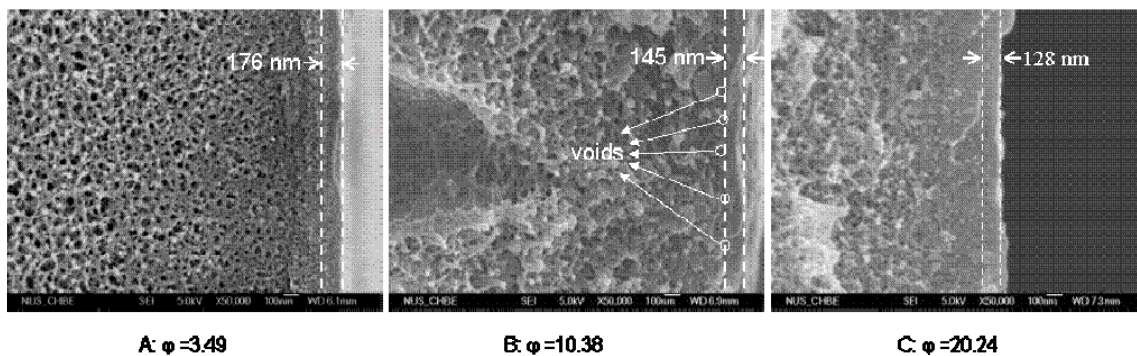
Figure 2.10. FESEM images of the near outer layer of Torlon® PAI NF hollow fiber membranes spun at different take-up speeds.

Table 2.4. Effects of take-up speed on roughness and nodule size of the outer surface of Torlon® PAI NF hollow fiber membranes.

Fiber ID	R_a (nm)	R_{ms} (nm)	R_{max} (nm)	Dimension of nodules in x-direction (nm)	Dimension of nodules in y-direction (nm)
A	0.72 (0.12)	0.93 (0.15)	10.71 (1.50)	72.5 (5.1)	70.6 (5.0)
B	1.41 (0.25)	1.74 (0.17)	14.33 (1.87)	50.9 (4.5)	50.9 (4.7)
C	1.55 (0.21)	1.97 (0.14)	16.30 (1.65)	35.2 (5.5)	35.2 (4.2)

R_a : mean roughness; R_{ms}: root mean square of Z values; R_{max}: Maximum vertical distance between the highest and lowest data points. The values in the brackets are standard deviation. y-direction is the spinning direction

To further verify the enhancement of molecular orientation in the skin layer, characterization with polarized FTIR was carried out because it can detect information from only a thin surface with a depth of less than approximately 150 nm [84]. The selective layer thicknesses of all membranes that we developed, as shown in the FESEM images in Figure 2.10 are within this range thus applicable for this technique. The FTIR spectra are shown in Figure 2.111. The blue bold line represents the spectra measured with the polarization parallel to the spinning direction, while the pink normal line represents the spectra with the polarization perpendicular. There was only a small difference in reflectance between the parallel and perpendicular polarization measured for the membranes spun at a low take-up speed. However, as the take-up speed increases, the difference becomes larger, indicating that a perpendicularly oriented skin was formed on the PAI hollow fiber membrane. These results indirectly confirm a significant difference in macromolecular stretch and orientation induced by the elongation stress during hollow fiber spinning that may create fiber-like nodules and elongated pores with enhanced rejection.
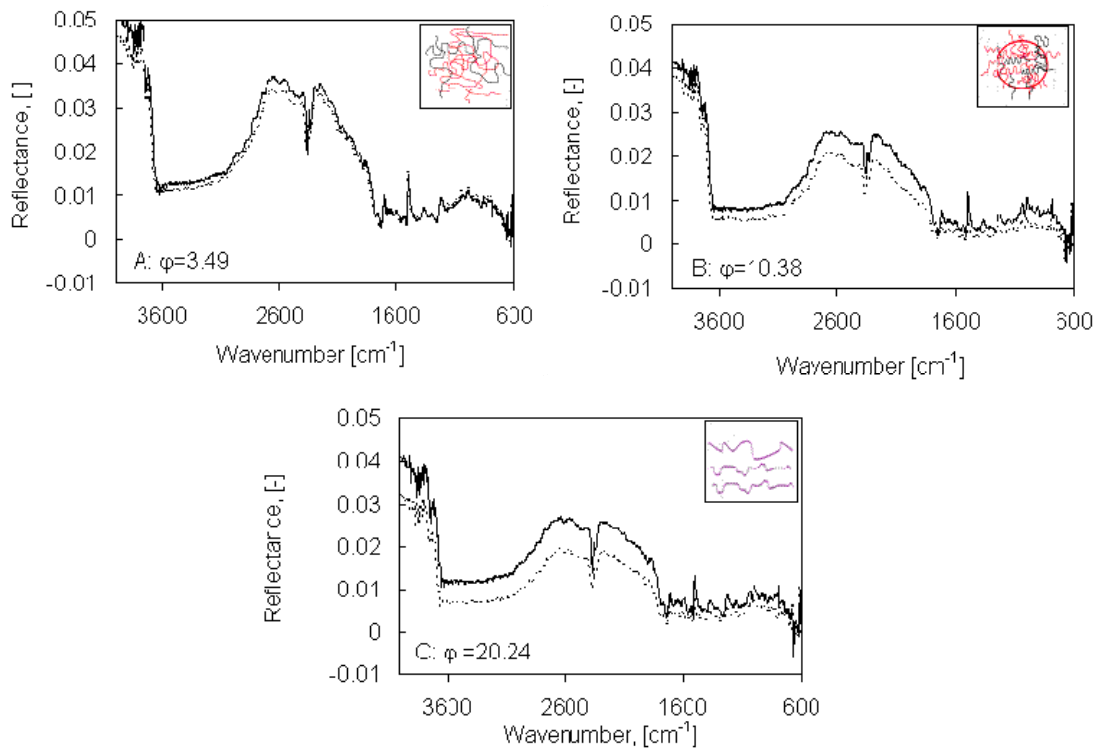
Figure 2.11. Polarized FTIR spectra of Torlon® PAI NF hollow fiber membranes. (bold line) Parallel to spinning direction; (dotted line) Perpendicular to spinning direction. (The small images in the upper right corner are the proposed structures of polymer molecules near the surface.)

2.4 Conclusions

A novel Torlon® polyamide-imide nanofiltration hollow fiber membrane was developed by the dry-jet wet-spinning process. We found that the external stretching had a great influence on membrane structure, nano-pore formation, and nanofiltration performance. AFM images demonstrate that a high take-up speed favors the "spinodal decomposition" rather than "nucleation and growth", which increases surface porosity and thus increases pure water permeability. Polarized FTIR further verifies the enhanced molecular orientation towards the direction perpendicular to the spinning direction. Therefore, the pore size and the MWCO were decreased while the pure water permeability was increased with an increase in take-up

speed. The Torlon® PAI hollow fiber membrane spun at 54.6 m/min has a mean pore radius of 0.46 nm and a narrow pore size distribution. The pure water permeability was achieved at 5.39 L m^{-2} bar^{-1} h^{-1}.

<center>**CHAPTER THREE**</center>

<center>**CHARACTERIZATION OF CHARGE PROPERTIES OF POLYAMIDE-IMIDE NANOFILTRATION HOLLOW FIBER MEMBRANES AND REJECTION OF GLUTATHIONE**</center>

3. 1. Introduction

As introduced in Chapter One, Torlon® polyamide-imide is a relatively new material employed in membrane field. To the best of our knowledge, we are the first to apply this polymer to fabricate NF membranes. Therefore, the characterization of the charge properties of the resultant NF membranes is very important. In this chapter, the charge properties of the Torlon® polyamide-imide NF membranes fabricated in Chapter One were characterized systematically in terms of zeta-potential, reflection coefficient, effective charge density, single salts rejection and binary salts rejections.

After characterizing the charge properties of the NF hollow fiber membrane, its NF performance will be tested with a drug compound, i.e. glutathione (Figure 1.2). As discussed in Chapter One, Glutathione is a tripeptide which is the most abundant non-protein thiol compound in living organisms. The valuable functions of glutathione on human body lead to an urgent need to explore effective technologies to recover, concentrate and purify this compound. NF is a promising candidate because of its separation mechanisms involves not only steric (size exclusion) effect, but also an electrostatic partitioning interaction (Donnan exclusion) between membrane and external solution. Therefore, if the target compound can be ionized in an aqueous solution, Donnan exclusion would be a suitable approach to increase

rejection by properly choosing the membrane material and solution pH [2]. In this chapter, the rejection of glutathione by the Torlon® polyamide-imide NF hollow fiber membrane is presented.

3. 2 Experimental

3.2.1 Materials

Several analytical-grade salts, i.e. NaCl, MgCl$_2$, MgSO$_4$, and Na$_2$SO$_4$ (Merck, Germany) were used to characterize the charge property of the membranes. Glutathione (C$_{10}$H$_{17}$N$_3$O$_6$S, MW 307.33, white powder) was purchased from Sigma-Aldrich. All chemicals were used as received.

3.2.2 Zeta-potential measurements

In order to characterize the membrane surface charge characteristics, streaming potential measurements of Torlon® PAI flat membranes were performed by a SurPASS electrokinetic analyzer (Anton Paar GmbH, Austria). Torlon® PAI flat membranes were prepared by casting the polymer solution (with the same concentration as spinning hollow fiber) on a glass plate by a blade with a 60 μm gap. Then the as-cast membranes were immediately immersed into water. The zeta potential of membranes was based on the measurement of streaming potential along the membrane surface [85]. A solution of 0.01M NaCl was circulated through the measuring cell containing the membrane sample. A relative movement of the charges in the electrochemical double layer occurred and gave rise to the streaming potential. This

streaming potential was detected by Ag/AgCl electrodes placed at both sides of the membrane sample. The electrolyte solution conductivity, temperature and pH value were measured simultaneously. The classic Helmholtz–Schmoluchowski equation was applied without any corrections to calculate the apparent zeta potentials [86]. Manual titration with 0.1M HCl and 0.1M NaOH was carried out to study the pH dependence of the zeta potential and thus determine the isoelectrical point (IEP).

3.2.3. Nanofiltration experiments of salt and glutathione with PAI NF hollow fiber membranes

Nanofiltration experiments of salt and glutathione solutions were conducted by following the procedure described in section 2.2.4.

(1) NaCl solutions with different concentrations were prepared. The ion rejection by membranes was measured at different pressures in order to characterize the effective charge density of the membranes.

(2) Different electrolyte solutions were prepared by dissolving single salts in DI water with the concentration 0.01 mol L^{-1}. The same experiment procedures as described in the Step (1) were employed to measure the salts rejection.

(3) The NaCl/Na$_2$SO$_4$ binary salt mixture solutions with different concentration ratios were prepared to test the ion fractionation performance of the membranes.

(4) Glutathione solutions (200ppm) were prepared by dissolving glutathione powder in DI water. NaOH (1.0 M) and HCl (1.0 M) solutions were used to modify the pH of the feed solutions; the solute rejection experiments were performed following Step (1) procedure with testing sequences from pH 3.3 to 8.8.

Concentrations of single electrolyte solutions were measured with an electric conductivity meter (Schott Instruments, Lab 960, Germany). Concentrations of different ions in electrolyte mixtures were measured with an ion chromatography (Metrohm, 792 Basic, Switzerland). Concentrations of the neutral solute solutions were measured with a total organic carbon analyzer (TOC ASI-5000A, Shimazu, Japan). The solution pH was measured by a pH meter (Horiba pH meter D-54, Japan).

3.3. Results and Discussions

3.3.1 Membrane characterization using single electrolyte solutions

In addition to pore size characterizations, the charge characteristics of Torlon® PAI NF membranes were studied in terms of zeta potential, reflection coefficient, effective charge density and rejection of single electrolyte solutions. As shown in Figure 3.1, the Torlon® PAI membrane has a slightly positive zeta potential below the isoelectric point at approximately pH 3.2, and is negatively charged above pH 3.2. This type of zeta potential curve is a characteristic of amphoteric surfaces consisting of carboxyl and amine functional groups on the membrane surface, in accordance with the molecular structure of Torlon® PAI illustrated in Figure 1.4. Therefore, the protonation of the amine functional groups may lead to a positive surface charge below the isoelectric point, while the de-protonation of the carboxyl groups would result in a negative charge above the isoelectric point [87].
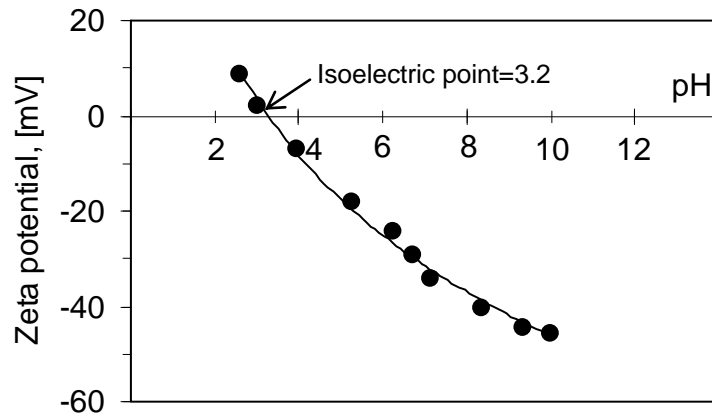
Figure 3.1. Zeta potential of Torlon® NF membrane as a function of pH. (Experiments were carried out with 0.01 M NaCl.)

The reflection coefficient and charge density of the PAI hollow fiber membranes were investigated through the transport and separation of NaCl at different pressures and different concentrations over a range of 1.0 to 50.0 mM. By means of fitting the real rejection data to the Spiegler–Kedem model as written in Eq. (1.10), membrane parameters (σ and P) can be determined from Figure 3.2 and Table 3.1 lists their values. Based on the Teorell–Meyer–Sievers model as written in Eq. (1.11) and Eq. (1.13), the effective charge density (ΦX) of the NF membranes can be determined from σ at different NaCl concentrations, as shown in Figure 3.3. It can be obviously found that the membrane with a smaller pore size has a higher rejection and a higher effective charge density. Interestingly, for each membrane the rejection was decreased as shown in Figure 3.2 while the effective charge density was increased as shown in Figure 3.3 with an increase in electrolyte concentration. This is due to the reduction of electrical double layer thickness within the pores when the concentration of the electrolyte was increased [88].
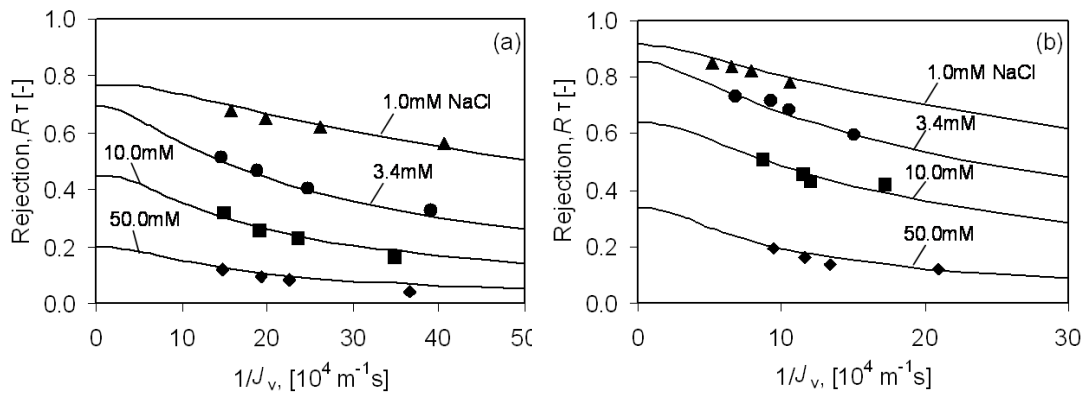
Figure 3.2. Rejections as function of permeate volume flux J_v with different NaCl concentrations. (a) Membrane A with r_p=0.58nm; (b) Membrane C with r_p=0.46nm. The curves are fitted by the Spiegler–Kedem equations.

Table 3.1. Reflection coefficient and Permeability of various concentrations of NaCl determined from the Spiegler–Kedem equations.

Membrane ID	A		C	
NaCl (mM)	Reflection coefficient, σ	Permeability, P ($\times$ 10^{-2} ms^{-1})	Reflection coefficient, σ	Permeability, P ($\times$ 10^{-2} ms^{-1})
1.0	0.857	0.72	0.898	0.66
3.4	0.692	1.19	0.850	1.11
10.0	0.435	1.62	0.550	1.19
50.0	0.201	2.40	0.363	4.64
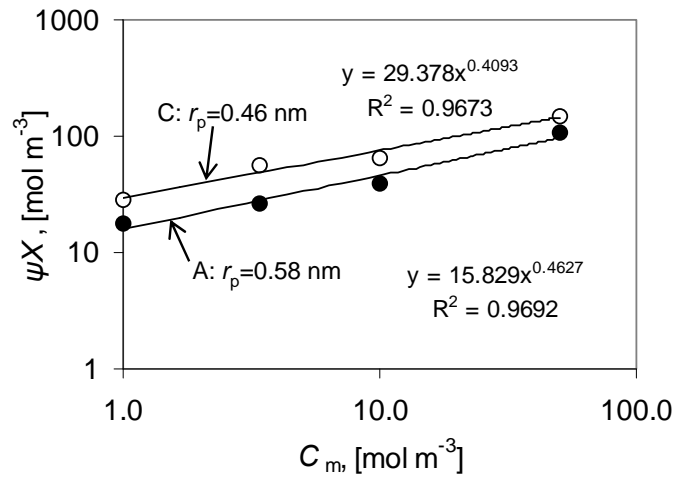
Figure 3.3. The effective charge density as a function of bulk NaCl molar concentration. The curves are fitted according to Eq. (1.13).

Because the NF membranes are negatively charged at pH 5.75, they show different rejections to anions and cations with different valences. At the same molar concentration (0.01 mol L^{-1}), the rejections of four kinds of electrolytes were measured at different pressures, as shown in Figure 3.4. They show an order of $R(Na_2SO_4) > R(MgSO_4) > R(NaCl) > R(MgCl_2)$. In other words, the membranes show a higher rejection to divalent anions with higher co-ion charge than monovalent anions, and a less rejection to divalent cations with higher counter-ion charge, corresponding with Donnan exclusion [89]. A slight deviation is the higher rejection of MgSO$_4$ than NaCl. According to Donnan exclusion, the rejection of theses 1:1 type electrolytes should be equal. This deviation is due to the larger hydrated radii and smaller diffusivities of the Mg^{2+} and SO$_4^{2-}$ ions than those of Na$^+$ and Cl$^-$ [90]. It can also be observed from Figure 3.4 that the solute rejection increases with increasing pressures. This is due to the fact that the water permeate flux through the membrane is linearly related to the applied pressure difference, whereas the solute flux is dependent on several factors: (1) the concentration gradient over the membrane; (2) the interaction between solute and fluid; and

41

(3) the water permeate flux. As a result, when increasing the pressure difference, the water flux increases relatively faster than the solute flux, which causes a decrease in solute permeate concentration and an increase in solute rejection.
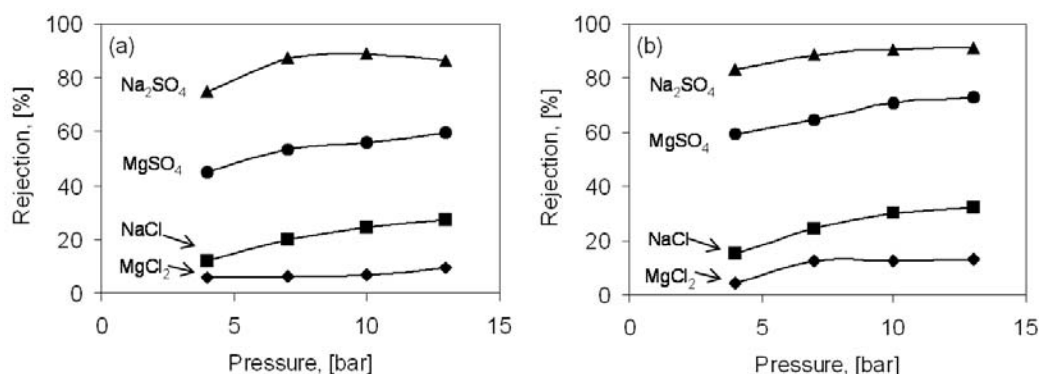
Figure 3.4. The rejection of different salts at different pressures.
(a) Membrane A with rp=0.58nm; (b) Membrane C with rp=0.46nm. (The bulk solution concentration: 0.01 mol L−1, pH 5.75)

3.3.2 Ion fractionation by PAI NF membranes in the electrolyte mixture solutions

Generally, most electrolyte solutions may contain several salts that need to be separated through the membrane process. In this section, a standard binary salt mixture containing Na_2SO_4 and NaCl was used to test the ion fractionation performance of the as-spun PAI NF membrane. The concentration of Na_2SO_4 was kept at 0.01 mol L^{-1} while NaCl was added to the system stepwise from 0.005 mol L^{-1} to 0.04 mol L^{-1}. As shown in Figure 3.5, more than 90% of Na_2SO_4 was rejected by the membrane while a negative rejection of NaCl at a low concentration was observed. This is due to the fact that Cl^- ions are forced to permeate preferentially compared to SO_4^{2-} ions since Cl^- has a lower valence, higher diffusivity and smaller hydrated radius [91]. Na^+ ions also permeate together with Cl^- to maintain electroneutrality at both sides of the membrane, which is in accordance with the Donnan

exclusion [89]. When the concentration of Cl⁻ was increased, the priority of Cl⁻ over SO_4^{2-} to permeate the membrane was lowered, thus increasing the rejection of Cl- and decreasing the rejection of SO_4^{2-}. The results shown in Figure 3.5 indicate that at a high concentration ratio of SO_4^{2-} to Cl⁻, these two ions could be effectively fractionated by the negatively charged Torlon® PAI NF membranes.
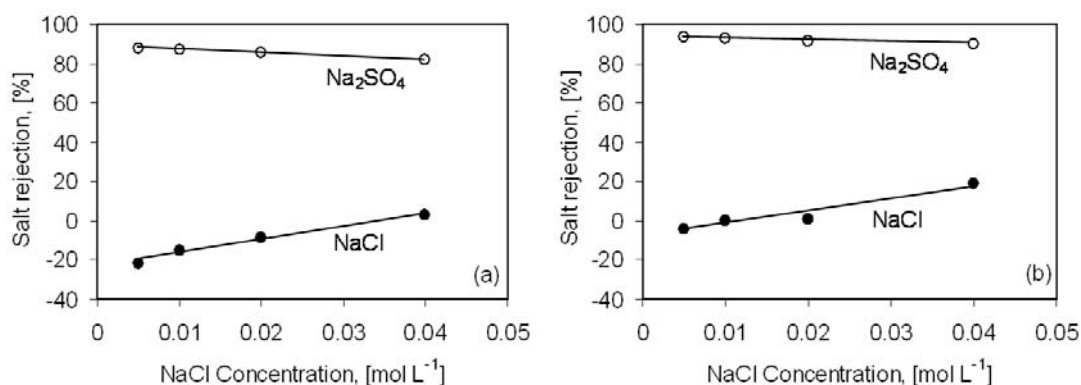
Figure 3.5. Ion rejection of the binary mixture of NaCl/Na2SO4 solution as a function of NaCl concentration. (a) Membrane A with rp=0.58nm; (b) Membrane C with rp=0.46nm. (Na2SO4 concentration was kept at 0.01 mol L-1, pH 5.75)

3.3.3 Rejection of glutathione by PAI NF hollow fiber membranes

As an amphoteric electrolyte molecule in the aqueous solution, glutathione acts as both base (proton acceptor) and acid (proton donor), given that glutathione molecules have the amino group (–NH₂), the carboxyl group (–COOH) and thiol group (-SH). As illustrated in Figure 1.2, glutathione is positively charged below pH 2.12 and negatively charged above pH 3.59. Within the range of 2.12 < pH < 3.59, the molecule becomes net neutral. Based on the dissociation constants (pK_a values) of the amino groups in glutathione, the fraction of different ionization states at different pH values can be expressed by the following Henderson–Hasselbalch equation [92] plotted in Figure 3.6 (light dark curves):

$$pH = pK_a + \log\left(\frac{[\text{proton acceptor}]}{[\text{proton donor}]}\right) \qquad (3.1)$$

Because Torlon® PAI NF membranes are also negatively charged at pH > 3.2 as shown in Figure 3.6, glutathione can be rejected by the NF membranes over a wide range of pH.
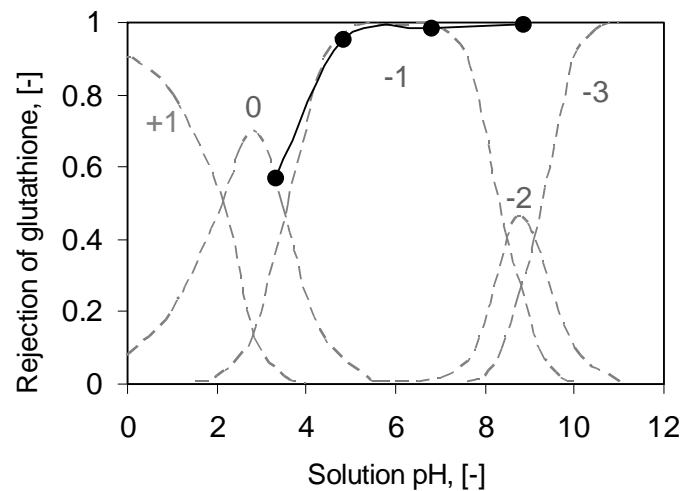
Figure 3.6. Rejection of glutathione (200 ppm) as affected by solution pH by membrane C with rp=0.46nm.

In this section, nanofiltration rejection of glutathione by membrane C with r_p= 0.46 nm was performed at 10 bar. As illustrated in Figure 3.6, more than 99.5% glutathione is rejected above pH 4.5. At pH values around the pI (2.12~3.59), the rejection of glutathione (~57.1%) is slightly higher than that of saccharose (~50.6%) which has almost the same molecular weight with glutathione. These results confirm that solution pH has the dominant effect on the separation of glutathione because pH determines the ionization states of the glutathione molecules and surface charge characteristics of the PAI membranes. The rejection of glutathione is also dependent on the pore size (steric exclusion) and the electrostatic interaction between solutes and membrane.

3.4 Conclusions

The Torlon® PAI NF membranes show higher rejections to divalent anions, lower rejections to monovalent ions, and the lowest rejections to divalent anions, which is in accordance with the Donnan exclusion. Zeta-potential measurements indicate that the isoelectric point of Torlon® PAI membrane is pH 3.2, above which the membrane is negatively charged. During treating the binary NaCl/Na$_2$SO$_4$ mixture solution, the negative rejection of Cl$^-$ and high rejection of SO$_4^{2-}$ was observed. Thus, these two ions can be effectively fractionated in their mixtures.

A greater than 99.5% rejection of glutathione molecules was obtained using the newly-developed Torlon® PAI NF hollow fiber membrane on appropriate adjustment of the feed solution pH. Therefore, based on the interaction between the charged membrane surface and the ionized glutathione molecules under different pH conditions, these new membranes hold great potential for the effective recovery, concentration and purification of glutathione and like molecules from aqueous solution containing lower molecular weight impurities.

CHAPTER FOUR

FABRICATION OF POLYAMIDE-IMIDE/CELLULOSE ACETATE DUAL-LAYER HOLLOW FIBER MEMBRANES FOR NANOFILTRATION

4.1 Introduction

As discussed in Chapter One, most conventional NF membranes are fabricated in two types. One type is the wholly integrated asymmetric membrane which is generally formed by phase inversion of cellulose acetate or other common polymers [6, 43]. The advantages of this kind of membrane include easy fabrication and low cost while the disadvantages are the limited flux and limited rejection. The other type is TFC membrane which consists of a thick, porous, nonselective support layer covered by an ultrathin barrier layer, and is prepared by interfacial polymerization, coating or chemical modification [44-46]. By adjusting various processing parameters, a tailor-made membrane is possible that provides a higher flux and rejection compared to the asymmetric membrane. However, the production of high flux TFC membranes for NF applications is not trivial.

The co-extrusion method is a technological breakthrough in membrane fabrication that makes it possible to prepare composite hollow fiber membranes in one step [93]. It allows the use of two different polymers to form a dual-layer hollow fiber membrane. The inner layer is usually porous and serves as a mechanical support for the selective outer layer, while the outer layer made from a high performance polymer may be asymmetric but contains a selective dense skin layer. Dual-layer hollow fiber membranes prepared by the co-extrusion technique retain all the advantages of conventional single-layer hollow fiber membranes: (1)

high membrane area per unit membrane module volume, resulting in a higher productivity; (2) self-mechanical support, allowing the membrane to be back-flushed for liquid separation; and (3) good flexibility and ease of handling during module fabrication and system operation [94, 95]. Furthermore, dual-layer hollow fiber membranes are more attractive than traditional hollow fiber membranes because it has the advantages of (1) significantly reducing material costs; (2) eliminating the complex post-treatment process because it is a one-step fabrication; (3) maximizing membrane performance by using a functional material of high performance as the selective layer [93].

Nevertheless, research on the fabrication of dual-layer hollow fiber membranes is still under-developed. Since the first attempt by Du Pont in 1992 [96], most of the researchers have focused on morphological studies [97-99], and applications in gas separation [100-105], membrane distillation [106, 107], pervaporation [77, 108, 109] and ultrafiltration [110]. Wessling and his co-workers first produced NF membranes by employing the dual-layer hollow fiber spinning technique [111]. They used sulfonated polyethersulfone (SPES) as the outer layer and polysulfone (PSf) as the inner layer. By increasing the outer dope concentration, they obtained dual-layer hollow fiber membranes with good adhesion between the two layers. However, the NF performance of the dual-layer hollow fiber membrane was inferior to that of the single layer asymmetric membranes. This was possibly due to the lack of comprehensive knowledge that available to bridge the fabrication conditions and their influence on the NF performance of the resultant dual-layer hollow fiber membranes. Therefore, it is our purpose to conduct a systematic study on the molecular engineering and design of dual-layer hollow fiber membranes in terms of their pore size, pore size distribution and pure water permeability as a function of spinning conditions. Such a study may be useful

in developing tailor-made high-performance NF membranes for various industrial applications.

In this chapter, Torlon® 4000TF polyamide-imide (PAI), as shown in Figure 1.4, was adopted as the outer layer material not only because of its superior mechanical properties, high thermal stability and solvent resistance, but also due to the charge characteristics introduced by the amide group in the polymer chains. In Chapter 2 and 3, we developed Torlon® hollow fibers with good NF performance, which stimulated our interest to further explore whether this high performance material can be employed in the fabrication of dual-layer hollow fiber membranes with conventional polymers. Cellulose acetate (CA) as shown in Figure 4.1, was chosen as the inner supporting layer because of: (1) its highly porous structure providing low transport resistance; (2) its inherent fouling resistance due to high hydrophilicity; and (3) its reasonable low price and ready availability. As a result, the combination of Torlon® and CA may take advantages of the strengths of both materials, while significantly lowering the material cost of the dual-layer hollow fiber membranes [94, 112].
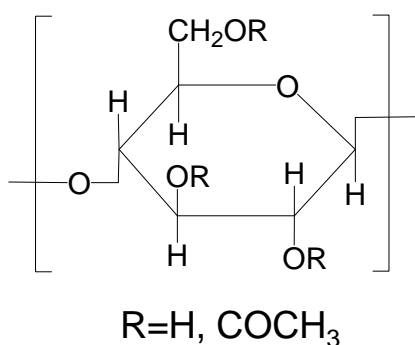
Figure 4.1. The chemical structures of cellulose acetate (CA-398-30).

Therefore, the objectives of this chapter are: (1) to fabricate PAI/CA dual-layer hollow fiber membranes for nanofiltration; (2) to molecularly engineer membrane structure for enhanced

NF performance by investigating various controlling parameters such as dope additives and spinneret temperature; and (3) to fundamentally understand the correlation between the NF performance and the morphological evolution at a molecular level.

4.2 Experimental

4.2.1 Materials

Torlon$^®$ 4000TF polyamide-imide was purchased from Solvay Advanced Polymers. Cellulose acetate (CA-389-30) was purchased from Eastman Chemical Company, USA. N-methyl-2-pyrrolidinone (NMP) was purchased from Merck and used as the solvent for the spinning solution. Methanol, ethanol, 2-propanol (IPA) were used as non-solvent additives in the polymer dope. Several uncharged neutral solutes of glucose, saccharose, raffinose, and α-cyclodextrin (Sigma-Aldrich, USA) were utilized to characterize membrane structure parameters. Molecular weights, diffusivities and Stokes radii of neutral solutes are listed in Table 2.1 [63]. Several analytical-grade salts, i.e. NaCl, $MgCl_2$, $MgSO_4$, and Na_2SO_4 (Merck, Germany) were used to characterize the charge properties of the membranes. Magnesium perchlorate, Mg $(ClO_4)_2$, was purchased from (Sigma-Aldrich, USA). All the chemicals were used as received.

4.2.2 Preparation and characterization of polymer dope solutions

The polymer concentrations of the outer dope and the inner dope were chosen as 27 wt% and 16 wt%, respectively, close to the critical concentration (26 wt% and 18 wt%, respectively)

required to form a macrovoid-free morphology [56, 78]. The detailed dope compositions are presented in Tables 4.1. The dried PAI and CA powders were dissolved in NMP at 70 °C and room temperature respectively. Both dopes were stirred for 24 hours to form homogeneous polymer solutions, which were then set aside for 2 days to eliminate air bubbles that may have been trapped in the solutions.

In order to investigate the effects of non-solvent additives on the NF performance, 10 wt% of methanol, ethanol or IPA was added into the outer dope respectively, as listed in Table 4.1. Each inner dope contained the same non-solvent as that in the outer dope to avoid additional complexities during the comparison. To prepare a dope for the outer layer with non-solvent additives, the homogenous PAI/NMP solution was allowed to cool to ambient temperature before slowly adding the non-solvent. The cooling was to prevent the evaporation of the non-solvents, i.e. methanol, ethanol and 2-propanol. 1.5 wt% $Mg(ClO_4)_2$ was added into the inner dope and served as a pore former in order to reduce substructure resistance [113, 114].

The rheological properties of the dope solutions were determined with an ARES Rheometric Scientific rheometer using a 25mm cone-and-plate fixture at room temperature. The ternary phase diagrams of various dope formulations were investigated using cloud-point experiments by water titration.

Table 4.1. The dope compositions of PAI/CA dual-layer hollow fiber membranes.

ID	Outer layer composition	Outer layer concentration (wt%)	Dope viscosity (cp)[a]	Inner layer composition	Inner layer concentration (wt%)	Dope viscosity (cp)[a]
Effects of inner dope additives						
DL1				CA/NMP	16/76	25230
DL2				CA/NMP/Water/Mg(ClO$_4$)$_2$	16/67.5/15/1.5	30420
DL3	PAI/NMP	27/73	14250	CA/NMP/Methanol/Mg(ClO$_4$)$_2$	16/67.5/15/1.5	12510
DL4				CA/NMP/Ethanol/Mg(ClO$_4$)$_2$	16/67.5/15/1.5	15450
DL5				CA/NMP/IPA/Mg(ClO$_4$)$_2$	16/67.5/15/1.5	22180
Effects of outer dope additives						
DL6	PAI/NMP/Methanol	27/63/10	14470	CA/NMP/Methanol/Mg(ClO$_4$)$_2$	16/67.5/15/1.5	-
DL7	PAI/NMP/Ethanol	27/63/10	17750	CA/NMP/Ethanol/Mg(ClO$_4$)$_2$	16/67.5/15/1.5	-
DL8	PAI/NMP/IPA	27/63/10	29170	CA/NMP/IPA/Mg(ClO$_4$)$_2$	16/67.5/15/1.5	-

[a] Dope viscosity was measured at 25 °C with shear rate 10 s^{-1}.

4.2.3 Fabrication of PAI/CA NF dual-layer hollow fiber membranes

The dual-layer hollow fiber membranes were fabricated by the co-extrusion technique using a dual-layer spinneret with an indent premixing feature, as shown in Figure 4.2. The dope solution and the bore fluid were fed into the spinneret separately by three ISCO syringe pumps. The outer dope and inner dope were premixed before exiting the spinneret in order to improve the integration of two layers. After that, the dopes and the bore fluid met at the tip of the spinneret, and passed through an air gap region before entering the coagulation (water) bath. Finally, the as-spun hollow fibers were collected by a take-up drum. The detailed dope compositions and spinning conditions are summarized in Table 4.2. After spinning, the as-spun hollow fiber membranes were rinsed in a clean water bath for 3 days to remove the residual solvent. The hollow fiber membranes were then divided into two groups for post-treatments. One group was dipped in a 40 wt% glycerol aqueous solution for 2 days and dried in air at room temperature to be used in the making of membrane modules for pore size and flux measurements. The soaking of membranes in a liquid pore stabilizer such as an aqueous glycerol solution is a standard post-treatment method in industry to prevent pores from closing during drying. The other group was directly freeze dried for further morphological characterizations.
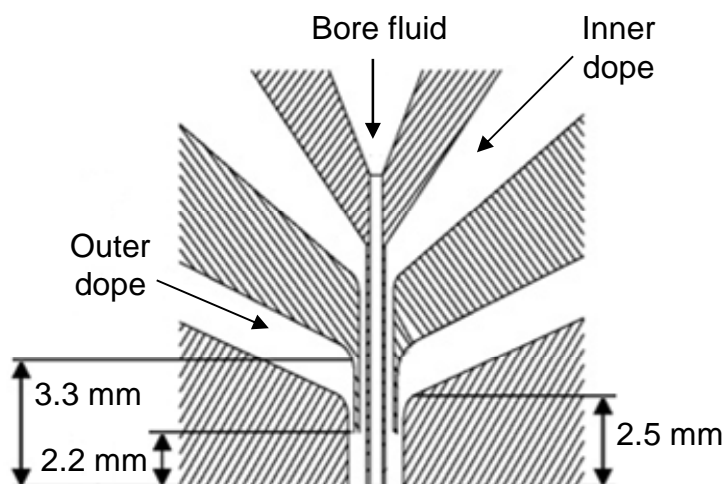
Figure 4.2. Diagram of the dual-layer spinneret with indented premixing feature.

Table 4.2. Spinning conditions of the dual layer hollow fiber membranes.

Bore fluid composition (wt%):	NMP/Water=70/30
External coagulant:	Water
Outer dope flow rate (ml/min)	0.5
Inner dope flow rate (ml/min)	3.0
Bore fluid flow rate (ml/min)	1.5
Air Gap (cm)	2.5
Take-up speed (m/min)	15
Spinneret dimension (mm):	0.84/1.0/1.58/1.74/2.0
Spinneret temperature (°C):	25 (DL8), 50 (DL9)

4.2.4 Characterization of PAI/CA NF dual-layer hollow fiber membranes

4.2.4.1 Morphology

The morphology of the dual-layer hollow fiber membranes was observed by a field emission scanning electron microscope (FESEM JEOL JSM-6700F). Before observation, the freeze dried hollow fibers were immersed in liquid nitrogen, fractured and then coated with platinum using a JEOL JFC-1300 Platinum coater.

4.2.4.2 Nanofiltration experiments with PAI/CA dual-layer hollow fiber membranes

NF experiments were conducted in a lab-scale circulating filtration unit, described in Chapter 2. For each hollow fiber sample, two modules with an outer diameter of 3/8 inch were tested simultaneously to ensure good repeatability. Every module comprised 10 hollow fiber membranes with an outer diameter of around 500 μm and an effective length of around 17 cm. Since the outer surface of the hollow fibers was the selective layer, the feed solution was pumped into the shell side, while the permeate solution exited from the lumen side of the hollow fibers. A high flow rate of 1.4 l/min was applied so that the effect of concentration polarization was minimized ($Re > 4000$). Then, each membrane sample was subjected to the pure water permeation experiment at 1 bar to measure the pure water permeability, PWP ($l\ m^{-2}\ bar^{-1}\ h^{-1}$), which was calculated using the equation

$$PWP = \frac{Q}{\Delta P \cdot A} \tag{4.1}$$

where Q is the water permeation volumetric flow rate (L/h), A is the effective filtration area (m^2), and ΔP is the transmembrane pressure drop (bar).

The membranes were then characterized by solute separation experiments with several neutral organic solutes and inorganic salts. The procedures for the nanofiltration experiments were as follows:

(1) Feed solutions were prepared by dissolving neutral solutes in deionized (DI) water at a concentration of about 200 ppm. The pressure difference across the membrane and the feed temperature were kept at 1 bar and 25°C respectively for all the

experiments. The feed solutions were circulated for about 0.5 h until the system reached steady state. Both feed and permeate solutions were collected to measure the concentrations.

(2) NF experiments were conducted with neutral organic solutes of progressively higher molecular weights, as listed in Table 2.1. Between runs of different solutes the membrane was flushed thoroughly with DI water. The solute separation data were further used for the estimation of mean pore size, pore size distribution and molecular weight cut-off (MWCO), which is referred to as the molecular weight above which 90 percent of the solute in the feed solution is retained by the membrane. The detailed procedure is described in Chapter 1.

(3) Different electrolyte solutions were prepared by dissolving single salts in DI water at a concentration of 0.01 mol L^{-1}. HCl (1.0M) and NaOH (1.0M) were used to adjust the solution to pH 7.0. The same experimental procedures as described in the Step (1) were employed to measure salt rejection.

Concentrations of the neutral solute solutions were measured with a total organic carbon analyzer (TOC ASI-5000A, Shimazu, Japan), while those of single electrolyte solutions were measured with an electric conductivity meter (Schott Instruments, Lab 960, Germany). The solution pH was determined using a pH meter (Horiba pH meter D-54, Japan). The apparent solute separation coefficient R_T (%) was calculated using the equation:

$$R_T(\%) = \left(1 - \frac{c_p}{c_f} \right) \times 100 \qquad (4.2)$$

where c_p and c_f are the solute concentrations in the permeate and the feed solutions, respectively.

4.3 Results and discussion

4.3.1 Effects of non-solvent additives on the overall morphology

When 27/73 wt% PAI/NMP and 16/84 wt% CA/NMP solutions were used with no non-solvent added to the dopes, severe delamination between the two layers occured, as shown in Figure 4.3 (a). No improvement in adhesion between these two layers was observed despite various attempts including changing the air-gap distance, the take-up speed, the flow rates of both dope and bore fluid, and the bore fluid composition, etc. This phenomenon maybe arise from the fact that PAI and CA are two polymers with different precipitation and shrinkage rates [98]. As shown in the ternary phase diagram, i.e. Figure 4.4, the distance between the cloud-point curve of CA/NMP solution (Figure 4.4 (a)) to the polymer/solvent axis is much larger than that of PAI/NMP (Figure 4.4 (b)). Therefore, the outer layer solidifies more quickly than the inner layer. Since the outer layer has a higher polymer concentration and faster precipitation rate than the inner layer, the outer layer has a larger diameter with less shrinkage than the inner layer, and thus delamination occurs. In addition, after the external coagulant (water) has passed through the thin outer layer (about 10 μm), a large amount of water might accumulate inside the gap between the outer and inner layers [98, 99].

Figure 4.3. Effects of non-solvent additives on the delamination of the dual-layer hollow fiber membranes (Scale bar 50μm). (a) DL1 (Outer layer: PAI/NMP:27/73; inner layer: CA/NMP:16/84); (b) DL2 to DL5 (Outer layer: PAI/NMP:27/73; inner layer: CA/NMP/additive/Mg(ClO$_4$)$_2$=16/67.5/15/1.5); (c) DL6 to DL8 (Outer layer: PAI/NMP/additive:27/63/10; inner layer: CA/NMP/additive/Mg(ClO$_4$)$_2$=16/67.5/15/1.5).

The situation was improved by adding 15 wt% non-solvent additives (DL2 to DL5) into the inner dope solutions, as demonstrated in Figure 4.3 (b). The addition of non-solvents brought the cloud-point curve of the CA/NMP solution much closer to the polymer-solvent axis. A more rapid precipitation was induced from the inner lumen skin and through the inner layer by a 70/30 NMP/water bore fluid solution. As a result, the outer diameter of the inner layer increased, greatly reducing the gap between the two layers [100, 115]. However, the interfacial gap was still not fully eliminated.

The inter-layer diffusion can be facilitated by increasing the spinneret temperature [102] or delaying the time for the external coagulant (i.e., water) to reach the interface [111]. However, the water flux of the resultant membrane may be sacrificed because of the formation of a dense interfacial layer due to demixing of dope compositions between the two layers or the formation of a dense outer surface due to rapid solvent evaporation at high spinneret temperatures.
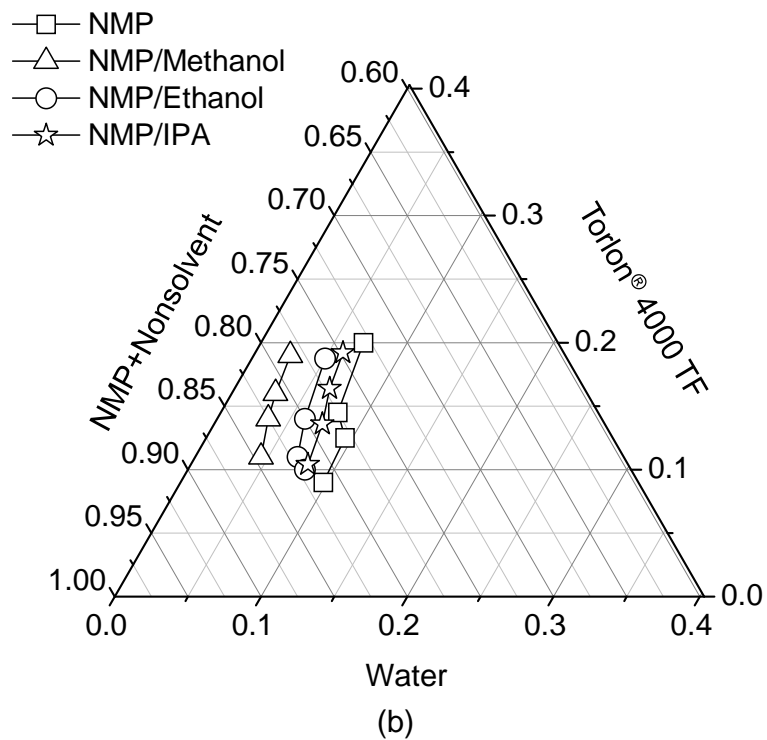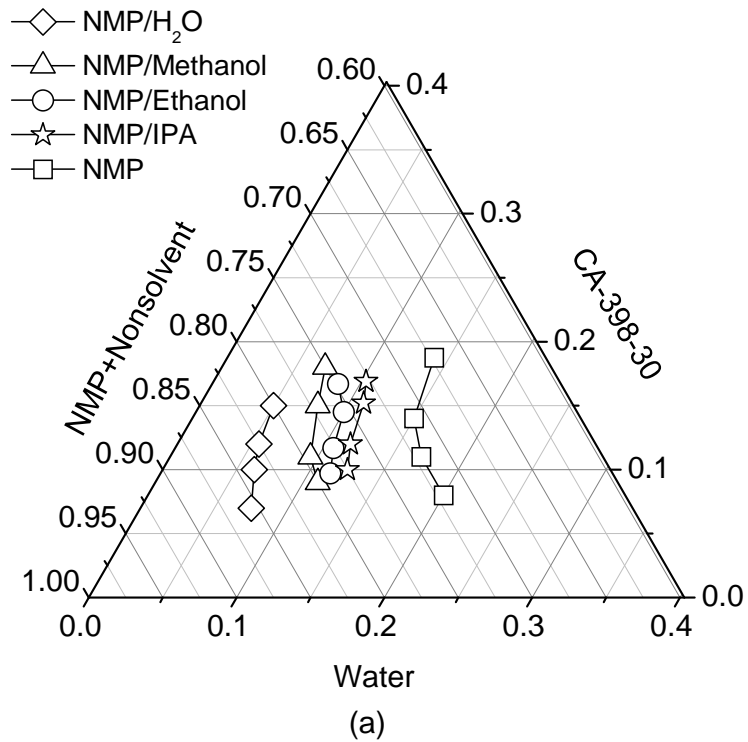
Figure 4.4. Phase diagrams for (a) CA/NMP+nonsolvent/Mg(ClO$_4$)$_2$/Water; (b) Torlon® 4000TF/NMP+nonsolvent/Water system.

In our study, we developed a different method by adding 10 wt% non-solvents to the outer dope solution. Compared to the dual-layer hollow fiber spun with pure

PAI/NMP solution, the attachment of both layers is superior with no obvious delamination observed by optical microscopy, as shown in Figure 4.3 (c). Based on the above findings, we propose that two factors may play an important role in eliminating the delamination; namely, the enhanced precipitation rate of the inner layer and the enhanced viscosity of the outer layer. The former results in a large diameter of the inner layer and reduces the gap between the inner and outer layers, while the latter retards the water diffusion across the outer layer so that significant inter-layer diffusion may occur and eliminate the gap. Table 4.1 reveals that the dope viscosity is increased when non-solvents, especially IPA, are added to the outer dope. It is worthy to note that the measured viscosity of the PAI/NMP/methanol dope solution (DL6) is not significantly higher than that of the PAI/NMP dope solution (DL3). However, due to its high volatility, the methanol would vaporize quickly in the air gap region during the hollow fiber spinning process, and thus the real viscosity of DL6 would be much higher than that of DL3.

The typical morphology of PAI/CA dual-layer hollow fiber membranes spun from sample DL8 (PAI/NMP/IPA=27/63/10 wt %) is shown in Figures 4.5 and 4.6. The cross-section FESEM image demonstrates that the outer and inner layers are interconnected although there is a clear boundary between them. Such a cross-section structure is quite desirable since it does not contribute significant transport resistance while it still ensures retention of good mechanical strength. Both the outer layer and the inner layer have asymmetric structures. There exists a dense and nodule-like selective layer at the outer edge of the outer layer. The thickness of the dense selective layer is approximately 170nm, as estimated from the FESEM image at a high magnification (×100,000). The inner support layer is macrovoid free and fully porous,

indicating CA is a good candidate as the support for dual-layer hollow fiber membranes. The effects of non-solvent additives on the micro-scale morphology of dual-layer hollow fiber membranes, which is closely related to the NF performance, will be discussed in detail in the following section.
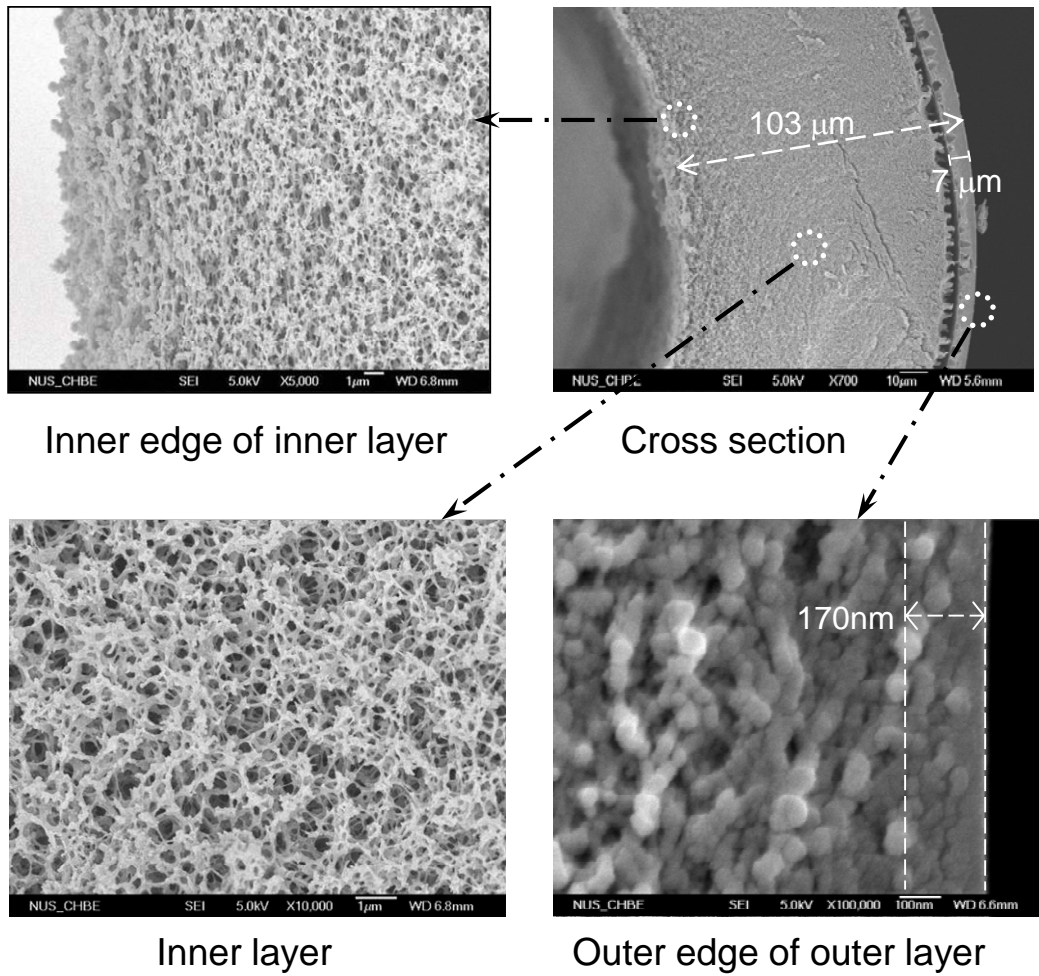
Figure 4.5. Cross section images of the dual-layer hollow fiber membranes. Outer dope: PAI/NMP/IPA=27/63/10 wt%, Inner dope: CA/NMP/IPA/Mg(ClO$_4$)$_2$=16/67.5/15/1.5.
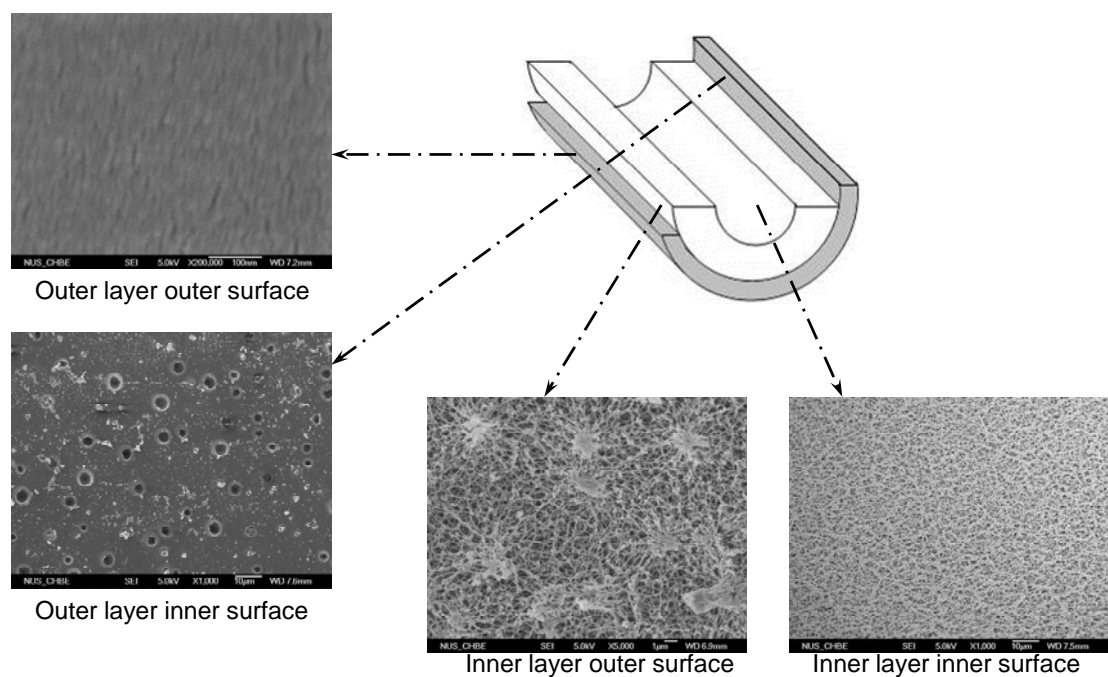
Figure 4.6. FESEM images of the different surfaces of the dual-layer hollow fiber membranes. Outer dope: PAI/NMP/IPA=27/63/10 wt%, Inner dope: CA/NMP/IPA/Mg(ClO$_4$)$_2$=16/67.5/15/1.5.

4.3.2 Effects of non-solvent additives on NF performance

4.3.2.1 Effects of non-solvent additives on pure water permeability, pore size, pore size distribution and molecular weight cutoff

In order to understand the effects of non-solvent additives on the NF performance, the newly developed PAI/CA NF dual-layer hollow fiber membranes were characterized by the solute transport method, as described in the experimental section, to obtain the mean effective pore size, pore size distribution and MWCO. The relationship between solute rejection and solute Stokes radius is shown on the log-normal probability graph in Figure 4.7. Linear relationships are obtained with reasonably high correlation coefficients ($r^2 > 0.95$). It is observed that the non-solvent additives have a significant influence on the NF performance of the dual-layer hollow fiber membranes. As shown in Figure 4.7, the solute rejection of membranes containing different non-solvent additives follows the order of methanol>ethanol>IPA. The difference is not so

obvious for low molecular solute rejection such as glucose, but such difference becomes greater for larger solutes, i.e. sucrose, raffinose and α-cyclodextrin.
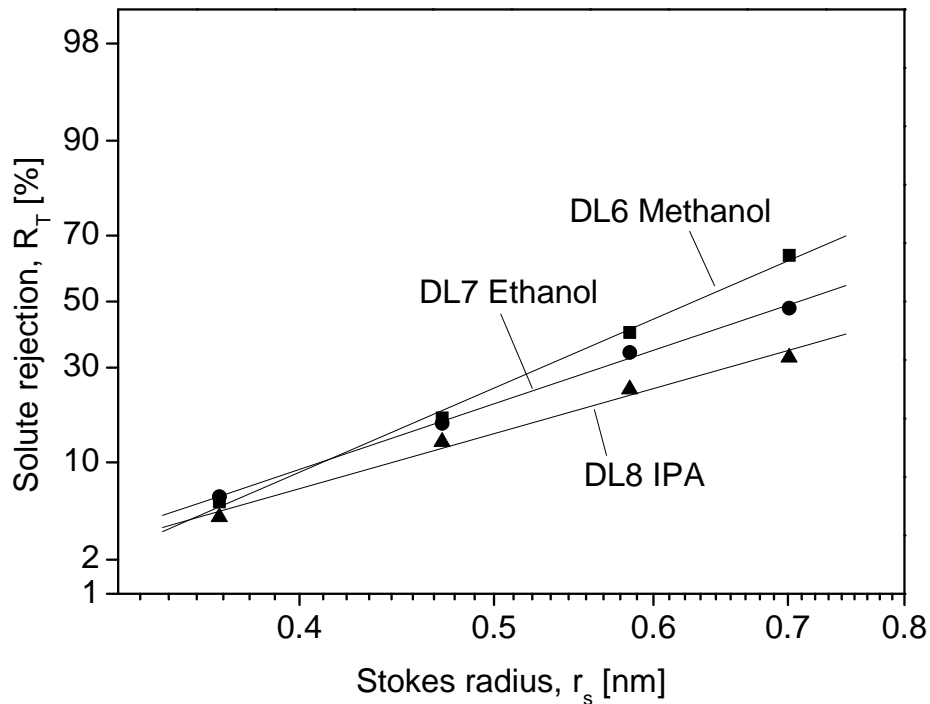
Figure 4.7. Log-normal probability plots of the effective rejection curves (solute rejections vs. their Stokes radii) for dual-layer hollow fiber membranes spun with different non-solvent additives.

In order to further analyze the structure change of the selective layer, the mean effective pore radius r_p at $R_T = 50\%$, the MWCO and the geometric standard deviation σ_p were calculated from Figure 4.7. The data are summarized in Table 4.3. The pure water permeabilities, which were obtained from Eq. (4.1), of hollow fiber membranes spun with different non-solvent additives, are also listed in Table 4.3. The cumulative pore size distribution curves and probability density function curves of PAI/CA dual-layer hollow fiber membranes calculated from the solute transport method are depicted in Figures 4.8 (a) and (b), respectively.

Table 4.3. Mean effective pore radius (r_p), geometric standard deviation (σ_p), molecular weight cut off (MWCO), and pure water permeability (PWP) of dual-layer NF hollow fiber membranes spun with different non-solvent additives.

ID	Non-solvent additive	r_p (nm)	σ_p	MWCO (Da)	PWP ($\mathrm{lm^{-2}bar^{-1}h^{-1}}$)
DL6	Methanol	0.63	1.38	1910	11.93
DL7	Ethanol	0.71	1.54	3694	7.43
DL8	IPA	0.85	1.69	8175	5.51

From Table 4.3 and Figure 4.8, it can be clearly seen that both pore size and MWCO of the membranes follow the order of IPA>ethanol>methanol. The pore size distribution shifts towards the left and becomes narrower when the non-solvent additive is changed from IPA to ethanol to methanol. Furthermore, Table 4.3 shows that different non-solvent additives also have tremendous influence on the pure water permeability of dual-layer hollow fiber membranes. Interestingly, the order of pure water permeability decreases in the order of methanol>ethanol>IPA, which is contrary to that of pore size. This phenomenon possibly arises from the following reasons:
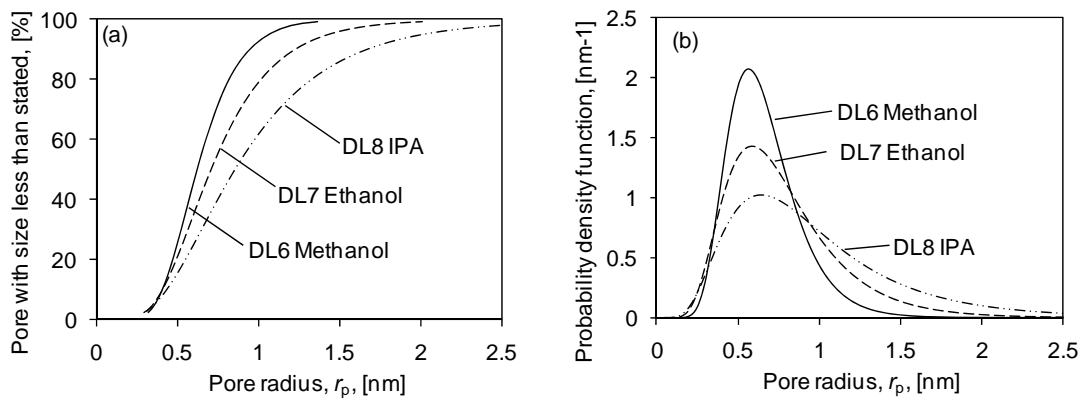
Figure 4.8. (a) Cumulative pore size distribution curves and (b) probability density function curves for the dual-layer NF hollow-fiber membranes spun with different non-solvent additives.

(1) Table 4.4 compares the properties of various non-solvent additives used in this research [116, 117]. The solubility parameter difference between additive and water increases in the order of methanol<ethanol<IPA while the difference between additive and NMP is reversed. A smaller solubility parameter difference usually implies a better mutual compatibility [118]. Meanwhile, the molecular volume of the additives also follows the order of methanol<ethanol<IPA. Therefore, methanol has the highest mass exchange rate with water at the precipitation front, followed by ethanol and IPA. Due to these factors, the nodules in the skin layer were smaller and more closely packed when methanol was introduced as the additive, compared to ethanol and IPA. A denser but thinner selective layer is formed, as shown in the FESEM image (Figure 4.9 (a)) at a high magnification ($\times$100,000). The denser packing ensures a higher rejection for large solutes, while the thinner selective layer results in a reduced transport resistance that allows for the enhanced water flux. We have observed a similar structure induced by external stretching of hollow fiber membranes under high take-up speeds [119].

Table 4.4. Properties of solvent and non-solvents.

	Molecular volume (Å^3)	Boiling point at 1 atm (°C)	Vapor pressure (mmHg at 20 °C)	Specific gravity	Viscosity (cP)	δ_t $(\text{J/cm}^3)^{1/2}$
Water	30	100	17.5	1.00	1.00	47.80
Methanol	67	64.5	96	0.792	0.60	29.60
Ethanol	97	78	43.9	0.789	1.22	26.50
IPA	127	82	33	0.790	2.40	23.50
NMP	160	202	-	1.026	1.65	22.90

Figure 4.9. Effects of non-solvent additives on the cross section of the dual-layer hollow fiber membranes. (a) Outer edge of the outer layer; (b) the interface between the outer layer and inner layer.

(2) It is interesting to observe that the addition of methanol results in many macrovoids in the outer layer while those with added ethanol and IPA lead to almost macrovoid-free structure (Figure 4.9 (b)). The interpenetration of the polymer chains between the outer and inner layers for the methanol-added membrane (the high magnification image at the left lower corner of Figure 4.9 (b)) is not as intimate or sophisticated as the latter two. However, the former membrane has a more porous inner surface of the outer layer than the latter two (Figure 4.10 (b)). Furthermore, the substructure immediately beneath the outer dense layer of the former is much more porous than the latter. The high porosity in the inner surface of the outer layer and the highly porous substructure are essential for the functioning of the dual-layer NF membranes with high water fluxes. Such morphological evolution can be attributed to the different physicochemical properties of the additives, coagulation paths and rheological properties of dope solutions. According to the phase diagram in Figure 4.4,

the dope containing methanol is much closer to the polymer-solvent axis than that containing ethanol and IPA. Due to extra phase instability, the dope added with methanol tends to experience instantaneous liquid–liquid demixing which may lead to small nodules and the formation of macrovoids [98]. Since the viscosity of dopes containing various additives increases in the order of methanol<ethanol<IPA, the water intrusion during coagulation was retarded when ethanol and IPA were introduced into the outer dope, possibly due to enhanced polymer chain entanglement [120]. As a consequence of the aforementioned factors, the interlayer adhesion is enhanced in the order of methanol<ethanol<IPA, while the substructure resistance is increased in the same order, which results in a decreased water permeation flux.
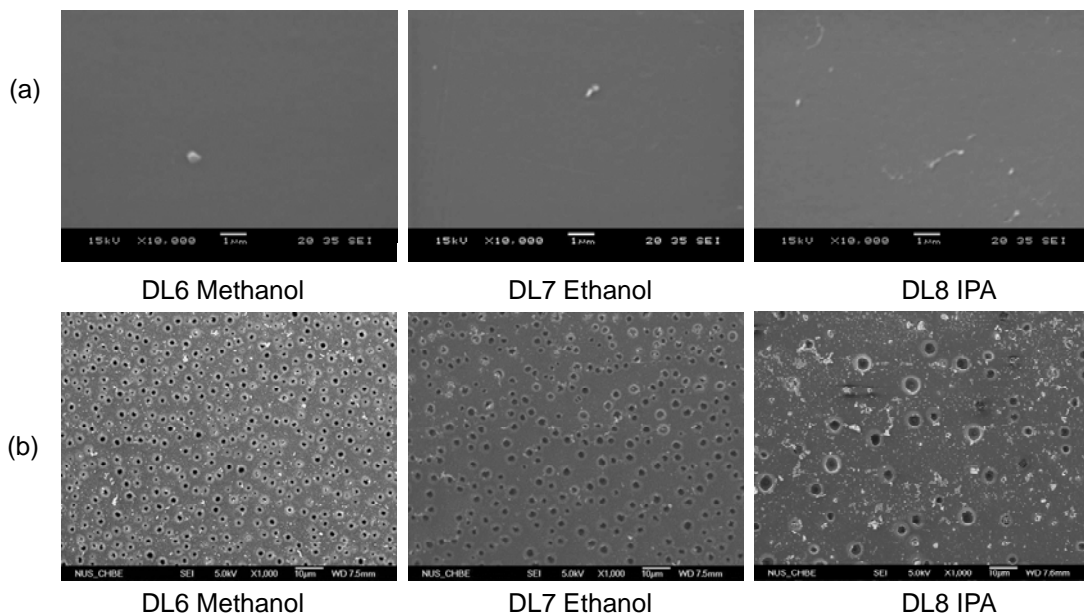
Figure 4.10. Effects of non-solvent additives on the surfaces of the dual-layer hollow fiber membranes. (a) The outer surface of the outer layer; (b) The inner surface of the outer layer.

As a result of these synergistic effects, the dual-layer hollow fiber membrane with methanol as an additive possesses better NF performance than those containing ethanol and IPA. The resultant NF membrane has a relatively higher pure water

permeability of 11.93 l m^{-2}bar^{-1}h^{-1} with a mean effective pore radius of 0.63 nm. Clearly, we have demonstrated that, by appropriately selecting non-solvent additives in both inner and outer layers without changing other spinning conditions, we can develop tailor-made NF dual-layer hollow fiber membranes with a smaller pore size but a higher pure water permeability.

4.3.2.2 Effects of non-solvent additives on salt rejection

In our previous work, we conducted a systematic characterization of the charge properties of Torlon$^{®}$ PAI NF membranes and proved that the isoelectric point of Torlon$^{®}$ PAI membranes is approximately 3.2 [119]. The membrane is slightly positively charged below this value and is negatively charged above it. Therefore, the NF hollow fiber membranes may show different rejections for anions and cations with different valences. In the current work, the rejections of four kinds of electrolytes were tested at the same molar concentration (0.01 mol L^{-1}), pH (7.0) and pressure (1 bar). As shown in Figure 4.11, the salt rejections of membranes containing different types of non-solvent additives follow the order of methanol>ethanol>IPA, which is similar to the trend of the neutral solutes tested in the previous section. For each type of membrane, the rejection of these salts decreases in the order $R(Na_2SO_4) > R(MgSO_4) > R(NaCl) > R(MgCl_2)$. In other words, the membranes show a higher rejection of divalent anions with higher co-ion charge than monovalent anions, and a lower rejection of divalent cations with higher counter-ion charge, corresponding to the Donnan exclusion principle [89].
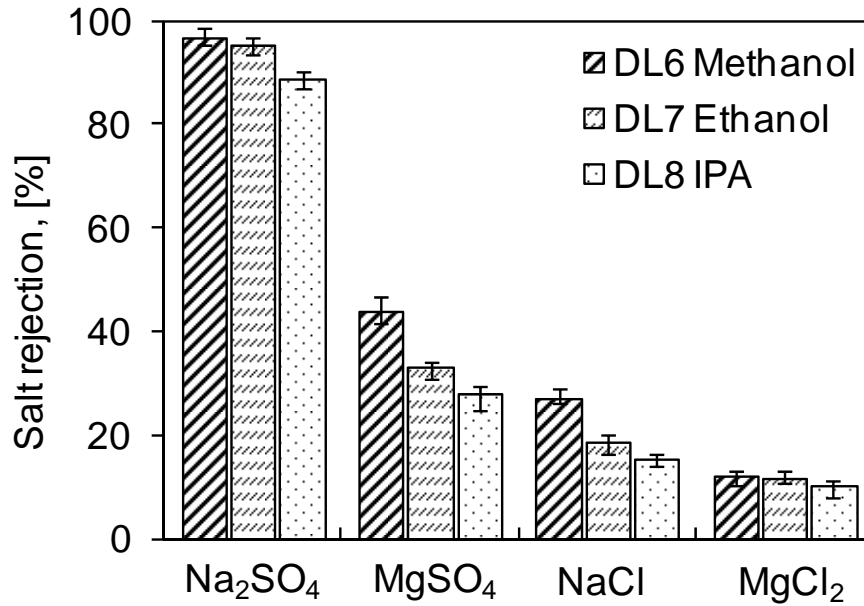
Figure 4.11. Effects of non-solvent additives on the rejections of different single salts.

4.3.3 Effects of spinneret temperature on NF performance

Figures 4.12 and 4.13 present the effects of spinneret temperature on the rejections of neutral solutes and electrolytes, respectively. The rejections by the dual-layer hollow fiber membrane spun at 50°C are obviously higher than by that spun at 25°C. From the solute transport method described in the previous section, the mean pore size and MWCO were obtained from Figure 4.12 and are summarized in Table 4.5 together with the pure water permeability. Clearly, the NF performance of the dual-layer hollow fiber membranes is very sensitive to the spinneret temperature. As the spinneret temperature was increased from 25°C to 50°C, the mean pore radius and MWCO were reduced from 0.85 nm to 0.50 nm and from 8175 to 1115 Dalton, respectively. The membrane spun at 50°C has a much steeper and narrower pore size distribution, as shown in Figure 4.14. Meanwhile, compared to membranes spun at room temperature, the pure water permeability of the dual-layer hollow fiber

membranes spun at 50°C becomes lower (Table 4.5). The significant influence of spinneret temperature on solute rejection and pure water permeability can be explained by the morphology changes in the two regions, i.e. the selective skin layer and the interface between the two layers of the dual-layer hollow fiber membranes, both of which are shown in Figure 4.15.
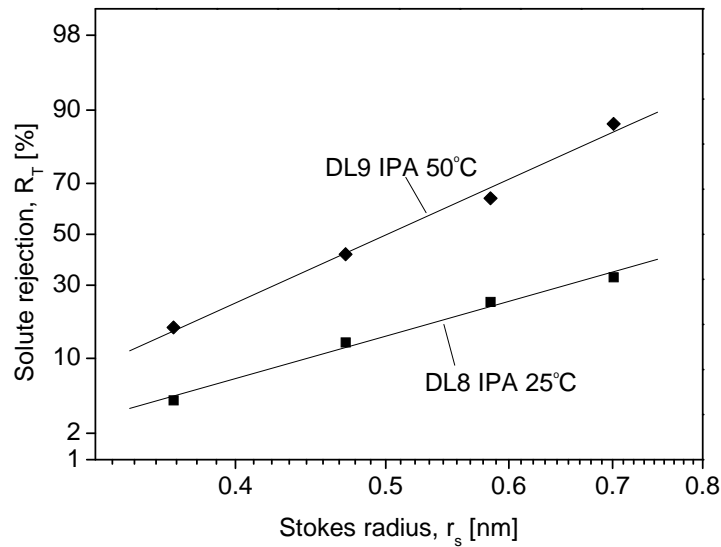
Figure 4.12. Log-normal probability plots of the effective rejection curves (solute rejections vs. their Stokes radii) for dual-layer hollow fiber membranes spun at different spinneret temperatures.
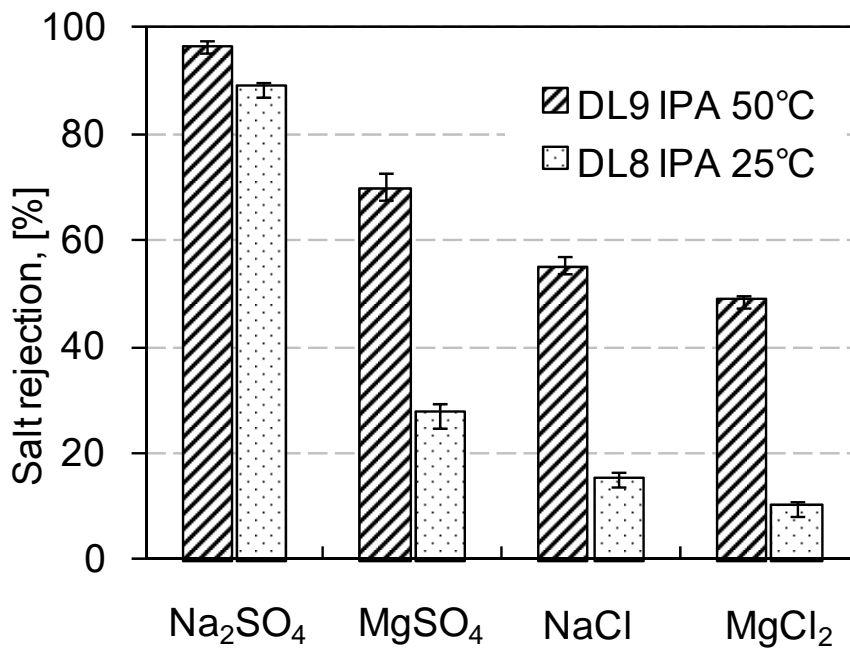
Figure 4.13. Effects of spinneret temperature on the rejections of different single salts.

Table 4.5. Mean effective pore radius (r_p), geometric standard deviation (σ_p), molecular weight cut off (MWCO), and pure water permeability (PWP) of dual layer NF hollow fiber membranes spun at different spinneret temperature.

ID	Spinneret temperature (°C)	r_p (nm)	σ_p (-)	MWCO (Da)	PWP ($lm^{-2}bar^{-1}h^{-1}$)
DL8	25	0.85	1.69	8175	5.51
DL9	50	0.50	1.40	1115	1.98

Firstly, it is widely accepted that the selective skin layer is formed as a result of a phase inversion process across the nascent hollow fiber with a concentration gradient. The local polymer concentration near the outermost region of a nascent membrane is higher than that of the bulk solution [121]. In this study, IPA, which was employed here as the non-solvent additive, is a volatile alcohol, as indicated in Table 4.4. When the spinneret temperature increases from 25°C to 50°C, it evaporates more quickly from the dope solution in the air gap region. Therefore, the polymer concentration in the outermost region becomes higher, which results in a less defective but thicker dense selective skin. Similar phenomena have been reported in our earlier work on single-layer hollow fiber membrane formation [120].
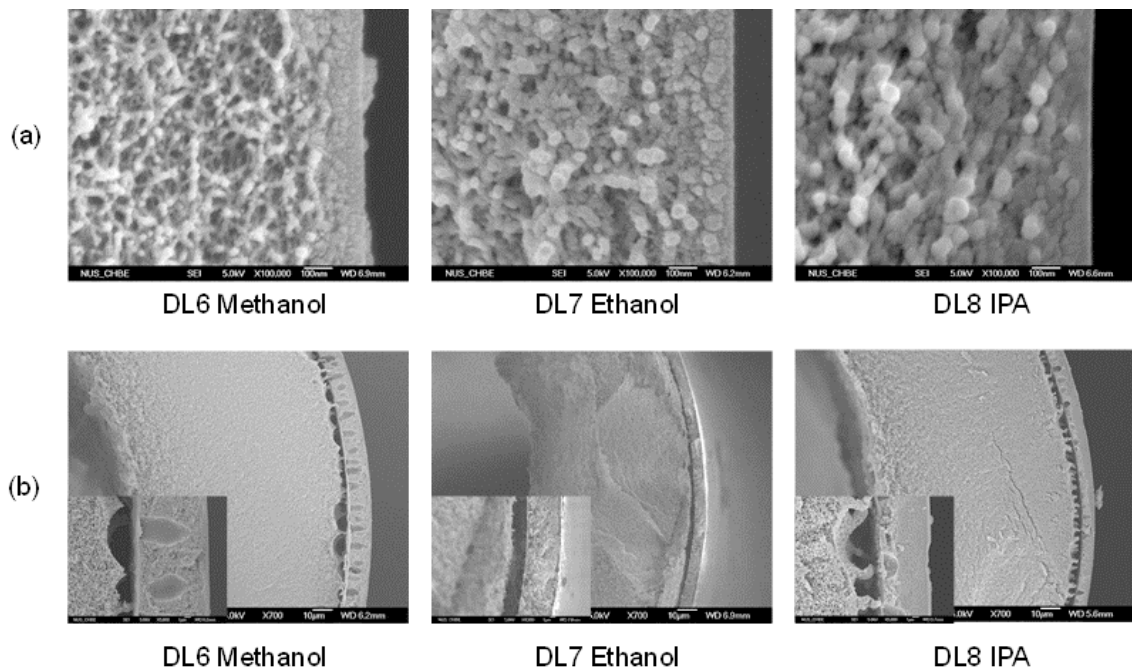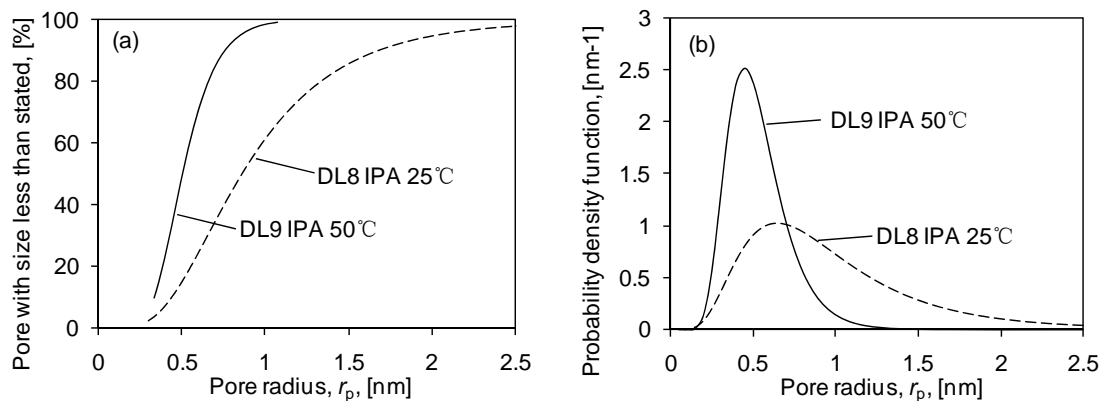

Figure 4.14. (a) Cumulative pore size distribution curves and (b) probability density function curves for the dual-layer NF hollow-fiber membranes spun at different temperature.

Secondly, the fabrication process for the dual-layer hollow fiber membrane is more complex than for the single-layer one. One reason is that the interface between the two layers may also serve as a barrier in addition to the outer selective layer [102]. In the current work, when the dual-layer hollow fiber membrane is spun at 25°C, the two layers are loosely connected to each other, as shown in Figure 4.15. However, when the spinneret temperature is increased to 50°C, the inter-layer diffusion is facilitated because of lower dope viscosities and higher molecular diffusion rates. As a result, a more compact interface is formed which creates higher resistance for both water and organic compounds to pass through. When spun at 50°C, we can obtain a NF membrane with a mean effective radius of 0.50 nm and a pure water permeability of 1.98 $lm^{-2}bar^{-1}h^{-1}$. A high rejection of Na_2SO_4 was achieved at more than 96.9%.
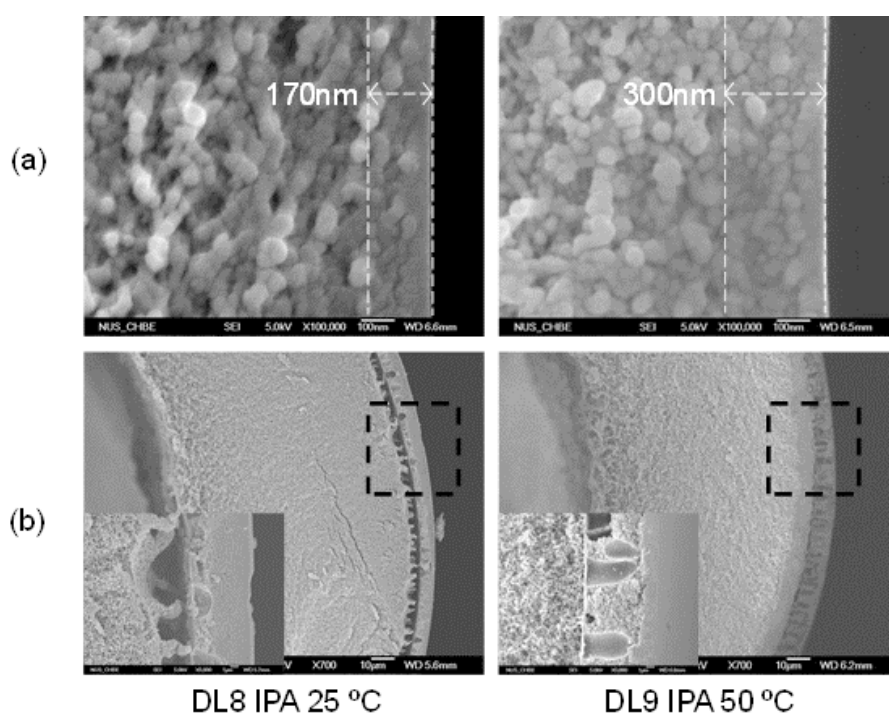
Figure 4.15. Effects of spinneret temperature on the morphology of dual-layer hollow fiber membranes. (a) outer edge of the outer layer; (b) the interface between the outer layer and inner layer.

4.4 Conclusions

Through co-extruding two polymer dopes from a triple-orifice spinneret, dual-layer composite nanofiltration hollow fiber membranes have been fabricated. Non-solvent additives and spinneret temperature are crucial parameters which influence the resultant morphology and the NF performance of PAI/CA dual-layer hollow fiber membranes. The following conclusions can be drawn from this study:

(1) In order to obtain a delamination-free structure for PAI/CA dual-layer hollow fiber membrane, the thermodynamic and kinetic properties of both spinning dopes should be considered. By adding non-solvents into the inner dope, more rapid precipitation of the inner layer can be induced, which may reduce the gap between the two layers. By introducing volatile non-solvents, such as methanol, ethanol and IPA, into the outer dope, water intrusion is hindered by the increased viscosity. Thus, a delamination-free dual-layer hollow fiber can be obtained.

(2) The addition of different non-solvents has significant influence on the NF performance of the resultant dual-layer hollow fibers. When methanol, ethanol and IPA are added into the outer dope, the pure water permeability is improved in the order of IPA<ethanol<methanol while reduced pore radius is obtained in the order of IPA>ethanol>methanol. FESEM reveals that a strong non-solvent, like methanol, may facilitate the mass exchange with the external coagulant and produce a thinner but more closely packed nodule-like selective layer which may form smaller pore sizes but reduced substructure resistance. However, outer dopes containing a weak non-

solvent, like IPA, favor delayed mixing which forms a thicker dense layer and macrovoid-free and delamination-free structure.

(3) Increasing spinneret temperature can significantly enhance the solute rejection while sacrificing water flux. As demonstrated in FESEM images, a denser surface skin and a more compact interface between the two layers are attributed to the phenomenon.

CHAPTER FIVE

HYPERBRANCHED POLYETHYLENEIMINE INDUCED CROSS-LINKING OF POLYAMIDE-IMIDE NANOFILTRATION HOLLOW FIBER MEMBRANES FOR EFFECTIVE REMOVAL OF CIPROFLOXACIN

5.1 Introduction

As introduced in Chapter 1, NF process is promising to remove pharmaceutical active compounds from water. We choose ciprofloxacin as a model solute because this antibiotic is widely used in antibacterial treatment. Recent studies have shown that inefficient removal of this compound from discharge streams before their release into aquatic environments may not only contaminate drinking water, thus posing a risk to public health, but also inhibit photosynthesis of plants and promote the growth of antibiotic-resistant bacteria, resulting in severe ecological issues [41, 42]. Therefore, effective removal of the compound from discharge streams to the environment becomes an important issue. Because the ciprofloxacin molecule consists of one carboxylic group and three amine groups, it possesses four pK_a values, i.e. 3.01, 6.14, 8.70, and 10.58, in aqueous solution [38]. The molecule is positively charged below pH 8.70 and neutral within the range of 8.70 < pH < 10.58. It becomes negatively charged above pH 10.58, which is an extremely basic condition. In order to obtain the optimum rejection of ciprofloxacin under mild conditions, a positively charged NF membrane is necessary. However, presently most NF membranes are negatively charged, which may result in inefficient rejection and a high fouling tendency during removal of the positively charged ciprofloxacin [122]. In addition, most NF modules are made in spiral-wound configuration using flat-sheet composite membranes

generally fabricated by sophisticated fabrication steps [7]. Recently, there is a growing interest to develop novel hollow fiber membranes for NF applications such as membrane bioreactor and forward osmosis [7, 123], because hollow fiber module may provide high surface area per unit volume that reduces manufacture costs [5]. However, the knowledge to fabricate high performance NF hollow fiber membranes is still limited. Therefore, our aim is to develop a positively charged NF hollow fiber membrane for removal of ciprofloxacin with high rejection and low fouling tendency.

Polyamide-imide (PAI), commercially known as Torlon$^{®}$, was adopted as the membrane material because it has not only superior mechanical properties, which allows NF operation at high pressures, but also good chemical stability over a wide pH range, which is demonstrated in literature [49] and also shown in our work in Chapter 3. Furthermore, the carbonyl groups of imide rings in the polymer chains are able to react with amines to form amide groups. Recently, several studies have shown that cross-linking of polyimides with polyethyleneiminne (PEI) is a promising approach to prepare a positively charged membrane by introducing additional amine group on membrane surface [124-126]. However, as a polyelectrolyte, the molecular weight of PEI varies from several hundred to tens of thousands. In order to achieve the best membrane performance, how to select an appropriate PEI molecular weight becomes a crucial issue. To the best of our knowledge, no in-depth work has been reported on the effects of PEI molecular weight on the properties of NF membranes such as pore size, pore size distribution and pure water permeability, or on the rejection and fouling capacity of pharmaceutical compounds by the NF membranes. Therefore, this work also aims to understand fundamentally the effects of PEI modification on the mechanisms of ciprofloxacin removal from water. This study may

provide guidelines for developing high rejection, anti-fouling NF hollow fiber membranes for various industrial applications.

5.2 Experimental

5.2.1 Materials

Torlon® 4000T-MV polyamide-imide with the chemical structure shown in Figure 1.4 was purchased from Solvay Advanced Polymers. N-methyl-2-pyrrolidinone (NMP) and ethylene glycol (EG) were purchased from Merck and used as solvent and non-solvent, respectively, for the spinning solution. Hyperbranched polyetheleneimine (Figure 5.1) with molecular weights of 60 kg/mol (Acro, USA), 25 kg/mol and 2 kg/mol (Sigma-Aldrich, USA) were used as modification agents. Uncharged neutral solutes of glucose, saccharose, raffinose, and α-cyclodextrin (Sigma-Aldrich, USA) were utilized to characterize membrane structure parameters. Molecular weights, diffusivities and Stokes radii of neutral solutes [63] are listed in Table 2.1. Several analytical-grade salts, i.e. NaCl, $MgCl_2$, $MgSO_4$, and Na_2SO_4 (Merck, Germany) were used to characterize the charge properties of the membranes. Ciprofloxacin ($C_{17}H_{18}FN_3O_3$, MW 331.3, >98%) was purchased from Sigma-Aldrich. Cephalexin ($C_{16}H_{17}N_3O_4S \cdot H_2O$, MW 365.4, $pK_{a,1}$: 2.56, $pK_{a,2}$: 6.88; Log K_{ow}:0.076, [123]) was purchased from MP Biomedicals (Heidelberg, Germany).
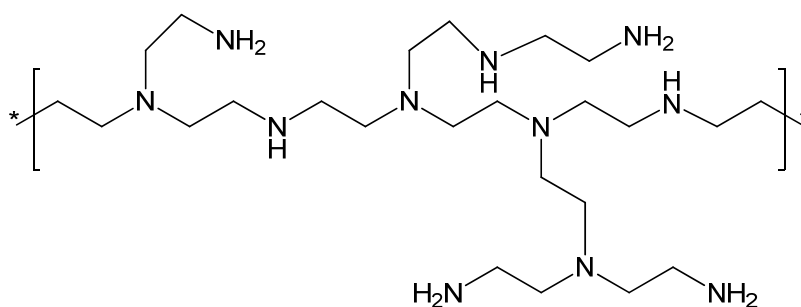
Figure 5.1. The chemical structures of hyperbranched polyethyleneimine.

5.2.2 Preparation of PAI hollow fiber membrane support

The hollow fiber membranes were prepared by the dry-jet wet-spinning process. Torlon® polymer was first dried in a vacuum oven at 120 °C overnight to remove moisture. Then, a dope solution containing 23.5wt% PAI, 13.5wt% EG and 63wt% NMP was prepared by adding the PAI polymer to a mixture of EG and NMP. The mixture was stirred in an oil bath at 70 °C for 12 hours to form a homogeneous polymer solution, which was then set aside for 1 day to eliminate air bubbles that may have been trapped in the solution. The dope solution and the bore fluid were fed into the annulus and the inner tube of the spinneret separately by two ISCO syringe pumps. After the dope and the bore fluid met at the tip of the spinneret, they passed through an air gap region before entering the coagulation (water) bath. Finally, the as-spun hollow fibers were collected by a take-up drum. The experimental setup and the spinneret are described in Figure 2.1. The detailed spinning conditions for the PAI NF hollow fiber membranes are listed in Table 5.1. After spinning, the as-spun hollow fiber membranes were rinsed in a clean water bath for 3 days to remove the residual solvent. The hollow fiber membranes were then divided into two groups for post-treatments. One group was dipped in a 30 wt% glycerol aqueous solution for 2 days and dried in air at room temperature to be used in the making of membrane modules

for flux and rejection measurements. Every module comprised 10 hollow fiber membranes with an outer diameter of around 420 μm and an effective length of around 15 cm. The other group was directly freeze dried for further morphological characterizations.

Table 5.1. Spinning conditions of Torlon[®] PAI NF hollow fiber membranes.

Torlon[®] dope solution	(wt. %)	Torlon[®] / EG/NMP (23.5/13.5/63.0)
Dope flow rate	(ml/min)	5.0
Bore fluid composition	(wt. %)	NMP/Water (95: 5)
Bore fluid flow rate	(ml/min)	3.0
Air gap	(cm)	5
Take-up speed	(m/min)	37.5
External coagulant	(-)	Tap water, 26 ± 1 ºC
Dope temperature	(ºC)	26 ± 1
Bore fluid temperature	(ºC)	26 ± 1
Room humidity	(%)	$65 \sim 70$
Dimension of spinneret	(mm)	i.d./o.d. (1.05/1.6)
Die length L of spinneret	(mm)	6.5

5.2.3 Chemical modification

Hyperbranched polyetheleneimine (Figure 5.1) with molecular weights of 60 kg/mol (Acro, USA), 25 kg/mol and 2 kg/mol (Sigma-Aldrich, USA) were used as modification agents. A 1.0 wt% cross-linking solution was prepared by dissolving hyperbranched polyethyleneimine in a 1:1 mixture of 2-propanol and water. The fabricated hollow fiber module was first flushed with DI water to remove glycerol contained in the membranes. Then, the cross-linking solution was flowed through the shell side of hollow fiber module at 70 °C and 500 ml/min for 20 minutes. Figure 5.2

exhibits the chemical modification procedure. Finally, the modified PAI membrane was carefully rinsed with DI water to remove excess cross-linking agent, and then kept in DI water for performance testing.

5.2.4 Characterizations

5.2.4.1 Morphology

The morphology of the hollow fiber membranes was observed by a scanning electron microscope (SEM JEOL JSM-5600LV). Before observation, the freeze dried hollow fibers were immersed in liquid nitrogen, fractured and then coated with platinum using a JEOL JFC-1300 Platinum coater.

5.2.4.2 ATR-FTIR and XPS

ATR-FTIR (Perkin-Elmer FT-IR spectrometer, Norwalk, CT) was used to examine the degree of chemical cross-linking. The X-ray photoelectron spectroscopy (XPS) measurements were carried out by a Kratos AXIS Hsi spectrometer (Kratos Analytical Ltd., Manchester, UK).

5.2.4.3 Water contact angle

The contact angle of water on the hollow fiber membranes was measured using a Sigma 701 Tensiometer from KSV Instruments Limited. The hollow fiber with an effective length of 5 mm was immersed in ultrapure water and the advancing contact

angle was calculated with the aid of the computer software. Five readings were measured and an average was obtained from the results.

Step I

Flushing with water to remove glycerol

Step II

Flowing with cross-linker solution to modify fiber outer surface

Step III

Water flushing to remove the residual modification agent, then immersing in water for testing or treating fiber for future use
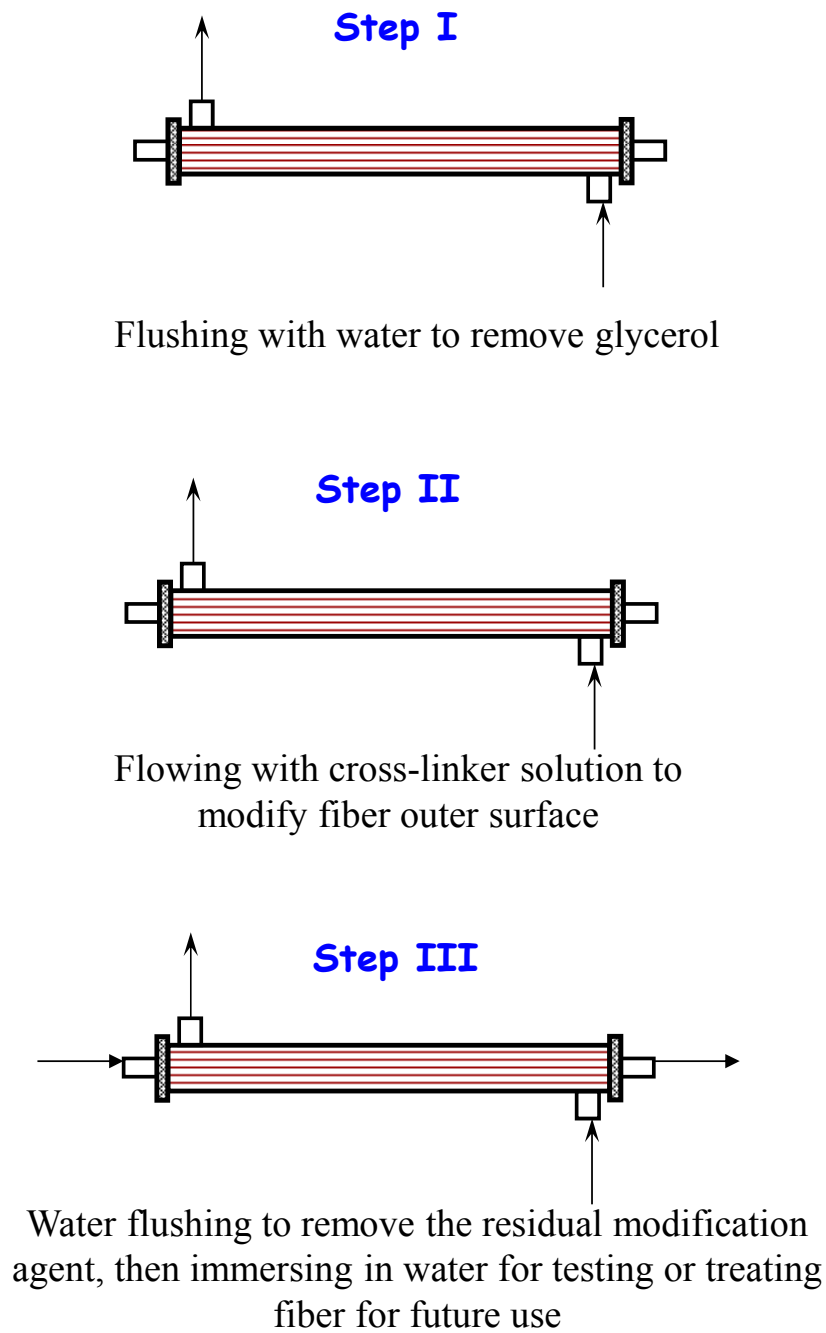
Figure 5.2. Procedure of PAI hollow fiber membrane cross-linking by polyethyleneimine

5.2.4.4 Streaming potential

The membrane surface charge characteristics were studied by streaming potential measurements with a SurPASS electrokinetic analyzer (Anton Paar GmbH, Austria). A 0.01M NaCl solution was used first to measure the zeta-potential at pH 5.75. After that, manual titrations with 0.1M HCl and 0.1M NaOH were carried out to study the pH dependence of the zeta potential and thus determine the isoelectric point with the method described in Chapter 3.

5.2.4.5 Adsorption measurements

In order to test the adsorption capacity of the original and modified membranes, ten fibers with an effective length of 5 cm per fiber for each modification condition were sealed at both ends by epoxy. These fibers were then immersed in 25ml 20 ppm ciprofloxacin solutions with a pH value of 6.8 and shaken at 60 rpm continuously for 48 hours. Meanwhile, a control experiment was conducted to verify the adsorption of ciprofloxacin on the epoxy by only immersing a small piece of cured epoxy into the ciprofloxacin solution. The ciprofloxacin concentration in all solutions was assessed by a UV–visible spectrophotometer (Biochrom Libra S32). The adsorption capacity of different membranes was calculated through the equation, $n = v(c_0 - c_1)/A$, where n is the adsorption capacity (μmol cm^{-2}), v is the volume of the ciprofloxacin solution (ml), A is the membrane surface area (cm^2), c_0 is the original concentration and c_1 is the concentration (ppm) after 48 hours.

5.2.4.6 Nanofiltration experiments

NF experiments were conducted in a lab-scale circulating filtration unit, described in Chapter 2. Since the outer surface of the hollow fiber was the selective layer, the feed solution was pumped into the shell side, while the permeate solution exited from the lumen side of the hollow fibers. Before testing, the hollow fiber membranes were conditioned at 12 bar for 6 hours. Then, each membrane sample was subjected to the pure water permeation experiment at a constant flow rate (1.7 L/min) and pressure (10 bar) to measure the pure water permeability, PWP (L m^{-2} bar^{-1} h^{-1}), which was calculated using the equation

$$\mathrm{PWP} = \frac{Q}{\Delta P \cdot A}$$

(5.1)

where Q is the water permeation volumetric flow rate (L/h), A is the effective filtration area (m^2), and ΔP is the transmembrane pressure drop (bar).

The membranes were then characterized by solute separation experiments with: (1) 200 ppm neutral organic solutes (Table 2.1) at pH 5.75 to estimate pore size, pore size distribution and MWCO according to the solute transport method described in Chapter 1; (2) various salt solutions at 0.01 mol L^{-1} (pH 5.75) to study the charge properties of the membranes; (3) 1ppm ciprofloxacin solutions with various pH from 3 to 9, adjusted by NaOH (1.0 M) and HCl (1.0 M) solutions. For each experiment, the feed solution was circulated at 10 bar for 1 hour before the concentrations of both feed and permeate were measured. The samples were collected 3 times for consecutive time intervals of 30 minutes. The variation of rejection was less than 2%. Between runs of different solutes the membrane was flushed thoroughly with DI water.

5.2.4.7 Chemical analyses

Concentrations of neutral solute solutions were measured by a total organic carbon analyzer (TOC ASI-5000A, Shimazu, Japan), while those of single electrolyte solutions were measured by an electric conductivity meter (Schott Instruments, Lab 960, Germany). The pH of the ciprofloxacin solutions was determined using a pH meter (Horiba pH meter D-54, Japan). The ciprofloxacin concentrations were determined by HPLC (Agilent technology 1200) with a variable wavelength detector. The Genesis C18 column (250×4.6mm, 4μm) and the guard column (10×4mm, 4μm) were purchased from Grace (IL, USA). The mobile phase consisted of solution A: 0.1% trifluoroacetic acid with water; and solution B: 0.1% trifluoroacetic acid with acetonitrile in the ratio of 20/80 (v/v). The flow rate was 1 ml/min. Detection was performed at a wavelength of 272 nm. The solute rejection R_T (%) was calculated using the equation:

$$R_{\mathrm{T}}(\%) = \left(1 - \frac{c_p}{c_f} \right) \times 100$$

(5.2)

where c_p and c_f are the solute concentrations in the permeate and the feed solution, respectively.

5.3 Results and discussions

5.3.1 Morphology of PAI hollow fiber membranes

The typical morphology of Torlon® PAI hollow fiber membranes is shown in Figure 5.3. The outer diameter is around 420 μm and the inner diameter is around 280 μm. The as-spun PAI hollow fiber membrane consists of a dense and nodule-like selective layer (about 150nm) at the outer edge, and a fully porous, macrovoid-free support layer (about 70μm). Such a sponge-like structure is quite different from that of our previously reported PAI hollow fiber membrane in Chapter 2, where a polymer (PAI)/solvent (NMP) binary system resulted in finger-like macrovoids throughout the cross-section. However, in the current study, the addition of non-solvent additive (EG) into the polymer solution increases viscosity, suppresses macrovoid formation and facilitates relatively uniformly spinodal decomposition across the membranes during the phase inversion process, as demonstrated in literature [120] and Chapter 4. As a result, macrovoid formation is completely eliminated. Meanwhile, the membrane support beneath the thin selective layer is full of interconnected open-cell pores. This so-called sponge-like cross-sectional structure is critical to minimize the transport resistance for water permeation under high pressures.
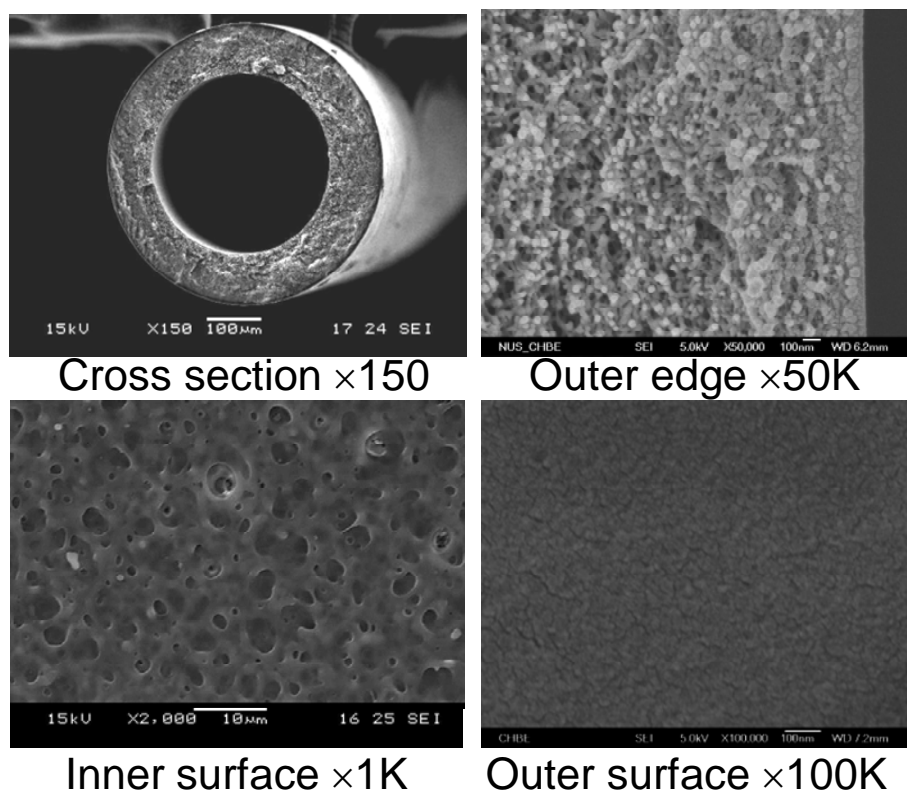
Figure 5.3. Morphology of Torlon® PAI NF hollow fiber membranes.

5.3.2 Characterization of modified PAI hollow fiber membranes

Figure 5.4 shows the ATR-FTIR spectra of the plain PAI membrane and those cross-linked with different PEI polymers. With an increase in PEI molecular weight, the characteristic peaks for the imide group at around 1773, 1709, and 1350 cm^{-1} gradually decrease, indicating the reduction of imide bonds. Meanwhile, the characteristic peaks for amide groups at 1640 cm^{-1} (C=O stretching) and 1521 cm^{-1} (C-N stretching of the C-N-H group) increase progressively, which implies the formation of amide bonds [64].
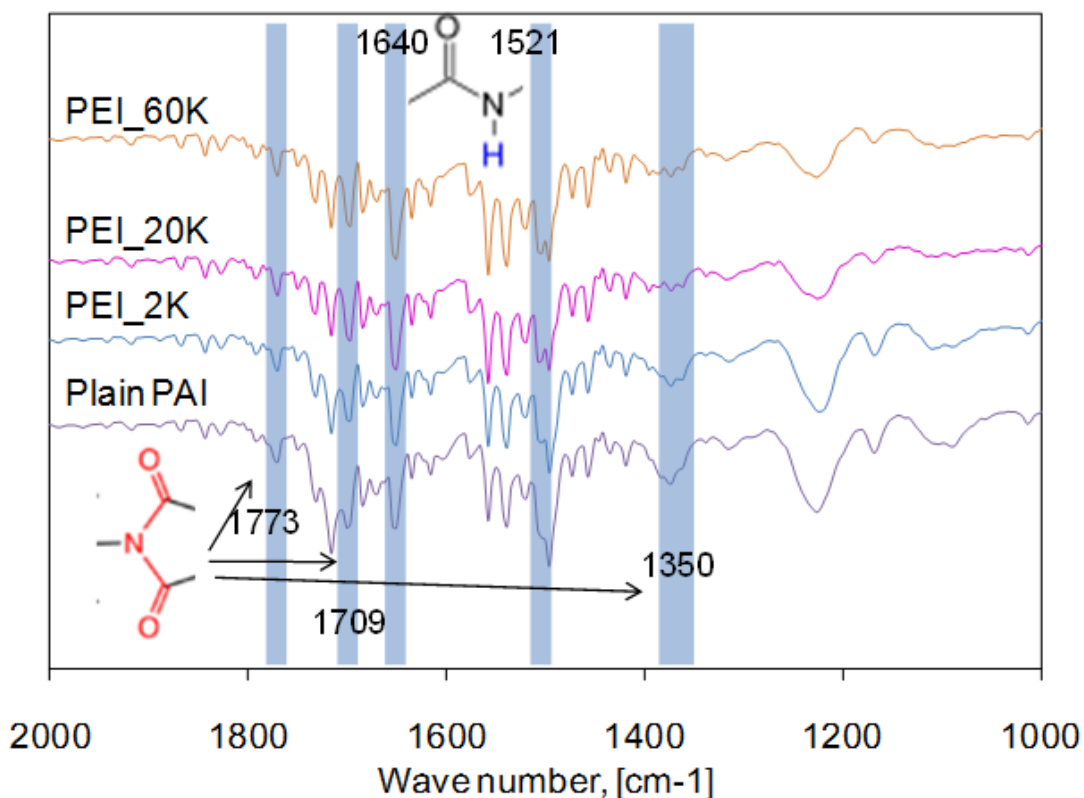
Figure 5.4. ATR-FTIR spectra of PAI NF hollow fiber membranes modified by PEI with various molecular weights.

XPS results, as listed in Table 5.2, also suggest the growth of nitrogen content on the surface of PEI modified membranes. Because the cross-linking process does not introduce or destroy oxygen molecules, the content of O_{1s} element on the membrane surface remains constant. Thus, oxygen content can be used as a reference, and the ratio of N_{1s} to O_{1s} can thus be considered as an indication of the degree of cross-linking. As compared to the plain PAI membrane, the ratio of N_{1s} to O_{1s} increases significantly after the PEI modification. Among these cross-linking agents, the N_{1s} to O_{1s} ratio increases progressively as the PEI molecular weight increases. This is probably because the penetration of PEI molecules into the membrane support becomes more difficult when the molecular size becomes larger. As a result, the amine concentration at the outer surface follows the order PEI_60K> PEI_20K> PEI_2K [124]. On the basis of FTIR and XPS results, a reaction mechanism is

proposed in Figure 5.5, which is similar to the cross-linking of polyimide with dendrimer [127].

Table 5.2. XPS Analysis of the original and PEI modified NF hollow fiber membranes.

	$C_{1s}(\%)$	$N_{1s}(\%)$	$O_{1s}(\%)$	N_{1s}/O_{1s}
Plain PAI	78.05	5.48	16.47	0.33
PEI_2K	74.58	9.99	15.43	0.65
PEI_20K	72.62	10.98	16.40	0.67
PEI_60K	72.46	14.00	13.54	1.03

As more amine groups are attached on the membrane surface, both of the hydrophilicity and the charge property are modified. The water contact angle data for the PAI hollow fiber membranes under different PEI modifications are shown in Table 5.3. The contact angle of the plain PAI hollow fiber membrane is 87.9±2.5º, which is similar to that of the PAI dense film (87.3º) reported in literature [50]. Such data indicate that PAI is a slightly hydrophilic material, mainly because of the amide group in polymer chains. Compared to the plain PAI membrane, the contact angle of the PEI functionalized membranes decreases to close to 70 º, indicating a more hydrophilic material has been formed.
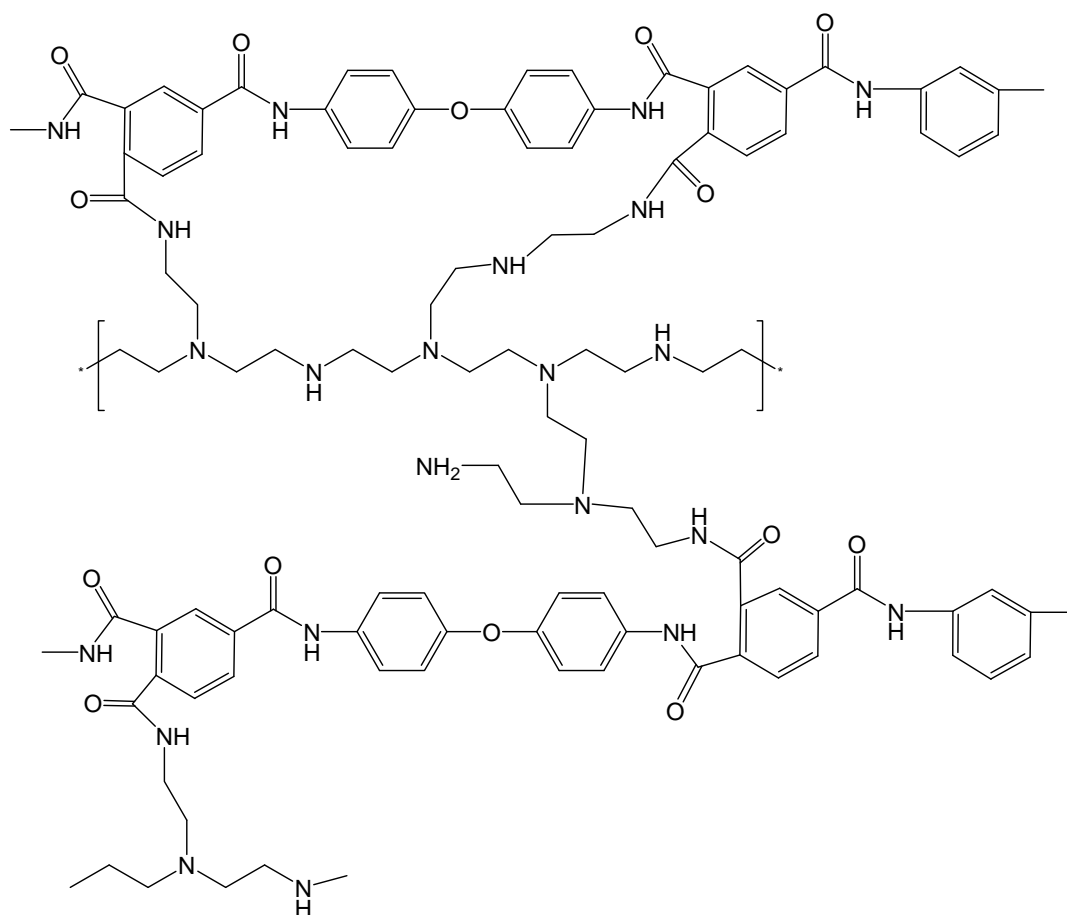
Figure 5.5. The possible chemical structure of polyamide-imide cross-linked by hyperbranched polyethlyeneimine.

Table 5.3. Contact angle, isoelectric point, zeta-potential, and adsorption capacity of the original and PEI modified NF hollow fiber membranes.

	Contact angle (º)	Zeta-potential (mv)[a]	Isoelectric point (-)[b]	Adsorption (μmol cm^{-2})[c]
Plain PAI	87.9±2.5	-32.5	3.8	2.68
PEI_2K	71.1±1.6	-4.77	5.1	0.84
PEI_20K	69.1±2.0	16.9	6.3	0.82
PEI_60K	68.6±1.3	25.1	8.0	0.80

Zeta-potential versus pH curves of PAI membranes modified by PEI with various molecular weights are shown in Figure 5.6. The isoelectric point derived from the plot, and the zeta-potential measured at neutral pH are listed in Table 5.3. The isoelectric

point of plain PAI membrane is 3.8, similar to our previously reported result in Chapter 3. The PAI membrane has a slightly positive charge below pH 3.8 due to protonation of the amine group, and is negatively charged above pH 3.8 because of de-protonation of the carboxyl group. However, since more amine groups are introduced on the membrane surface after the PEI modification, the zeta-potential curve shift towards the right, and thus the isoelectric point increases as the PEI molecular weight increases. Similar results were reported in literature [125]. Compared to the plain PAI membrane, the isoelectric point of the PEI_60K modified membrane is higher at about 8.0, which implies that the previously negatively charged PAI membrane had become positively charged when the pH is below 8.0.

Adsorption of pharmaceutical compounds has been considered as an important factor in membrane separations [128, 129]. The adsorption capacity of the plain PAI membrane and those PEI modified membranes were measured according to the method described in supporting information. As shown in Table 5.3, the adsorption of ciprofloxacin on the membranes correlates well with the hydrophilicity and the charge properties of the membranes. As discussed above, PEI modification changed the slightly hydrophilic and negatively charged membrane into a much more hydrophilic and positively charged membrane. Therefore, the positively charged ciprofloxacin molecule has a much lower tendency to adsorb on the PEI modified membrane surface, because of enhanced charge repulsion and increased membrane hydrophilicity [122]. This adsorption-resistant membrane may have great potential to reduce fouling during nanofiltration tests with ciprofloxacin solutions, which will be discussed later.
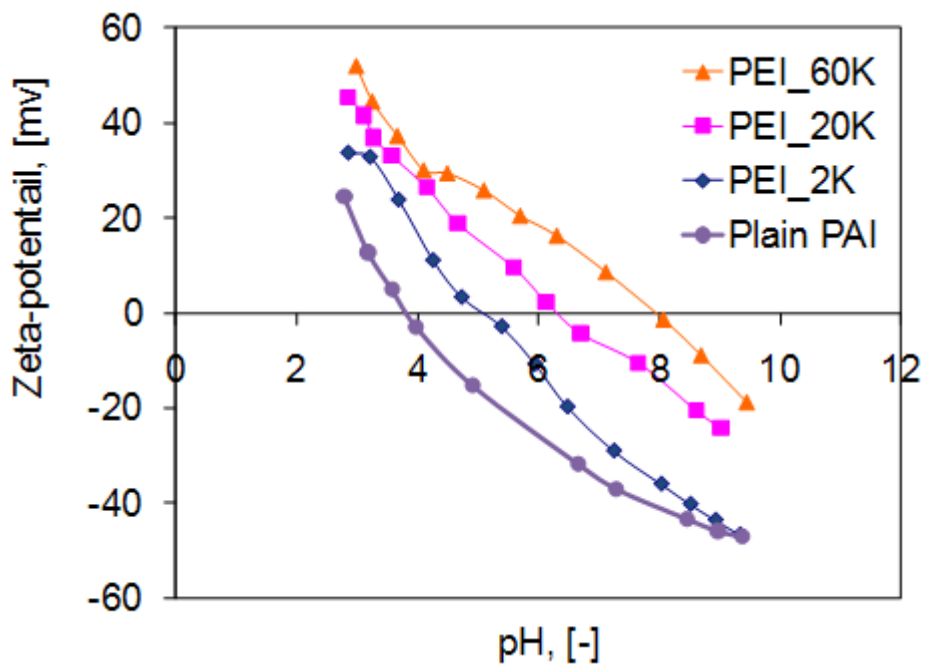
Figure 5.6. Zeta potential vs. pH curves of PAI NF membranes modified by PEI with various molecular weights. Experiments were carried out with 0.01 M NaCl.

5.3.3 Nanofiltration performance of PEI modified membranes

5.3.3.1 Effects of PEI modification on pure water permeability, pore size, pore size distribution and molecular weight cutoff

In order to understand the effects of PEI modification on the NF performance, the plain PAI and the PEI modified hollow fiber membranes were characterized by the solute transport method with a series of organic solutes, as described in the experimental section. The relationship between solute rejection and solute Stokes radius is shown on the log-normal probability graph in Figure 5.7. The mean effective pore radius r_p at $R_T = 50\%$, the MWCO and the geometric standard deviation σ_p were calculated from Figure 5.7 and summarized in Table 5.4. The PWP, which were obtained from Eq. (5.1), are also listed in Table 5.4. The cumulative pore size distribution curves and probability density function curves, calculated using the solute transport method are depicted in Figures 5.8 (a) and (b), respectively.
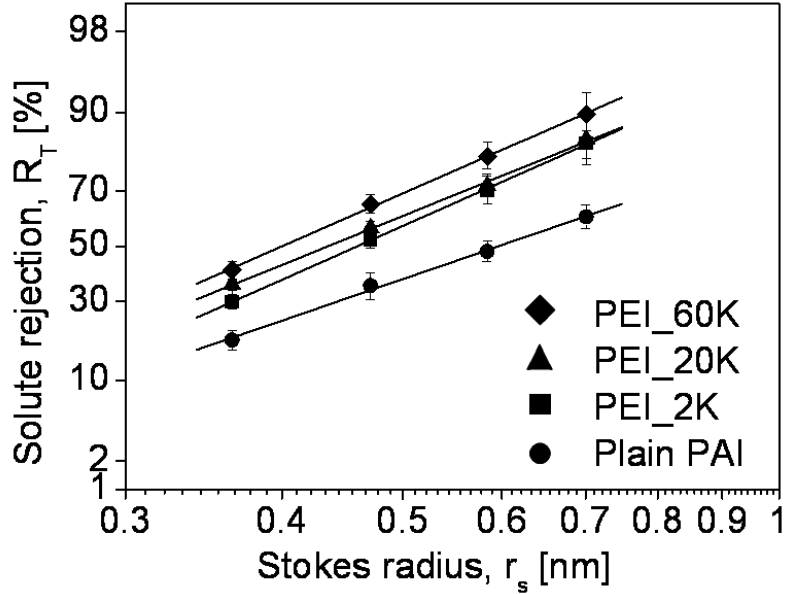
Figure 5.7. Effects of PEI modification on rejection of neutral solutes at pH 5.75.

Table 5.4. Mean effective pore radius (r_p), geometric standard deviation (σ_p), molecular weight cut off (MWCO), and pure water permeability (PWP) of the original and PEI modified NF hollow fiber membranes.

ID	r_p (nm)	σ_p	MWCO (Da)	PWP ($lm^{-2}bar^{-1}h^{-1}$)
Plain PAI	0.62	1.67	3675	15.10
PEI_2K	0.46	1.53	1278	6.37
PEI_20K	0.43	1.62	1278	4.85
PEI_60K	0.40	1.56	912	3.58

It can be seen clearly that the PEI modification has a significant impact on the nanostructures of the membrane surface. The mean effective pore radius and the MWCO decrease dramatically after modification. The pure water permeability is decreased, may be because the pore size is reduced and the cross-link structure becomes more rigid, thus limiting the molecular movement [126]. An enhanced solute rejection can also be observed, possibly due to the decreased pore size and the increased membrane hydrophilicity [130]. The results suggest that the membrane

structure and subsequent separation performance can be manipulated effectively through carefully chemical modification with polyethyleneimine. Comparing to membranes modified by smaller cross-linking agents (PEI_20K and PEI_2K), the PEI_60K cross-linked membrane has the smallest MWCO (about 1000) with a narrow pore size distribution.
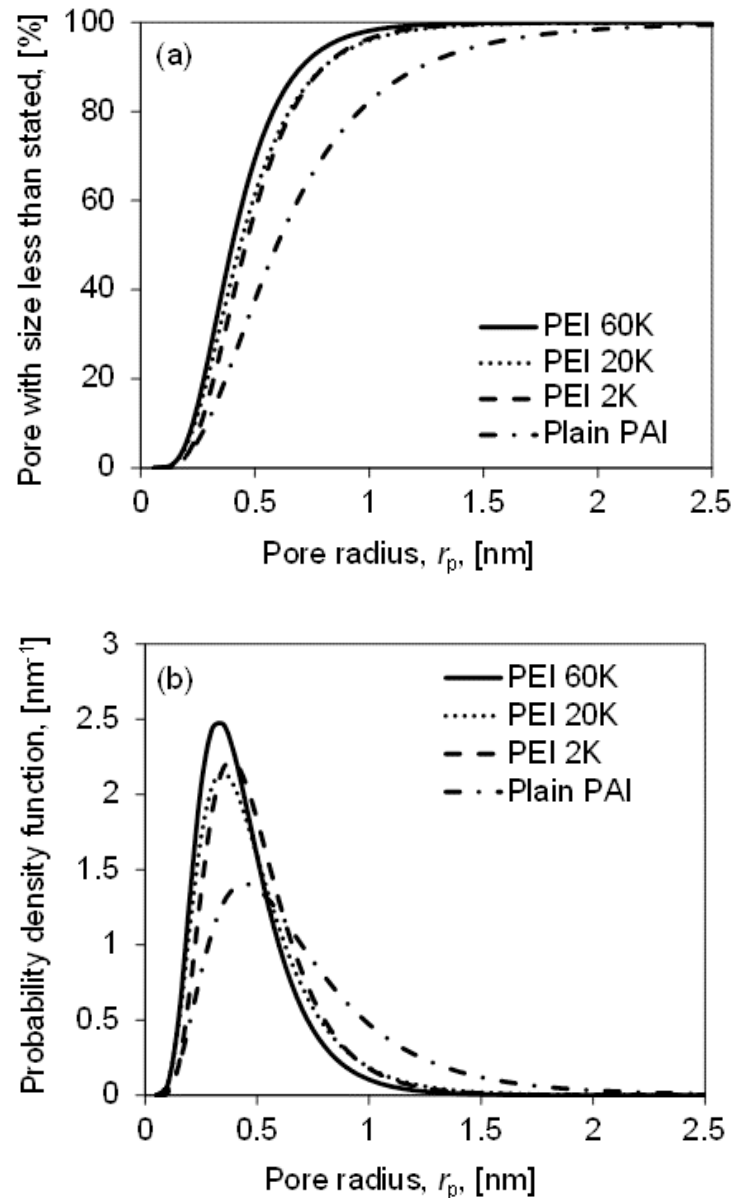
Figure 5.8. (a) Cumulative pore size distribution curves and (b) probability density function curves of PAI NF hollow fiber membranes modified by PEI with various molecular weights.

5.3.3.2 Effects of PEI modification on salt rejection

In order to further analyze the effects of PEI modification on the charge properties of the PAI hollow fiber membranes, the rejections of four kinds of electrolytes were tested at the same molar concentration (0.01 mol L^{-1}), pH (5.75) and pressure (10 bar). For the plain PAI membrane, the rejection of these salts decreases in the order $R(Na_2SO_4) > R(MgSO_4) > R(NaCl) > R(MgCl_2)$, as shown in Figure 5.9. Interestingly, such order is reversed after PEI modification. This phenomenon is mainly determined by the Donnan exclusion effect [89]. Because the plain PAI membrane is negatively charged, as verified by zeta-potential tests in previous section, it shows a higher rejection of divalent anions (SO_4^{2-}) with a higher co-ion charge than monovalent anions (Cl$^-$), and a lower rejection of divalent cations (Mg^{2+}) with a higher counter-ion charge. However, after the PEI modification, the membrane becomes positively charged. Thus the co-ions have changed to (Mg^{2+}) and (Na^+), while the counter-ions have changed to (SO_4^{2-}) and (Cl$^-$). Our work shows that the PEI modification dramatically increases the rejection of $MgCl_2$, NaCl and $MgSO_4$. Furthermore, among the PEI modified membranes, the rejection for each electrolyte increases in the order PEI_60K>PEI_20K>PEI_2K. This phenomenon can be explained by the steric-hindrance effect as the PEI modification reduces the membrane pore size in the sequence of PEI_60K<PEI_20K<PEI_2K.
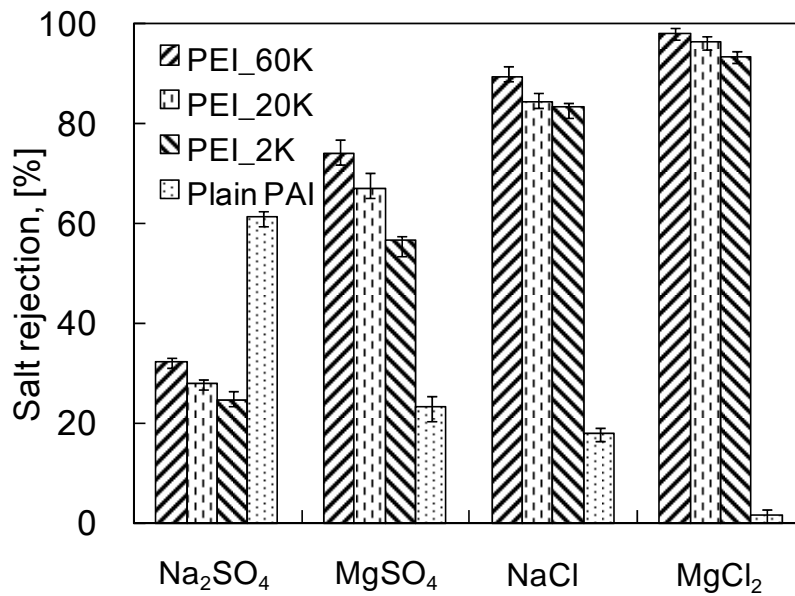
Figure 5.9. Effects of PEI modification on rejection of electrolyte solutions at pH 5.75.

5.3.3.3 Effects of PEI modification on rejection of ciprofloxacin

Based on the four pK_a values of ciprofloxacin (Figure 1.3), the fraction of different ionization states at different pH values can be calculated according to the method described in Chapter 3 by utilizing Eq. (3.1). The result is shown in Figure 5.10. As an amphoteric molecule, ciprofloxacin is positively charged below pH 8.70 and negatively charged above pH 10.58. Within the range of 8.70 < pH < 10.58, the molecule becomes net neutral.
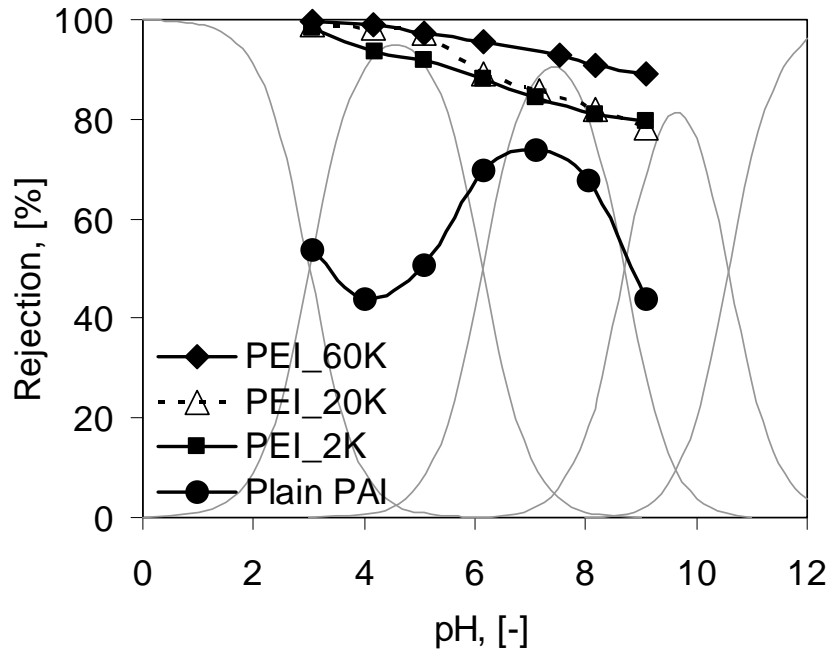
Figure 5.10 Effects of PEI modification on rejection of ciprofloxacin solutions as a function of pH.

Figures 5.10 and 5.11 present the rejection and the permeate flux, respectively, for the plain PAI and PEI modified hollow fiber membranes as a function of pH during nanofiltration tests of ciprofloxacin solutions at 10 bar. A control experiment to study the effect of pH on clean water flux for each membrane is shown in Figure 5.12 (a) and the normalized flux, J/J_0 (%), which is the ratio of permeate flux of ciprofloxacin solution, J (L m^{-2} h^{-1}), to the pure water flux, J_0 (L m^{-2} h^{-1}), at various pH, is shown in Figure 5.12 (b) of SI. For the plain PAI membrane, it is very interesting to observe that pH has a strong impact on ciprofloxacin rejection. As verified in zeta-potential tests, the isoelectric point of the plain PAI membrane is about pH 3.8. From pH 3 to pH 4, the charge of the membrane is changed from slightly a positive to the neutral state. Under such a condition, the electrostatic repulsion between the membrane and the positively charged ciprofloxacin molecule becomes less, thus the rejection is slightly decreased from 53.9% to 43.9%. However, from pH 4 to 7, the ciprofloxacin rejection is increased almost twice to 73.9%. This is probably attributed to the

following reasons: when the pH is above 4, the PAI membrane is negatively charged and only slightly hydrophilic, while the charge of ciprofloxacin molecules is still positive. As a result of this synergic effect, adsorption of ciprofloxacin molecules on the surface and in the bulk of the membrane becomes very severe, as demonstrated in an earlier section. The adsorbed ciprofloxacin molecules might block some of the membrane pores. Therefore, the rejection is increased while the permeate flux (Figure 5.11) is dramatically decreased. When pH is above 7, ciprofloxacin rejection decreases again and finally drops to 44.0% at pH 8.7, because the ciprofloxacin molecule has become neutral.
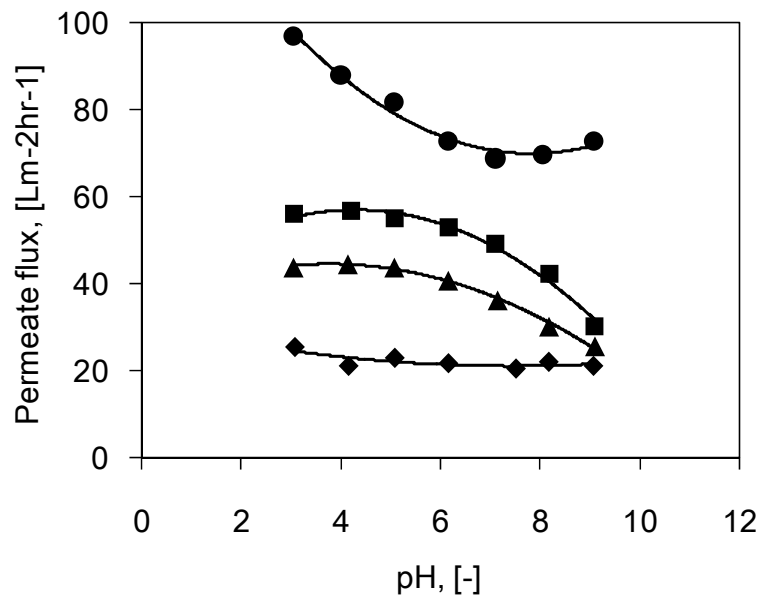
Figure 5.11 Effects of PEI modification on permeate flux of ciprofloxacin solutions as a function of pH.
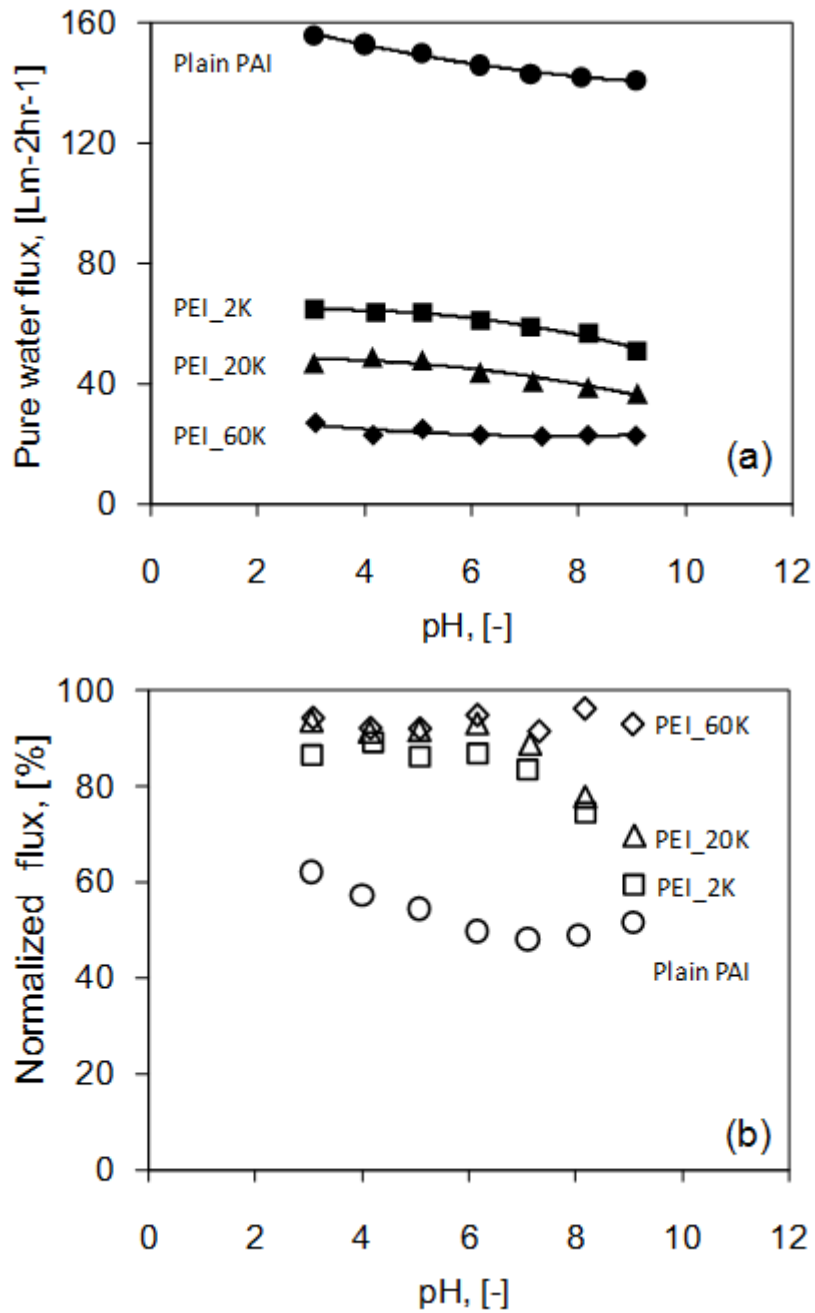
Figure 5.12. (a) Pure water flux as a function of pH at 10 bar and (b) normalized flux, J/J_0 at various pH.

After the PEI modification, the PAI hollow fiber membranes may possess the following characteristics: (1) the pore size becomes smaller, leading to a higher ciprofloxacin rejection because of the size-exclusion mechanism; (2) the membrane becomes more hydrophilic, resulting in less severe adsorption; (3) the membrane surface becomes positively charged; because of the Donnan exclusion mechanism,

ciprofloxacin rejection is increased while ciprofloxacin adsorption is reduced. As a result of these synergic effects, ciprofloxacin rejection is substantially increased, as shown in Figure 5.10.

The trend of ciprofloxacin rejection is similar for all three PEI modified membranes. At pH 3, the positively charged PEI modified NF hollow fiber membranes show extremely high rejections above 99%. As pH increases, the rejection decreases because ciprofloxacin molecules become less positively charged. However, after carefully examining the rejection versus pH curves, a very interesting phenomenon can be observed. From pH 3 to 5, the ciprofloxacin rejection of the membrane modified by PEI_20K is almost the same as that for PEI_60K and much higher than that for PEI_2K. But above pH 5, the rejection by membrane PEI_20K immediately drops to nearly the same as that for PEI_2K. A similar clue can be found in the permeate flux versus pH curves as illustrated in Figure 5.11. The permeate fluxes of both PEI_2K and PEI_20K do not vary much between pH 3 to 5, but they reduce gradually when the pH is above 5. The isoelectric points of PEI_2K and PEI_20K are 5.1 and 6.3 respectively (Table 5.3). PEI_20K has a higher positive charge than PEI_2K on the membrane surface (Figure 5.6), thus the higher charge repulsion leads to a higher rejection and less fouling tendency. Nevertheless, above pH 5, both of the membranes become less positively charged and start to show neutral and finally negative charge properties. Because these two membranes share a similar MWCO (1278Da), their rejections become quite similar [11]. Their permeate fluxes also drop gradually, due to fouling induced by the adsorption of positively charged ciprofloxacin on the negatively charged surface.

Compared to membranes modified by low molecular weight PEI (2K and 20K), the PEI_60K functionalized membrane has a smaller pore size, and a more hydrophilic and positively charged membrane surface. In this case, the membrane shows the highest rejection and the permeate flux almost remains constant over the whole pH range (3 to 9).

5.4 Conclusions

These results confirm that size exclusion, charge repulsion and solute-membrane affinity are all important parameters that determine the rejection of ciprofloxacin. The results also suggest that PEI molecule weight has an significant influence on the properties of the modified PAI hollow fiber membranes. The normalized water flux at various pH Figure 11 (b) shows that hyperbranched PEI_60k modified NF membrane has the lowest fouling tendency among all the tested membranes. Such positively charged membrane may also hold high potential to remove not only pharmaceutical active compounds with similar chemical structure, such as norfloxacin and enrofloxacin, but also some positively charged heavy metal ions, such as Cu^{2+}, Zn^{2+} and so on.

<center>**CHAPTER SIX**</center>

<center>**FABRICATION OF THIN-FILM COMPOSITE NANOFILTRATION
HOLLOW FIBER MEMBRANE VIA INTERFACIAL POLYMERIZATION
FOR EFFECTIVE REMOVAL OF EMERGING ORGANIC MATTERS
FROM WATER**</center>

6.1 Introduction

As discussed in Chapter 4, dual-layer hollow fiber membranes prepared by the co-extrusion technique retain all the advantages of conventional single-layer hollow fiber membranes. Meanwhile, the dual-layer hollow fiber membrane is more attractive than the traditional hollow fiber membrane because it allows the use of two different polymers or one polymer with different concentrations to form a composite membrane in one-step, which reduces manufacture cost [93]. Therefore, we aim to develop a novel thin-film composite NF membrane through interfacial polymerization on a dual-layer hollow fiber membrane support.

In this chapter, Torlon® 4000T-MV polyamide-imide (PAI), as shown in Figure 1.4, is employed for both outer and inner dope to eliminate the delamination issue, while different concentrations are chosen to reduce the sublayer water transport resistance. Hyperbranched polyethyleneimine (PEI) and isophthaloyl chloride (IPC), as shown in Figure 6.1, are chosen as the monomers to form an interfacial polymerized network on top of the dual-layer hollow fiber membrane. As a polyelectrolyte, PEI has attracted many interests to functionalize polyimide membranes through cross-linking the carbonyl groups of imide rings in the polymer chains with amines to form amide groups [124, 126, 131]. The resultant NF membrane has excellent solvent resistance

and positive charged selective layer over a wide pH range, which is demonstrated in the above literatures and also shown in our work in Chapter 5. However, cross-linking may not cover some large pores of the substrate if the pore size distribution is broad and the transport channels of the selective layer may be reduced after cross-linking. Consequently, the cross-linked membrane may suffer from limited solute rejection and limited water flux. However, such issues may be solved by creating an ultra-thin selective layer synthesized from interfacial polymerization of PEI and IPC. Several studies reported the interfacial polymerization with polyethyleneimine on polyacrylnitrile and polypropylene substrates [132, 133]. In order to form a homogeneous thin film, a pretreatment step was necessary to stabilize polyethyleneimine before the reaction, by forming carboxyl (–COOH) groups on the membrane surface. In contrast to these efforts, the utilization of the polyamide-imide material as the substrate could eliminate the pretreatment step because the carbonyl groups of imide rings in polymer chains are able to form covalent bonds with the amine groups, thus stabilizing the PEI molecules. To the best of our knowledge, no such studies have been reported before.

Two model solutions are selected to test the NF performance of the newly developed thin-film composite dual-layer hollow fiber membrane. The first is composed of either positively or negatively charged dye solution to represent waste streams from dye-houses in textile industry. The impact of solute charge on the NF performance of the membrane will be studied. We also choose cephalexin, a widely used antibiotic with therapeutically advantages and broad antibacterial activity, to investigate the pH effects on nanofiltration of this zwitterionic molecule. This study may provide guidelines for designing high performance NF dual-layer hollow fiber membranes for

sustainable manufacture applications, especially wastewater treatments in various industries.

6.2 Experimental

6.2.1 Materials

Torlon® 4000T-MV polyamide-imide with the chemical structure shown in Figure 1.4 was purchased from Solvay Advanced Polymers. N-methyl-2-pyrrolidinone (NMP) was purchased from Merck and used as solvent. Methanol and PEG 2000 were purchased from Sigma and used as additives for the spinning solutions. PEI with molecular weights of 2 000 (Sigma, Singapore) and 60 000 (Acro, USA) and IPC (Sigma, Singapore) were used for interfacial polymerization. Their chemical structures are shown in Figure 6.1. A series of uncharged neutral organic solutes with various molecular weights were utilized to characterize membrane structure parameters. Molecular weights, diffusivities and Stokes radii of neutral solutes are listed in Table 6.1. Several analytical-grade salts, i.e. NaCl, MgCl$_2$, MgSO$_4$, and Na$_2$SO$_4$ (Merck, Germany) were used to characterize the charge properties of the membranes. Safranin O ($C_{20}H_{19}N_4^+$, Cl$^-$, 350.84 Da) and orange II sodium salt ($C_{16}H_{11}N_2O_4S^-$, Na$^+$, 350.32 Da) were purchased from Sigma Singapore. Cephalexin ($C_{16}H_{17}N_3O_4S \cdot H_2O$, MW 365.4, p$K_{a,1}$: 2.56, p$K_{a,2}$: 5.88, Log K$_{ow}$=0.076) was purchased from MP Biomedicals (Heidelberg, Germany).

(a) Hyperbranched polyethyleneimine (PEI) (b) Isophthaloyl chloride (IPC)
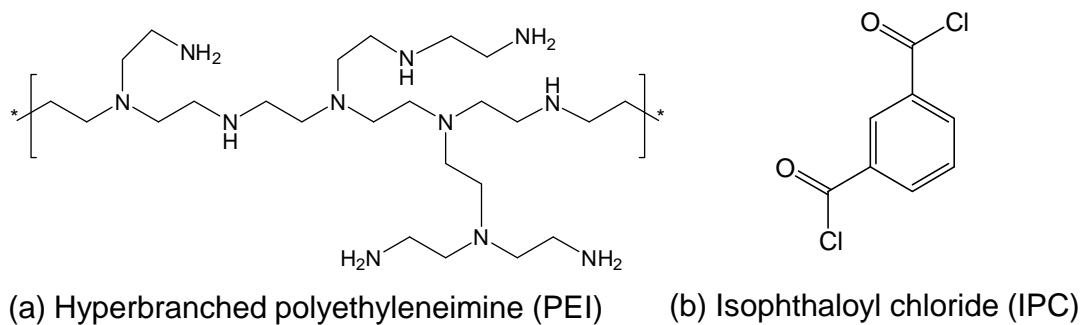
Figure 6.1. The chemical structures of (a) Hyperbranched polyethyleneimine, (b) Isophthaloylchloride.

Table 6.1. Diffusivities and Stokes radii of neutral solutes in aqueous solutions (at 25ºC).

Solute	MW [g·mol^{-1}]	D_s [$\times 10^{-9}$ m^2·s^{-1}]	r_s [nm]
Solutes used for calculating the pore size of NF membranes:			
Glycerol	92	0.78	0.260
Glucose	180	0.67	0.365
Saccharose	342	0.52	0.471
Raffinose	504	0.42	0.584
Solutes used for calculating the pore size of the support:			
PEG 2K	2 000	-	1.15
PEG 10K	10 000	-	2.82
PEG 20K	20 000	-	4.16
PEG 35K	35 000	-	5.68
PEO 100K	100 000	-	8.99

6.2.2 Fabrication of dual-layer PAI hollow fiber membrane support

The Torlon® PAI polymer was first dried in a vacuum oven at 120 °C overnight to remove moisture. Then two dopes were prepared according to the compositions listed in Table 6.2. The dopes were stirred at 70 °C for 24 hours to form homogeneous

polymer solutions, which were then set aside for 1 day to eliminate air bubbles that may have been trapped in the solutions.

Table 6.2. Spinning conditions of the dual-layer hollow fiber membranes.

Outer dope composition (wt%):	PAI/Methanol/NMP: 20.0/10.0/70.0
Inner dope composition (wt%):	PAI/PEG2K/NMP: 15.0/5.0/80.0
Bore fluid composition (wt%):	NMP/Water=80/20
External coagulant:	Water
Outer dope flow rate (ml/min)	0.5
Inner dope flow rate (ml/min)	4.0
Bore fluid flow rate (ml/min)	3.0
Air Gap (cm)	2.5
Take-up speed (m/min)	10
Spinneret dimension (mm):	0.84/1.0/1.58/1.74/2.0
Spinneret temperature (ºC):	26

The dual-layer hollow fiber membranes were fabricated by the co-extrusion technique using a tri-channel spinneret. The outer dope, inner dope and bore fluid were fed into the spinneret separately by three ISCO syringe pumps. After that, the dopes and the bore fluid met at the tip of the spinneret, and passed through an air gap region before entering the coagulation (water) bath. Finally, the as-spun hollow fibers were collected by a take-up drum. The detailed dope compositions and spinning conditions are summarized in Table 6.2. After spinning, the as-spun hollow fiber membranes were rinsed in a clean water bath for 3 days to remove the residual solvent. The hollow fiber membranes were then divided into two groups for post-treatments. One group was dipped in a 30 wt% glycerol aqueous solution for 2 days and dried in air at room temperature to be used in the making of membrane modules for interfacial

polymerization and nanofiltration experiments. The other group was directly freeze dried for further morphological characterizations.

6.2.3 Interfacial polymerization

Thin-film composite membranes were prepared via interfacial polymerization of PEI in aqueous phase and IPC in organic phase (n-hexane). The molecular weight and concentration of PEI were varied, as listed in Table 6.3, to study their effects on nanofiltration performance. The reaction was carried out at the outer surface of the hollow fiber membranes. First, the fabricated hollow fiber module was flushed with DI water to remove glycerol contained in the membranes. Then, the PEI solution was flowed through the shell side of hollow fiber module with a peristaltic pump at 100 ml/min for 60 minutes. The excess PEI solution was drained and the module was dried in air for 5 minutes. After that, the IPC solution was pumped through the module in the same way for 3 minutes. Subsequently, the excess IPC was drained and the module was cured in an oven at 110 ^{o} C for 10 minutes. Finally, the as-functionalized membrane was stored in DI water before NF tests.

Table 6.3. Effects of molecular weight and concentration of HPEI on pure water permeability (PWP), rejections of raffinose and $MgCl_2$.

PEI MW (Da)	PEI concentration (wt%)	IPC concentration (wt%)	PWP ($lm^{-2}bar^{-1}h^{-1}$)	Raffinose rejection (%)	$MgCl_2$ rejection (%)
PEI_2K	1	0.5	8.17	79.32	83.05
PEI_60K	1	0.5	5.87	86.29	92.55
PEI_60K	2	0.5	4.85	90.01	96.17
PEI_60K	4	0.5	1.91	91.36	96.99

Raffinose concentration: 200ppm, $MgCl_2$ concentration: 1mM. pH 5.75. Pressure: 5 bar.

6.2.4 Characterizations

The morphology of hollow fiber membranes was observed by a scanning electron microscope (SEM JEOL JSM-5600LV) and a field emission scanning electron microscope (FESEM JEOL JSM-6700F). Before observation, the freeze dried hollow fibers were immersed in liquid nitrogen, fractured and then coated with platinum using a JEOL JFC-1300 Platinum coater.

The surface topology of membranes before and after interfacial polymerization was examined using a Nanoscope IIIa atomic force microscope (AFM) from Digital Instruments Inc. For each membrane, an area of 250nm×250nm was scanned at a rate of 1 Hz using the tapping mode. The mean roughness (R_a) was used to quantify the differences between various membrane surfaces and was determined from the averages of at least 5 sections of several fibers.

The contact angle of water on hollow fiber membranes was measured using a Sigma 701 Tensiometer from KSV Instruments Limited. The hollow fiber with an effective length of 5 mm was immersed in ultrapure water and the advancing contact angle was calculated with the aid of the computer software. Five readings were measured and an average was obtained from the results.

6.2.5 Nanofiltration experiments

NF experiments were conducted in a lab-scale circulating filtration unit, described in Chapter 2. Every module comprised 15 hollow fiber membranes with an effective

area of around 60 cm^2. Since the outer surface of hollow fibers was the selective layer, the feed solution was pumped into the shell side, while the permeate solution exited from the lumen side of hollow fibers. Before testing, the hollow fiber membranes were conditioned at 6 bar for 6 hours. Then, each membrane sample was subjected to the pure water permeation experiment at a constant flow rate (1.5 L/min) and pressure (5 bar) to measure the pure water permeability, PWP (L m^{-2} bar^{-1} h^{-1}), which was calculated using the equation

$$\text{PWP} = \frac{Q}{\Delta P \cdot A}$$

(6.1)

where Q is the water permeation volumetric flow rate (L/h), A is the effective filtration area (m^2), and ΔP is the transmembrane pressure drop (bar).

The membranes were then characterized by solute separation experiments with: (1) 200 ppm neutral organic solutes (Table 6.1) at pH 5.75 to estimate pore size, pore size distribution and MWCO according to the solute transport method described in Chapter 1; (2) various salt solutions at 1 mM (pH 5.75) to study the charge properties of the membranes; (3) 50 ppm positively charged (safranin O) or negatively charged (orange II sodium salt) dye solutions at pH 5.75 to test the decolourization capabilities of the interracially polymerized membranes; (4) 200 ppm cephalexin solutions with various pH from 3 to 9, adjusted by NaOH (1.0 M) and HCl (1.0 M) solutions, to study the removal efficiency of this pharmaceutical active compound as a function of pH. For each experiment, the feed solution was circulated at 5 bar for 1 hour before the concentrations of both feed and permeate were measured. The samples were collected 3 times for consecutive time intervals of 30 minutes. The variation of rejection was less than 2%. Between runs of different solutes the membrane was flushed thoroughly with DI water.

6.2.6 Chemical analyses

Concentrations of neutral solute solutions were measured by a total organic carbon analyzer (TOC, ASI-5000A, Shimazu, Japan), while those of single electrolyte solutions were measured by an electric conductivity meter (Schott Instruments, Lab 960, Germany). Concentrations of dye solutions were assessed by a UV–visible spectrophotometer (Biochrom Libra S32). The pH of the cephalexin solutions was determined using a pH meter (Horiba pH meter D-54, Japan). Cephalexin concentrations were measured by a TOC. The solute rejection R_T (%) was calculated using the equation:

$$R_T(\%) = \left(1 - \frac{c_p}{c_f}\right) \times 100$$

(6.2)

where c_p and c_f are the solute concentrations in the permeate and the feed solution, respectively.

6.3 Results and discussions

6.3.1 Morphology of the PAI dual-layer hollow fiber membrane support

The morphology of the plain PAI dual-layer hollow fiber membrane is shown in Figure 6.2. The outer diameter is around 860 μm and the inner diameter is around 660 μm. The cross-section of the membrane is asymmetric and consists of three regions: (1) A sponge-like and defect-free selective layer with a thickness less than 1 μm is located at the outer edge of the membrane; (2) A 100-μm-thick middle layer is full of

large finger-like macrovoids; (3) A sponge-like and fully porous support with a thickness of 5 to 10 μm to withstand high pressures under NF operations. Such a unique sandwich-like structure is achieved through the following design criteria:

(1) The same polymer, i.e. Torlon® polyamide-imide, is employed in both of the outer dope and the inner dope. Consequently, the delamination issue which often occurs in fabricating dual-layer hollow fiber membranes using two incompatible dopes can be easily avoided. Meanwhile, as the polymer in the inner dope (15 wt%) is less concentrated than that of the outer dope (20 wt%), we could create a more porous structure than conventional single-layer hollow fiber membranes [107].

| Outer edge ×10K | Cross section ×100 | Cross section ×1K |
| Outer surface ×10K | Inner surface ×2K | Inner edge ×5K |
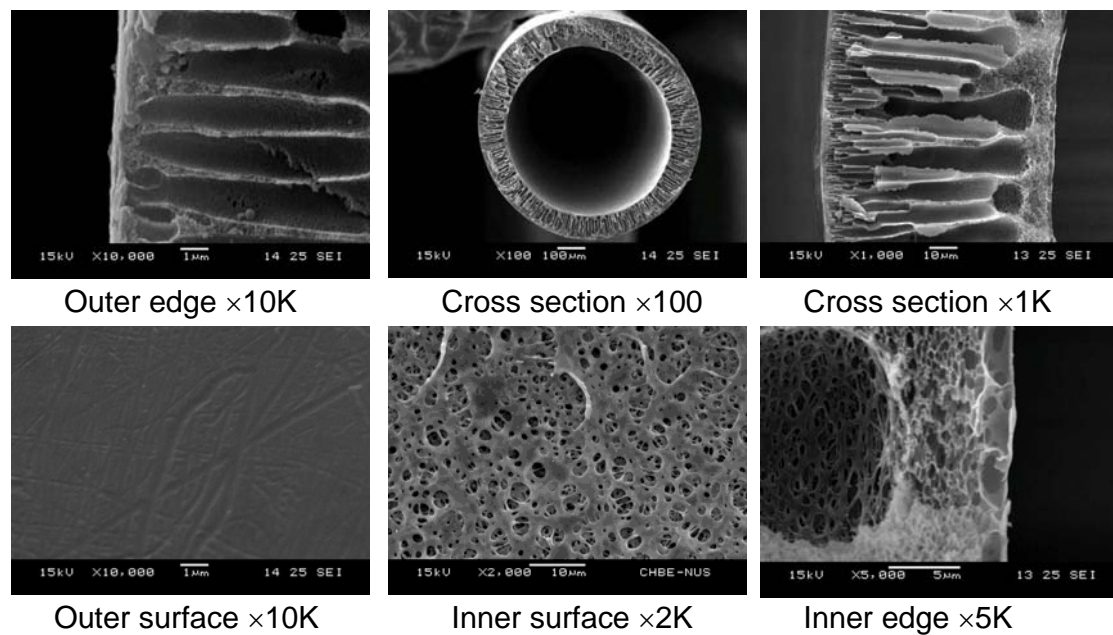
Figure 6.2. Morphology of the PAI dual-layer hollow fiber membranes.

(2) Methanol, which is a small molecular non-solvent additive, is introduced into the outer dope solution. Due to extra phase instability, the dope added with methanol tends to experience instantaneous liquid–liquid demixing which may lead to a thin

selective layer and the formation of macrovoids; the mechanism has been elaborated in Chapter 4.

(3) In contrast to the outer dope, the inner dope incorporates a larger polymeric additive, i.e. PEG 2000. This type of additive is not only a pore former but also causes delayed demixing when the nascent fiber is subjected to phase separation [98, 134]. As a result, a porous sponge-like layer can be formed at the inner edge of the hollow fiber membrane. Moreover, the excellent mutual compatibility between the two dopes may cause the inner dope to further dilute the outer dope after both of them have met in the air gap region. This is likely to results in a more porous inner support layer.

6.3.2 Effects of molecular weight and concentration of PEI on NF performance

Table 6.3 shows the effects of PEI molecular weight and concentration on the NF performance of the interfacial polymerized membranes. As the molecular weight of PEI increases from 2 000 to 60 000, the rejections of organic and inorganic solutes increase while the pure water permeability decreases, indicating the pore size becomes smaller. This is possibly because low-molecular-weight PEI may diffuse into the substrate when the PEI solution is in contact with the membrane. In contrast, high-molecular-weight PEI may prefer to stay on the surface, providing a higher amount of amine groups to react with IPC later. The phenomenon was proved by XPS characterizations in our previous paper in which PEI with various molecular weights were used to cross-link polyamide-imide membranes. With increasing PEI concentration, the rejections of organic and inorganic solutes increase gradually and finally become stable while the pure water permeability decreases throughout the

range. This is possibly because the reaction becomes faster in higher PEI concentration solutions. When the PEI concentration increases from 2 wt% to 4 wt%, only a slight increase in solute rejection is obtained. However, the pure water permeability decreases 2.5 folds. The membrane prepared with 2 wt% PEI was further characterized and tested for NF applications. The hollow fiber support is denoted as "Bef IP" while the interfacial polymerized NF membrane is denoted as "Aft IP".

6.3.3 Characterizations of the interfacial polymerized NF membranes

The outer surfaces of the interfacial polymerized NF membrane and the plain PAI dual-layer hollow fiber membrane were characterized by FESEM and AFM. As shown in Figure 6.3, the outer surface of the plain PAI membrane is quite smooth. The mean roughness is $R_a=0.99\pm0.15$ nm. There are no observable nodules even under ×100,000 magnification. However, for the interfacial polymerized membrane, it is clearly shown that nodules with a size of 20 to 50 nm are grown on the membrane surface. Therefore, the membrane possesses a much rougher outer surface ($R_a=3.00\pm0.30$ nm), which implies a thin layer polymerized by PEI and IPC is formed on top of the membrane.

The water contact angle of the plain PAI dual-layer hollow fiber membrane support is $56.0\pm4.5^\circ$, much lower than that of plain PAI hollow fiber membrane, i.e. $87.9\pm2.5^\circ$, which is shown in Table 5.3 of Chapter 5. The reason for the increased hydrophilicity can be explained by the migration of hydrophilic PEG polymer from the inner layer to the outer layer during the phase separation process. After interfacial polymerization, the contact angle decreases further to $41.7\pm0.5^\circ$, which is comparable to that of

commercial hydrophilic NF membranes, for example, Desal5DL.[135] The improved

hydrophilicity mainly arises from the increased amount of amine groups brought by

hyperbranched polyethyleneimine [124].
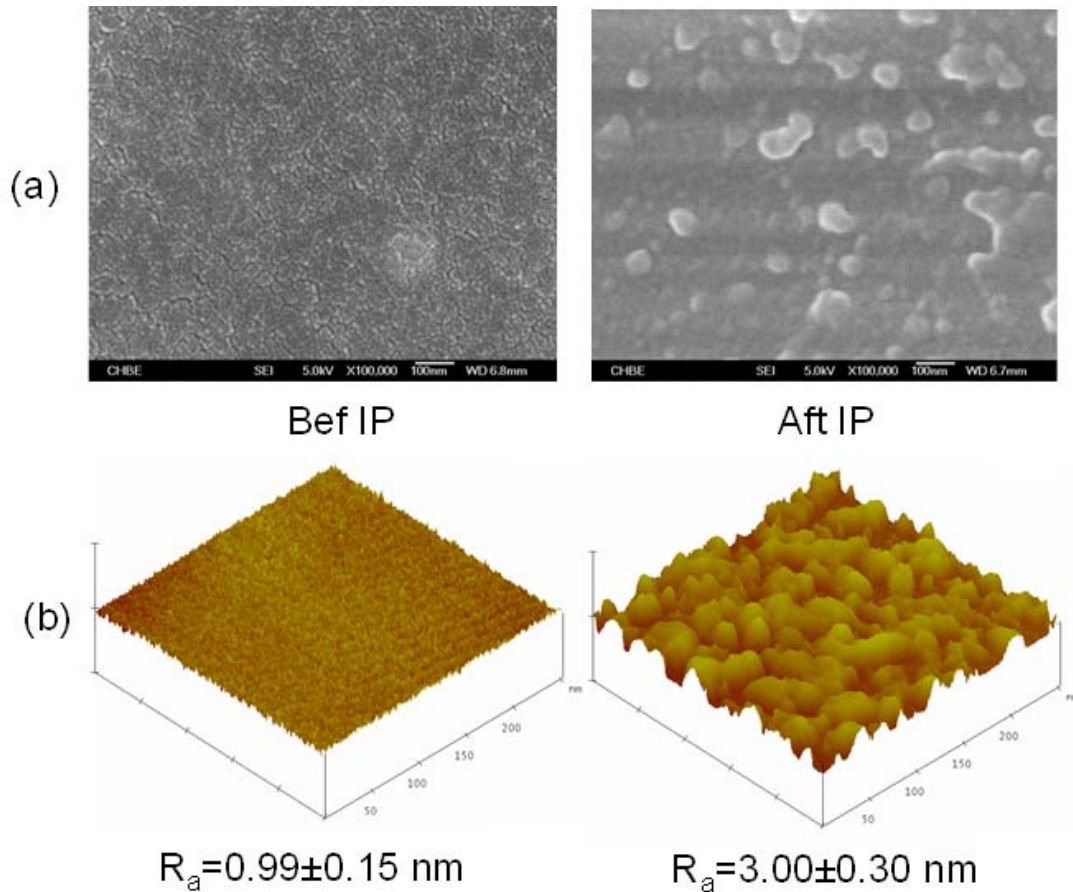
Figure 6.3. (a) FESEM and (b) AFM images of the outer surface before and after interfacial polymerization.

6.3.4 Effects of interfacial polymerization on pure water permeability, pore size, pore size distribution and molecular weight cutoff

The interfacial polymerized and the plain PAI dual-layer hollow fiber membrane were

then characterized by the solute transport method with a series of organic solutes

(Table 6.1), as described in the experimental section. The relationship between solute

rejection and solute Stokes radius is shown on the log-normal probability graph in

Figure 6.4. The mean effective pore radius r_p at $R_T = 50\%$, the MWCO and the geometric standard deviation σ_p were calculated from Figure 6.4 and summarized in Table 6.4. The PWP, which were obtained from Eq. (6.1), are also listed in Table 6.4. The cumulative pore size distribution curves and probability density function curves, calculated using the solute transport method are depicted in Figures 6.5 (a) and (b), respectively.
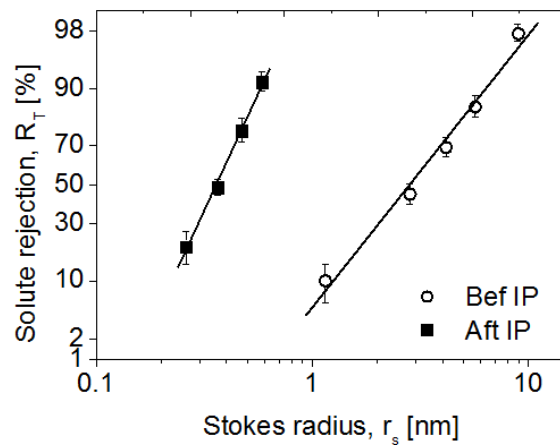
Figure 6.4. Rejections of neutral organic solutions by the membranes before and after interfacial polymerization.

Table 6.4. Mean effective pore radius (r_p), geometric standard deviation (σ_p), molecular weight cut off (MWCO), and pure water permeability (PWP) of the membrane before and after interfacial polymerization.

ID	r_p (nm)	σ_p (-)	MWCO (Da)	PWP ($lm^{-2}bar^{-1}h^{-1}$)
Bef IP	2.82	1.89	42000±1000	43.25
Aft IP	0.36	1.44	500±50	4.85

(The feed solution concentration: 200ppm, pH 5.75. Pressure:5 bar)
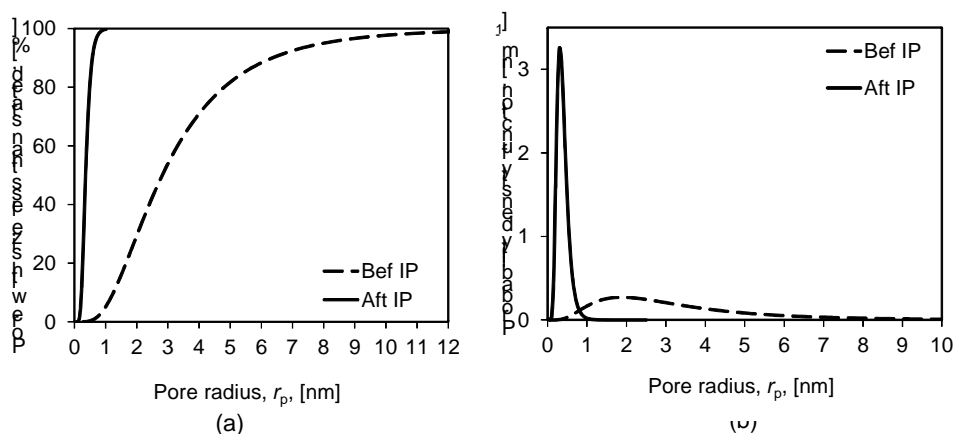
Figure 6.5. (a) Cumulative pore size distribution and (b) probability density function of the membranes before and after interfacial polymerization.

The plain PAI membrane has a mean effective pore radius about 2.82 nm and a MWCO around 46.2 KDa. The interfacial polymerized NF membrane has a sharp pore size distribution with a mean effective pore radius of 0.36 nm and MWCO of 489 Da. Nearly 100% pores are smaller than 1 nm, as illustrated in Figure 6.5 (b). In Chapter 5, we developed NF membranes by cross-linking PAI hollow fibers with PEI. The MWCO and PWP of those NF membranes are 912 to 1278 and PWP of 3.58 to 6.37 $lm^{-2}bar^{-1}h^{-1}$, respectively. However, the membrane developed here by interfacial polymerization shows a much smaller MWCO with similar PWP, i.e. 4.85 $lm^{-2}bar^{-1}h^{-1}$. This may be because the interfacial polymerized network formed with PEI and IPC (Figure 6.6) can eliminate defects or large pores on the membrane surface, thus increase solute rejections. However, for the cross-link method, if the pore size distribution of the membrane substrate is not narrow enough, there may be still some small defects after cross-link, leading to insufficient solute rejections compared to interfacial polymerization. Therefore, the interfacial polymerization method allows the membrane substrate has larger pores than the cross-link method. By preparing less concentrating dope solutions during the spinning process, one can get more porous membrane substrates to reduce the water transport resistance. The results suggest that

114

the membrane structure and subsequent separation performance can be manipulated effectively through interfacial polymerization of PEI and IPC.
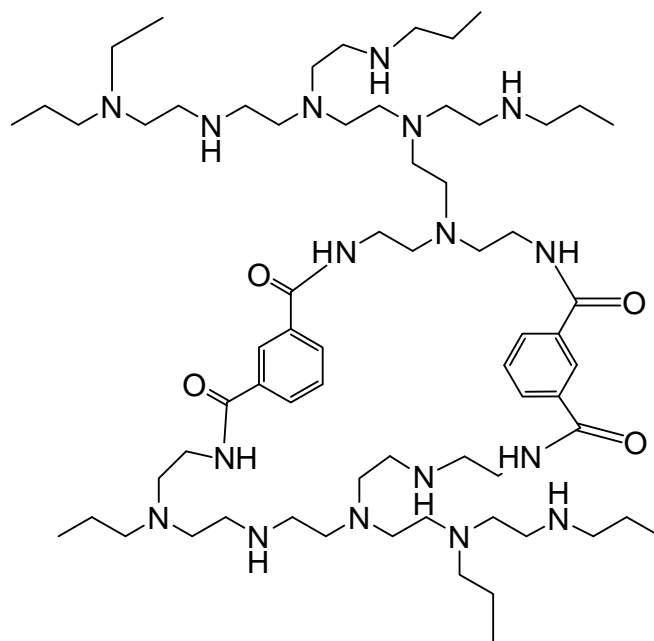
Figure 6.6. The possible chemical structure of the interfacial polymerized network formed with hyperbranched polyethyleneimine and isophthaloyl chloride.

6.3.5 Rejections of salt solutions by the PAI NF dual-layer hollow fiber membranes

The charge properties of the NF hollow fiber membranes before and after interfacial polymerization were characterized by testing the rejections of four kinds of electrolytes at the same molar concentration (1 mM), pH (5.75) and pressure (5 bar). As shown in Figure 6.7, the salt rejections of the plain PAI membrane decrease in the order $R(Na_2SO_4) > R(MgSO_4) > R(NaCl) > R(MgCl_2)$. This indicates that the plain PAI support is negatively charged at neutral pH, according to the Donnan exclusion principle [89]. The result is also consistent with zeta-potential tests, as shown in Chapter 3 and Chapter 5, demonstrating that the isoelectric point of plain PAI membranes is about 3.2 to 3.8.
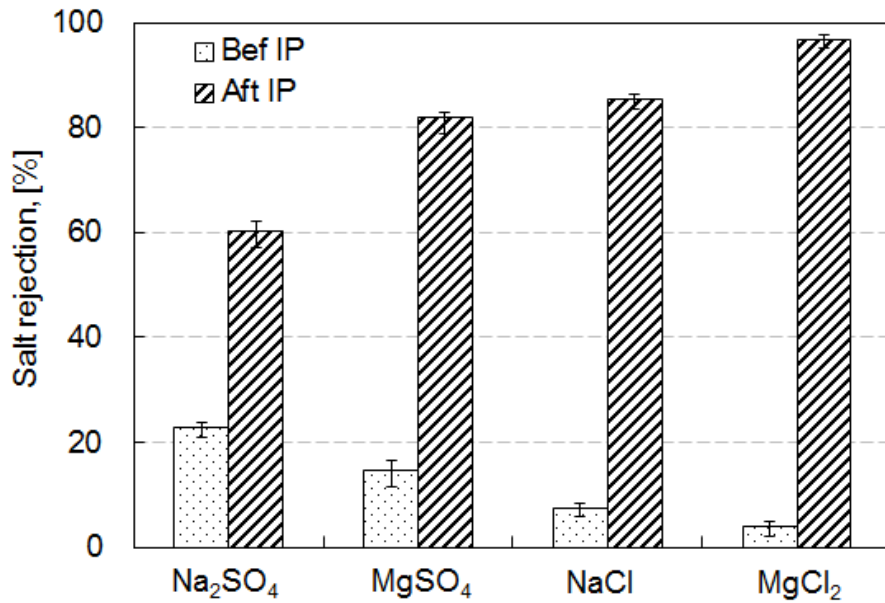
Figure 6.7. Salt rejections of the membranes before and after interfacial polymerization.
(The feed solution concentration: 1mM, pH 5.75. Pressure: 5 bar)

However, after interfacial polymerization, the order of salt rejections is interestingly reversed. It shows a higher rejection of divalent cations (Mg^{2+}) than monovalent cations (Na^+), and a lower rejection of divalent anions (SO_4^{2-}). This phenomenon is mainly determined by the Donnan exclusion effect [89], which implies that the membrane becomes positively charged after interfacial polymerization of PEI and IPC. Meanwhile, interfacial polymerization dramatically increases the rejection of $MgCl_2$, NaCl and $MgSO_4$ through a stronger steric hindrance effect imposed by the formation of the dense selective layer. A high rejection of $MgCl_2$ was achieved at more than 96.17%.

6.3.6 Rejections of dye solutions by the PAI NF dual-layer hollow fiber membranes

In order to study the effect of solute charge on the performance of the interfacial polymerized NF membrane, two types of dye solutions, i.e. safranin O ($C_{20}H_{19}N_4^+$, Cl^-,

350.84 Da) and orange II sodium salt ($C_{16}H_{11}N_2O_4S^-$, Na^+, 350.32 Da), were chosen as model solutions. Both of them share very similar molecular weights. The charge of safranin is positive while that of orange II is negative. The utility of the NF membrane for removal of these dyes from water is demonstrated in Figure 6.8. It is interesting to observe that the rejections for both of the dyes are superior to either NaCl (R_T=85.5%) or saccharose (R_T=76.4%, MW=342 Da), a neutral solute with similar molecular weight to the dye molecules.

Solute rejections are generally governed by several parameters: (1) the membrane pore size; (2) the size of the solute; (3) the solute-membrane charge interactions and (4) the solute electro-neutrality. The membrane pore size will not be considered for the comparison of solute rejections, as the employed membranes are fabricated in the same method. The superior rejections of the dye solutions over NaCl indicate that steric-hindrance effect is important for molecules with different sizes or molecular weights.
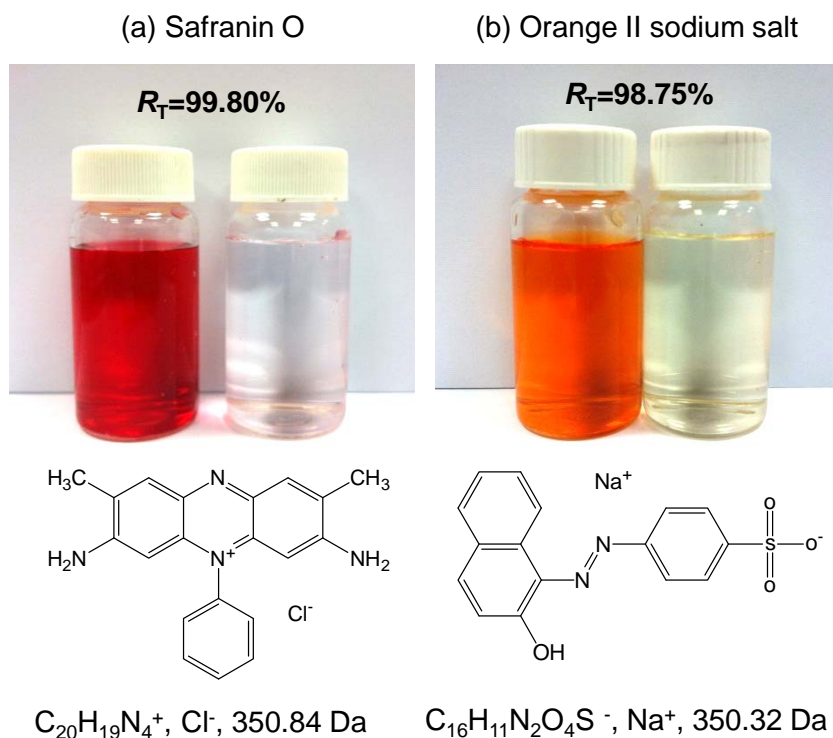
Figure 6.8. Rejection of (a) positively charged dye, Safranin O, and (b) negatively charged dye, Orange II sodium salt, solutions. The left bottle is the feed solution while the right bottle is the permeate. (The feed solution concentration: 50ppm, pH 5.75. Pressure:5 bar)

However, for the molecules with similar size, other mechanisms need to be taken into account. The molecular dimensions of safranin O, orange II sodium salt and saccharose, calculated with ChemBio3D software employing MM2 force-field parameters, are listed in Table 6.5. The molecular sizes of these molecules are not significantly different. The main difference between them is the solute-membrane charge interaction. According to the Donnan exclusion principle, a charged membrane tends to exclude co-ions and favors sorption of counter-ions [89]. As depicted in the previous section, the selective layer of the interracial polymerized membrane is positively charged while the support is negatively charged. In aqueous solutions, safranin O is dissociated into the form of $C_{20}H_{19}N_4^+$ and Cl^- ions. Therefore, it is expected that the positively charged selective layer preferentially rejects $C_{20}H_{19}N_4^+$ while let Cl^- pass through. However, in order to maintain the electroneutrality on both

sides of the membrane, the tendency of Cl$^-$ passage is dramatically lowered because $C_{20}H_{19}N_4^+$ is too large to pass through the membrane. Such situation is changed when filtrates Orange II sodium salt whose dissociated ions are $C_{16}H_{11}N_2O_4S^-$ and Na$^+$. One may predict the rejection of this dye molecule would be much lower than safranin O, or even lower than the neutral saccharose, as the dye functional ion, i.e. $C_{16}H_{11}N_2O_4S^-$, is negatively charged, which is the counter-ion of the positively charged selective layer. However, the observed high rejection (98.75%) is probably due to coupling effects from the following reasons (1) the charge repulsion between Na$^+$ and the positively charged membrane may decrease the sorption of $C_{16}H_{11}N_2O_4S^-$ into the membrane because of solute electro-neutrality; (2) the negatively charged support layer may serve as a secondary barrier to prevent $C_{16}H_{11}N_2O_4S^-$ from passing through the membrane. An evidence to prove the proposed mechanism is that the normalized water flux (Table 6.5), which is the ratio of permeate flux of the dye solution, J (L m^{-2} h^{-1}), to the pure water flux, J_0 (L m^{-2} h^{-1}), of orange II sodium salt is lower than that of safranin O and saccharose, implying that certain amount of the solute is retained in the selective layer, which leading to a more severe fouling. Compared to the dye molecules, the neutral solute saccharose exhibits the lowest rejection (76.39%) because size-exclusion is the only dominating mechanism. An illustration of the mechanisms for rejection of various molecules is shown in Figure 6.9.

Table 6.5. Structures, molecular dimensions, rejections and fluxes of dye molecules and saccharose filtrated by the interfacial polymerized membrane.

Solute	Safranin O	Orange II sodium salt	Saccharose
Molecular formula	$C_{20}H_{19}N_4^+,Cl^-$	$C_{16}H_{11}N_2O_4S^-,Na^+$	$C_{12}H_{22}O_{11}$
MW (Da)	350.84	350.32	342.30
Size (nm^3)	$1.10\times0.95\times0.49$	$1.10\times0.63\times0.70$	$1.05\times0.66\times0.73$
Rejection, (%)	99.80	98.75	76.39
Flux, ($L\ m^{-2}h^{-1}$)	22.71	20.60	21.35
J/J_0, (%)	93.65	84.95	88.04

$J_0 = 24.25\ L\ m^{-2}h^{-1}$
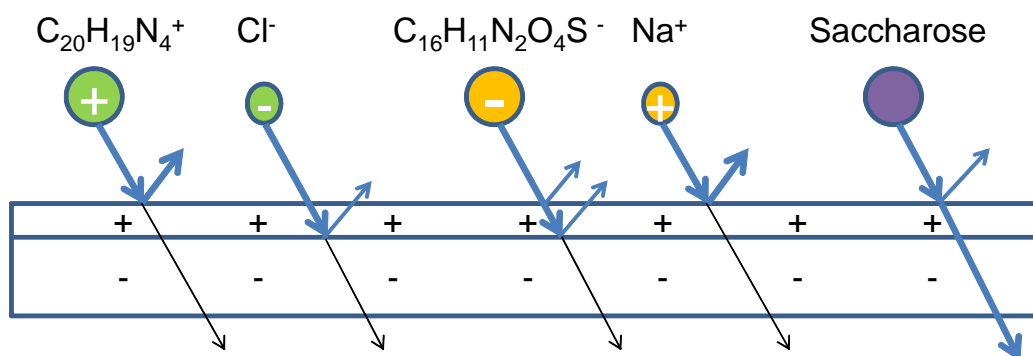
Figure 6.9. A schematic diagram showing solute transport through interfacial polymerized NF membranes.

6.3.7 Rejection of cephalexin by the PAI NF dual-layer hollow fiber membranes

The effect of pH on the NF performance of the interfacial polymerized membrane was studied with a pharmaceutical active compound, i.e. cephalexin. As an amphoteric electrolyte molecule, in aqueous solutions cephalexin acts as both base (proton acceptor) and acid (proton donor), given that cephalexin molecules include amino (–NH$_2$) and carboxyl (–COOH) groups. Based on the pK_a values of cephalexin (Figure 6.10), the fraction of different ionization states at different pH values can be calculated according to the method described in Chapter 3. Similar to amino acids, the

ionization states of cephalexin molecules is dependent on pH in the aqueous solution, as shown in Figure 6.11. The molecule is positively charged below pH 2.56 and negatively charged above pH 5.88. Within the range of 2.56 < pH < 5.88, the molecule becomes net neutral.
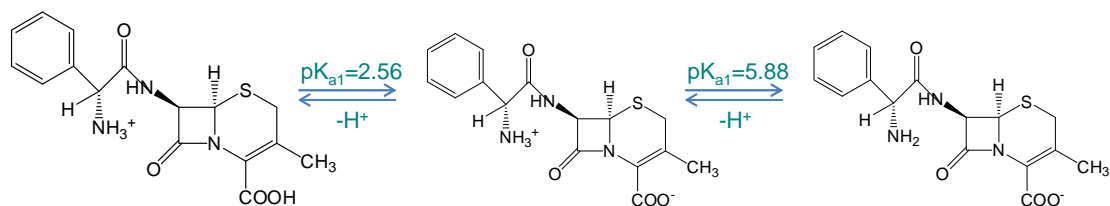
Figure 6.10. Ionization states of cephalexin at various pH values.
($pK_{a,1}$=2.56, $pK_{a,2}$=5.88)

The cephalexin rejection of the plain PAI membrane, as shown in Figure 6.11, is below 20% in a wide pH range. This is mainly because the pore size of this UF membrane (MWCO=42.6 KDa) is too large to prevent the molecule from passing through. After interfacial polymerization, the cephalexin rejection is significantly improved, because of the reduction of the pore radius from 2.82 to 0.36 nm. The result also shows a strong effect of pH on cephalexin rejection. As pH increases, the cephalexin molecule changes from positive, to neutral then to negative. Thus the positively charged NF membrane shows the highest rejection at low pH but the rejection decreases as the pH increases, which is in accordance to the Donnan exclusion principle, as discussed in previous sections.
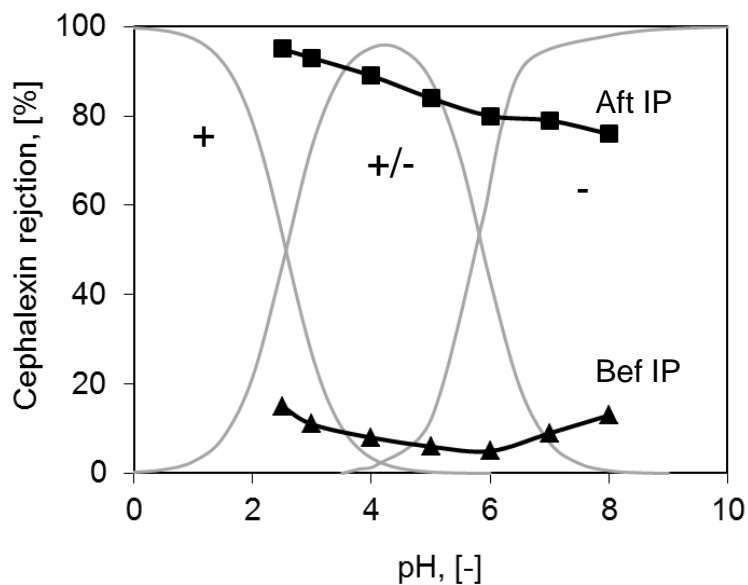
Figure 6.11. Cephalexin rejection of the membranes before and after interfacial polymerization as a function of pH.
(The feed solution concentration: 200 ppm. Pressure:5 bar)

6.4 Conclusions

The work in this chapter provides a novel thin-film composite NF membrane via interfacial polymerization of PEI and IPC on a Torlon® PAI dual-layer hollow fiber substrate. In order to obtain a highly permeable substrate with sufficient mechanical strength, a sandwich-like cross-section structure is proposed and achieved for the first time. The ultrathin spongy-like outer layer and the middle layer with asymmetric finger-like macrovoids are caused by a combined effect of the instantaneous liquid–liquid demixing, which is induced by adding methanol into the outer dope, and the utilization of a less concentrated inner dope to facilitate the growth of macrovoids. The spongy-like fully porous inner layer is mainly because of the delayed demixing induced by incorporation of PEG 2000 in the inner dope.

It is observed that both molecular weight and concentration of PEI play an important role in determining the NF performance of the interfacial polymerized membrane. As the PEI molecular weight increases, the membrane tends to have a smaller pore size leading to an increased rejection but a decreased flux. For a given PEI molecular weight, an optimum rejection is observed at a certain PEI concentration after which point no significant improvement can be attained but the water permeability is sacrificed. The optimized NF membrane has a mean effective pore radius of 0.36 nm, molecular weight cut off of 489 Da, and pure water permeability of 4.85 $\text{lm}^{-2}\text{bar}^{-1}\text{h}^{-1}$.

As demonstrated by a series of NF tests with single salt solutions, the NF membrane possesses a positively charged selective layer and a negatively charged substrate. Due to this double-repulsion effect, together with the steric-hindrance and the solute electro-neutrality effects, the newly developed NF membrane shows superior rejections for both positively and negatively charged dye molecules. By appropriate adjustment of feed pH, the zwitterionic antibiotic cephalexin can also be effectively removed from water.

CHAPTER SEVEN

CONCLUSIONS AND RECOMMENDATIONS

7. 1 Conclusions

In this thesis, fabrication of NF hollow fiber membranes with Torlon® polyamide-imide materials was systematically studied. It is found that membrane performance is related to both of the membrane structures and the properties of the membrane materials. Therefore, the first part of the thesis, including Chapter 2 to Chapter 4, focuses mainly on the fundamental study of the membrane structure effects on pore size, pore size distribution and water permeability. In order to gain more insights on the newly developed membrane, the charge properties of the resultant NF membrane was also systematically studied. After obtaining such fundamental knowledge, in the second part of the thesis, i.e. Chapter 5 and 6, chemical functionalization of the membrane materials were further explored in order to investigate possible ways to enhance the NF membrane performance for the applications in pharmaceutical and other areas. The relationship between the NF performance and membrane properties were also discussed in depth.

The Torlon® polyamide-imide hollow fiber membranes developed in this thesis were formed by phase inversion technique in the dry-jet wet-spinning process. It was found that the external stretching is an effective method to control the membrane structure, nano-pore formation, and nanofiltration performance. Through external stretching, the solute rejections and the water permeability is simultaneously increased, because a

high take-up speed favors the "spinodal decomposition" rather than "nucleation and growth", which increases surface porosity and reduces the membrane pore size.

Zeta-potential measurements indicate that the isoelectric point of Torlon® PAI membrane is pH 3.2, above which the membrane is negatively charged. Therefore, the Torlon® PAI NF membranes show higher rejections to divalent anions, lower rejections to monovalent ions, and the lowest rejections to divalent anions. Therefore, based on Donnan effect, the NF membrane was applied to effective separate Cl^- and SO_4^{2-}, and reject 99.5% glutathione molecules. The membrane holds great potential for the effective recovery, concentration and purification of glutathione and like molecules from aqueous solution containing lower molecular weight impurities.

In order to combine the advantages of higher performance polymer and conventional low-cost polymers, a PAI/CA dual-layer hollow fiber membrane was fabricated through co-extruding two polymer dopes from a triple-orifice spinneret. The delamination issue, which is the challenge for the real applications of dual-layer hollow fiber membranes, was solved by properly select non-solvent additives in both of the outer dope and the inner dope. This method not only increases the precipitation rate of the inner layer but also increases the viscosity of the outer layer. Through this method, the membrane pore structure was also controlled. The results in the thesis demonstrate that by properly selecting the non-solvent additives, it is able to simultaneously increase the solute rejection and the water permeability.

PEI modification significantly influences on NF performance through the mechanisms of size exclusion, charge repulsion and solute-membrane affinity. After the PEI

modification, the PAI hollow fiber membranes may possess the following characteristics: (1) the pore size becomes smaller, leading to a higher ciprofloxacin rejection because of the size-exclusion mechanism; (2) the membrane becomes more hydrophilic, resulting in less severe adsorption; (3) the membrane surface becomes positively charged. As a result of these synergic effects, the rejection of ciprofloxacin is substantially enhanced. Furthermore, experimental results show that an increase in PEI molecular weight enhances the rejection, and fouling tendency.

In order to fabricate high performance novel thin-film composite NF membranes, both the sublayer structure and the parameters of interfacial polymerization plays important role. A sandwich-like cross-section structure, which consists of a layer with asymmetric finger-like macrovoids in the middle and two thin spongy-like layers at the outer and inner edge, provides the membrane with highly water permeable channels and sufficient mechanical strength. It was also found that both molecular weight and concentration of PEI are important for the interfacial polymerization. There exists optimized molecular weight and concentration that result a NF membrane with a mean effective pore radius of 0.36 nm, molecular weight cut off of around 500 Da, and pure water permeability of 4.85 $lm^{-2}bar^{-1}h^{-1}$. The resultant NF membrane exhibits a unique double-repulsion effect because the membrane the NF membrane possesses a positively charged selective layer and a negatively charged substrate. As a result, the membrane shows superior rejections for both positively and negatively charged molecules. Therefore, the double repulsive membrane has great potential to treat waste water that consists of compounds with diverse charge properties.

In summary, this thesis demonstrates that Torlon® PAI is a promising material for the fabrication of NF hollow fiber membranes. The fundamental studies provide guidelines for future development of novel high-performance NF membranes through design of the membrane structure and functionalization of the membrane material. There is great potential to extend this study into applications of NF membranes into sustainable pharmaceutical manufacture and other various applications

7.2 Recommendations

Based on the experimental results obtained, the discussions presented and the conclusions made from this research, the following recommendations may be interesting for future investigation related to this topic:

1) Because the polyethyleneimine functionalized NF membranes possess small pore size and positively charged surface, they have high rejection properties toward divalent cations. Therefore, it is valuable to extend the present work to the application of the positively charged PAI NF membranes in the removal of positively charged pharmaceutical active compounds such as norfloxacin and enrofloxacin, and some positively charged heavy metal ions, such as Cu^{2+}, Zn^{2+} and so on.

2) The double –repulsive thin-film composite membranes have superior rejections to both cations and anions. Therefore, it has great potential to treat waste water that consists of compounds with diverse charge properties.

3) Recently, there is a growing need to develop solvent resistant nanofiltration membranes for solvent recovery in pharmaceutical, petrochemical and other

industries. Such applications request the membranes to be stable in organic solvents. The polyethyleneimine cross-linked PAI NF membrane may have excellent solvent stability for a wide range of organic solvent. Therefore, it will be interesting to further explore the present work to the application of PAI NF membranes in the organic solvent system.

4) The elongation induced nanopore evolution and the dual-layer hollow fiber membranes provides us ways to enhance water permeability of the substructures, while the polyethyleneimine functionalization is able to improve the salt rejections. Therefore, it is possible to fabricate a high-flux and low salt leakage forward osmosis membranes for seawater desalination and pharmaceutical concentration.

5) Couple the PAI NF hollow fiber membranes with reactor to form membrane reactors for pharmaceutical synthesis and removal of natural organic matters.

6) Explore the commercialization of the PAI NF hollow fiber membrane in the separation of pharmaceuticals and waste water treatment.

BIBLIOGRAPHY

[1] M.A. Shannon, P.W. Bohn, M. Elimelech, J.G. Georgiadis, B.J. Marinas, A.M. Mayes, Science and technology for water purification in the coming decades, Nature, 452 (2008) 301-310.

[2] S. Sarkar, A.K. Sengupta, P. Prakash, The Donnan Membrane Principle: Opportunities for Sustainable Engineered Processes and Materials, Environ. Sci. Technol., 44 (2010) 1161-1166.

[3] B. Kartal, J.G. Kuenen, M.C.M. van Loosdrecht, Sewage Treatment with Anammox, Science, 328 (2010) 702-703.

[4] P. Anastas, N. Eghbali, Green Chemistry: Principles and Practice, Chem. Soc. Rev., 39 (2010) 301-312.

[5] S.P. Nunes, K.V. Peinemann, Membrane Technology in the Chemical Industry, Wiley-VCH Verlag GmbH, Weinheim, 2001.

[6] M.H.V. Mulder, Basic principles of membrane technology, Kluwer academic publishers, Netherlands, 1996.

[7] A.I. Schäfer, A.G. Fane, T.D. Waite, Nanofiltration - Principles and Applications, Elsevier, Oxford, UK, 2002.

[8] B. Van der Bruggen, C. Vandecasteele, T. Van Gestel, W. Doyen, R. Leysen, A review of pressure-driven membrane processes in wastewater treatment and drinking water production, Environ. Prog., 22 (2003) 46-56.

[9] K. Sutherland, Developments in filtration: What is nanofiltration?, Filtr. Sep., 45 (2008) 32-35.

[10] K.Y. Wang, T.S. Chung, J.J. Qin, Polybenzimidazole (PBI) nanofiltration hollow fiber membranes applied in forward osmosis process, J. Membr. Sci., 300 (2007) 6-12.

[11] W. Peng, I.C. Escobar, Rejection efficiency of water quality parameters by reverse osmosis and nanofiltration membranes, Environ. Sci. Technol., 37 (2003) 4435-4441.

[12] K.K. Sirkar, Application of membrane technologies in the pharmaceutical industry, Curr. Opin. Drug Discov. Devel., 3 (2000) 714-722.

[13] K.Y. Wang, T.S. Chung, Polybenzimidazole nanofiltration hollow fiber for cephalexin separation, AICHE J., 52 (2006) 1363-1377.

[14] D.F. Stamatialis, B.J. Papenburg, M. Girones, S. Saiful, S.N.M. Bettahalli, S. Schmitmeier, M. Wessling, Medical applications of membranes: Drug delivery, artificial organs and tissue engineering, J. Membr. Sci., 308 (2008) 1-34.

[15] I. Sereewatthanawut, A.T. Boam, A.G. Livingston, Polymeric membrane nanofiltration and its application to separations in the chemical industries, Macromol. Symp., 264 (2008) 184-188.

[16] L.S. White, Development of large-scale applications in organic solvent nanofiltration and pervaporation for chemical and refining processes, J. Membr. Sci., 286 (2006) 26-35.

[17] S. Ghizellaoui, A. Chibani, Use of nanofiltration for partial softening of very hard water, Desalination, 179 (2005) 315-322.

[18] E.E. Chang, Y.W. Chen, Y.L. Lin, P.C. Chiang, Reduction of natural organic matter by nanofiltration process, Chemosphere, 76 (2009) 1265-1272.

[19] K.Y. Wang, T.S. Chung, Fabrication of polybenzimidazole (PBI) nanofiltration hollow fiber membranes for removal of chromate, J. Membr. Sci., 281 (2006) 307-315.

[20] J. Radjenovic, M. Petrovic, F. Ventura, D. Barcelo, Rejection of pharmaceuticals in nanofiltration and reverse osmosis membrane drinking water treatment, Water Res., 42 (2008) 3601-3610.

[21] N.F. Ghazali, F.C. Ferreira, A.J.P. White, A.G. Livingston, Enantiomer separation by enantioselective inclusion complexation-organic solvent nanofiltration, Tetrahedron-Asymmetry, 17 (2006) 1846-1852.

[22] P. Vandezande, L.E.M. Gevers, I.F.J. Vankelecom, Solvent resistant nanofiltration: separating on a molecular level, Chem. Soc. Rev., 37 (2008) 365-405.

[23] S. Chakraborty, M.K. Purkait, S. DasGupta, S. De, J.K. Basu, Nanofiltration of textile plant effluent for color removal and reduction in COD, Sep. Purif. Technol., 31 (2003) 141-151.

[24] R. Andras, J.M. Wang, C. Jozsef, H. Cecilia, V. Gyula, Experimental Investigation of the Sweet Whey Concentration by Nanofiltration, Food and Bioprocess Technology, 4 (2011) 702-709.

[25] K. Pan, Q. Song, L. Wang, B. Cao, A study of demineralization of whey by nanofiltration membrane, Desalination, 267 (2011) 217-221.

[26] M. Manttari, K. Viitikko, M. Nystrom, Nanofiltration of biologically treated effluents from. the pulp and paper industry, J. Membr. Sci., 272 (2006) 152-160.

[27] R.M. Gould, L.S. White, C.R. Wildemuth, Membrane separation in solvent lube dewaxing, Environ. Prog., 20 (2001) 12-16.

[28] S.S. Luthra, X.J. Yang, L.M.F. dos Santos, L.S. White, A.G. Livingston, Homogeneous phase transfer catalyst recovery and re-use using solvent resistant membranes, J. Membr. Sci., 201 (2002) 65-75.

[29] Q. Yang, K.Y. Wang, T.S. Chung, A novel dual-layer forward osmosis membrane for protein enrichment and concentration, Sep. Purif. Technol., 69 (2009) 269-274.

[30] D.W. Kolpin, E.T. Furlong, M.T. Meyer, E.M. Thurman, S.D. Zaugg, L.B. Barber, H.T. Buxton, Pharmaceuticals, hormones, and other organic wastewater contaminants in US streams, 1999-2000: A national reconnaissance, Environ. Sci. Technol., 36 (2002) 1202-1211.

[31] S.T. Glassmeyer, E.T. Furlong, D.W. Kolpin, J.D. Cahill, S.D. Zaugg, S.L. Werner, M.T. Meyer, D.D. Kryak, Transport of chemical and microbial compounds from known wastewater discharges: Potential for use as indicators of human fecal contamination, Environ. Sci. Technol., 39 (2005) 5157-5169.

[32] S. Beier, S. Koster, K. Veltmann, H.F. Schroder, J. Pinnekamp, Treatment of hospital wastewater effluent by nanofiltration and reverse osmosis, Water Sci. Technol., 61 (2010) 1691-1698.

[33] X.Y. Wei, Z. Wang, F.H. Fan, J.X. Wang, S.C. Wang, Advanced treatment of a complex pharmaceutical wastewater by nanofiltration: Membrane foulant identification and cleaning, Desalination, 251 (2010) 167-175.

[34] B. Van der Bruggen, M. Manttari, M. Nystrom, Drawbacks of applying nanofiltration and how to avoid them: A review, Sep. Purif. Technol., 63 (2008) 251-263.

[35] H. Sies, Glutathione and its role in cellular functions, Free Radic. Biol. Med., 27 (1999) 916-921.

[36] K. Sakato, H. Tanaka, Advanced control of glutahione fermentation process, Biotechnol. Bioeng., 40 (1992) 904-912.

[37] T. Gotoh, H. Iguchi, K.C. Kikuchi, Separation of glutathione and its related amino acids by nanofiltration, Biochem. Eng. J., 19 (2004) 165-170.

[38] Z.M. Qiang, C. Adams, Potentiometric determination of acid dissociation constants (pK(a)) for human and veterinary antibiotics, Water Res., 38 (2004) 2874-2890.

[39] K. Hylton, M. Sangwan, S. Mitra, Microscale membrane extraction of diverse antibiotics from water, Anal. Chim. Acta, 653 (2009) 116-120.

[40] E.M. Golet, A.C. Alder, W. Giger, Environmental exposure and risk assessment of fluoroquinolone antibacterial agents in wastewater and river water of the Glatt Valley Watershed, Switzerland, Environ. Sci. Technol., 36 (2002) 3645-3651.

[41] L. Aristilde, A. Melis, G. Sposito, Inhibition of Photosynthesis by a Fluoroquinolone Antibiotic, Environ. Sci. Technol., 44 (2010) 1444-1450.

[42] J.B. Belden, J.D. Maul, M.J. Lydy, Partitioning and photo degradation of ciprofloxacin in aqueous systems in the presence of organic matter, Chemosphere, 66 (2007) 1390-1395.

[43] P. van der Marel, A. Zwijnenburg, A. Kemperman, M. Wessling, H. Temmink, W. van der Meer, Influence of membrane properties on fouling in submerged membrane bioreactors, J. Membr. Sci., 348 66-74.

[44] R.J. Petersen, Composite reverse-osmosis and nanofiltration membranes, J. Membr. Sci., 83 (1993) 81-150.

[45] B. Van der Bruggen, Chemical Modification of Polyethersulfone Nanofiltration Membranes: A Review, J. Appl. Polym. Sci., 114 (2009) 630-642.

[46] T. Shintani, H. Matsuyama, N. Kurata, T. Ohara, Development of a chlorine-resistant polyamide nanofiltration membrane and its field-test results, J. Appl. Polym. Sci., 106 (2007) 4174-4179.

[47] R.W. Baker, Membrane Technology and Applications, John Wiley & Sons Ltd., West Sussex, England, 2004.

[48] G. Artug, Modelling and simulation of Nanofiltration membranes, in: Technical University of Hamburg Hargurg, 2007.

[49] G.P. Robertson, M.D. Guiver, M. Yoshikawa, S. Brownstein, Structural determination of Torlon (R) 4000T polyamide-imide by NMR spectroscopy, Polymer, 45 (2004) 1111-1117.

[50] Y. Wang, L.Y. Jiang, T. Matsuura, T.S. Chung, S.H. Goh, Investigation of the fundamental differences between polyamide-imide (PAI) and polyetherimide (PEI) membranes for isopropanol dehydration via pervaporation, J. Membr. Sci., 318 (2008) 217-226.

[51] M. Yoshikawa, A. Higuchi, M. Ishikawa, M.D. Guiver, G.P. Robertson, Vapor permeation of aqueous 2-propanol solutions through gelatin/Torlon((R)) poly(amide imide) blended membranes, J. Membr. Sci., 243 (2004) 89-95.

[52] A. Higuchi, M. Yoshikawa, M.D. Guiver, G.P. Robertson, Vapor permeation and pervaporation of aqueous 2-propanol solutions through the Torlono (R) poly(amide imide) membrane, Sep. Sci. Technol., 40 (2005) 2697-2707.

[53] M.M. Teoh, T.S. Chung, K.Y. Wang, M.D. Guiver, Exploring Torlon/P84 co-polyamide-imide blended hollow fibers and their chemical cross-linking modifications for pervaporation dehydration of isopropanol, Sep. Purif. Technol., 61 (2008) 404-413.

[54] N. Peng, T.S. Chung, The effects of spinneret dimension and hollow fiber dimension on gas separation performance of ultra-thin defect-free Torlon (R) hollow fiber membranes, J. Membr. Sci., 310 (2008) 455-465.

[55] M.R. Kosuri, W.J. Koros, Defect-free asymmetric hollow fiber membranes from Torlon (R), a polyamide-imide polymer, for high-pressure CO_2 separations, J. Membr. Sci., 320 (2008) 65-72.

[56] N. Peng, T.-S. Chung, J.-Y. Lai, The rheology of Torlon[®] solutions and its role in the formation of ultra-thin defect-free Torlon[®] hollow fiber membranes for gas separation, J. Membr. Sci., 326 (2009) 608-617.

[57] J.E. Wijaya, Formation and characterization of solvent resistant nanofiltration membranes, in, University of Ottawa, 2005.

[58] B. van der Bruggen, J. Schaep, D. Wilms, C. Vandecasteele, A comparison of models to describe the maximal retention of organic molecules in nanofiltration, Sep. Sci. Technol., 35 (2000) 169-182.

[59] P. Aimar, M. Meireles, V. Sanchez, A contribution to the translation of retention curves into pore-size distributions for sieving membranes, J. Membr. Sci., 54 (1990) 321-338.

[60] W.R. Bowen, A.W. Mohammad, Characterization and prediction of nanofiltration membrane performance - A general assessment, Chem. Eng. Res. Des., 76 (1998) 885-893.

[61] O. Kedem, A. Katchalsky, Thermodynamic analysis of the permeability of biological membranes to non-electrolytes, Biochim. Biophys. Acta, 27 (1958) 229-246.

[62] K.S. Spiegler, O. Kedem, Thermodynamics of hyperfiltration (reverse osmosis): criteria for efficient membranes, Desalination, 1 (1966) 311-326.

[63] X.L. Wang, T. Tsuru, S. Nakao, S. Kimura, The electrostatic and steric-hindrance model for the transport of charged solutes through nanofiltration membranes, J. Membr. Sci., 135 (1997) 19-32.

[64] X.Y. Qiao, T.S. Chung, Diamine modification of P84 polyimide membranes for pervaporation dehydration of isopropanol, AICHE J., 52 (2006) 3462-3472.

[65] R.W. Baker, Membrane Technology and Applications, John Wiley & Sons Ltd., West Sussex, England, 2004.

[66] M.J. Elhibri, D.R. Paul, Effects of uniaxial drawing and heat-treatment on gas sorption and transport in PVC, J. Appl. Polym. Sci., 30 (1985) 3649-3678.

[67] S.J. Shilton, G. Bell, J. Ferguson, The rheology of fiber spinning and the properties of hollow-fiber membranes for gas separation, Polymer, 35 (1994) 5327-5335.

[68] T.S. Chung, W.H. Lin, R.H. Vora, The effect of shear rates on gas separation performance of 6FDA-durene polyimide hollow fibers, J. Membr. Sci., 167 (2000) 55-66.

[69] A. Niwa, H. Kawakami, T. Kanamori, T. Shinbo, A. Kaito, S. Nagaoka, Surface orientation effect of asymmetric polyimide hollow fibers on their gas transport properties, J. Membr. Sci., 230 (2004) 141-148.

[70] J.J. Qin, J. Gu, T.S. Chung, Effect of wet and dry-jet wet spinning on the sheer-induced orientation during the formation of ultrafiltration hollow fiber membranes, J. Membr. Sci., 182 (2001) 57-75.

[71] W.L. Chou, M.C. Yang, Effect of take-up speed on physical properties and permeation performance of cellulose acetate hollow fibers, J. Membr. Sci., 250 (2005) 259-267.

[72] I.C. Omole, S.J. Miller, W.J. Koros, Increased molecular weight of a cross-linkable polyimide for spinning plasticization resistant hollow fiber membranes, Macromolecules, 41 (2008) 6367-6375.

[73] K.Y. Wang, D.F. Li, T.S. Chung, S.B. Chen, The observation of elongation dependent macrovoid evolution in single and dual-layer asymmetric hollow fiber membranes, Chem. Eng. Sci., 59 (2004) 4657-4660.

[74] K.C. Khulbe, T. Matsuura, Characterization of synthetic membranes by Raman spectroscopy, electron spin resonance, and atomic force microscopy; a review, Polymer, 41 (2000) 1917-1935.

[75] T.S. Chung, J.J. Qin, A. Huan, K.C. Toh, Visualization of the effect of die shear rate on the outer surface morphology of ultrafiltration membranes by AFM, J. Membr. Sci., 196 (2002) 251-266.

[76] J.E. Mark, Polymer Data Handbook, Oxford University Press, New York, 1999.

[77] R.X. Liu, X.Y. Qiao, T.S. Chung, Dual-layer P84/polyethersulfone hollow fibers for pervaporation dehydration of isopropanol, J. Membr. Sci., 294 (2007) 103-114.

[78] N. Peng, T.S. Chung, K.Y. Wang, Macrovoid evolution and critical factors to form macrovoid-free hollow fiber membranes, J. Membr. Sci., 318 (2008) 363-372.

[79] H.Z. Chen, Y.C. Xiao, T.S. Chung, Synthesis and characterization of poly (ethylene oxide) containing copolyimides for hydrogen purification, Polymer, 51 (2010) 4077-4086.

[80] K. Kokubo, K. Sakai, Evaluation of dialysis membranes using a tortuous pore model, AICHE J., 44 (1998) 2607-2619.

[81] S. Singh, K.C. Khulbe, T. Matsuura, P. Ramamurthy, Membrane characterization by solute transport and atomic force microscopy, J. Membr. Sci., 142 (1998) 111-127.

[82] T.-S. Chung, The limitations of using Flory-Huggins equation for the states of solutions during asymmetric hollow-fiber formation, J. Membr. Sci., 126 (1997) 19-34.

[83] Z.Z. Zhou, Y.C. Xiao, T.A. Hatton, T.S. Chung, Effects of spacer arm length and benzoation on enantioseparation performance of beta-cyclodextrin functionalized cellulose membranes, J. Membr. Sci., 339 (2009) 21-27.

[84] Y.C. Xiao, M.L. Chng, T.S. Chung, M. Toriida, S. Tamai, H.M. Chen, Y.C.J. Jean, Asymmetric structure and enhanced gas separation performance induced by in situ growth of silver nanoparticles in carbon membranes, Carbon, 48 (2010) 408-416.

[85] A.E. Childress, M. Elimelech, Effect of solution chemistry on the surface charge of polymeric reverse osmosis and nanofiltration membranes, J. Membr. Sci., 119 (1996) 253-268.

[86] M. Manttari, A. Pihlajamaki, M. Nystrom, Effect of pH on hydrophilicity and charge and their effect on the filtration efficiency of NF membranes at different pH, J. Membr. Sci., 280 (2006) 311-320.

[87] R.X. Liu, X.Y. Qiao, T.S. Chung, The development of high performance P84 co-polyimide hollow fibers for pervaporation dehydration of isopropanol, Chem. Eng. Sci., 60 (2005) 6674-6686.

[88] X.Y. Qiao, T.S. Chung, R. Rajagopalan, Zeolite filled P84 co-polyimide membranes for dehydration of isopropanol through pervaporation process, Chem. Eng. Sci., 61 (2006) 6816-6825.

[89] F.G. Donnan, Theory of membrane equilibria and membrane potentials in the presence of non-dialysing electrolytes, J. Membr. Sci., 100 (1995) 45-55.

[90] J. Schaep, B. Van der Bruggen, C. Vandecasteele, D. Wilms, Influence of ion size and charge in nanofiltration, Sep. Purif. Technol., 14 (1998) 155-162.

[91] X.Y. Qiao, T.S. Chung, W.F. Guo, T. Matsuura, M.M. Teoh, Dehydration of isopropanol and its comparison with dehydration of butanol isomers from thermodynamic and molecular aspects, J. Membr. Sci., 252 (2005) 37-49.

[92] L.L. Zhang, Y.C. Xiao, T.S. Chung, J.W. Jiang, Mechanistic understanding of CO2-induced plasticization of a polyimide membrane: A combination of experiment and simulation study, Polymer, 51 (2010) 4439-4447.

[93] H. Strathmann, Membrane separation processes: Current relevance and future opportunities, AIChE J., 47 (2001) 1077-1087.

[94] S.P. Nunes, K.-V. Peinemann, Membrane Technology in the Chemical Industry, Wiley-VCH Verlag GmbH, Weinheim, 2001.

[95] D.W. Wallace, C. Staudt-Bickel, W.J. Koros, Efficient development of effective hollow fiber membranes for gas separations from novel polymers, J. Membr. Sci., 278 (2006) 92-104.

[96] O.M. Ekiner, R.A. Hayes, P. Manos, Novel multicomponent fluid separation membranes, in, 1992.

[97] N. Widjojo, T.S. Chung, W.B. Krantz, A morphological and structural study of Ultem/P84 copolyimide dual-layer hollow fiber membranes with delamination-free morphology, J. Membr. Sci., 294 (2007) 132-146.

[98] D.F. Li, T.S. Chung, W. Rong, Morphological aspects and structure control of dual-layer asymmetric hollow fiber membranes formed by a simultaneous co-extrusion approach, J. Membr. Sci., 243 (2004) 155-175.

[99] C.C. Pereira, R. Nobrega, K.V. Peinemann, C.P. Borges, Hollow fiber membranes obtained by simultaneous spinning of two polymer solutions: a morphological study, J. Membr. Sci., 226 (2003) 35-50.

[100] D.F. Li, T.S. Chung, R. Wang, Y. Liu, Fabrication of fluoropolyimide/polyethersulfone (PES) dual-layer asymmetric hollow fiber membranes for gas separation, J. Membr. Sci., 198 (2002) 211-223.

[101] Y. Li, C. Cao, T.S. Chung, K.P. Pramoda, Fabrication of dual-layer polyethersulfone (PES) hollow fiber membranes with an ultrathin dense-selective layer for gas separation, J. Membr. Sci., 245 (2004) 53-60.

[102] L.Y. Jiang, T.S. Chung, D.F. Li, C. Cao, A. Kulprathipanja, Fabrication of Matrimid/polyethersulfone dual-layer hollow fiber membranes for gas separation, J. Membr. Sci., 240 (2004) 91-103.

[103] N. Widjojo, S.D. Zhang, T.S. Chung, Y. Liu, Enhanced gas separation performance of dual-layer hollow fiber membranes via substructure resistance reduction using mixed matrix materials, J. Membr. Sci., 306 (2007) 147-158.

[104] L.T. Duarte, C.C. Pereira, A.C. Habert, C.P. Borges, Polyurethane/polyethersulphone composite hollow fibers produced by simultaneous spinning of two polymer solutions, J. Membr. Sci., 311 (2008) 12-22.

[105] X.L. Ding, Y.M. Cao, H.Y. Zhao, L. Wang, Q. Yuan, Fabrication of high performance Matrimid/polysulfone dual-layer hollow fiber membranes for O-2/N-2 separation, J. Membr. Sci., 323 (2008) 352-361.

[106] M. Khayet, T. Matsuura, J.I. Mengual, Porous hydrophobic/hydrophilic composite membranes: Estimation of the hydrophobic-layer thickness, J. Membr. Sci., 266 (2005) 68-79.

[107] S. Bonyadi, T.S. Chung, Flux enhancement in membrane distillation by fabrication of dual layer hydrophilic-hydrophobic hollow fiber membranes, J. Membr. Sci., 306 (2007) 134-146.

[108] K.Y. Wang, T.S. Chung, R. Rajagopalan, Dehydration of tetrafluoropropanol (TFP) by pervaporation via novel PBI/BTDA-TDI/MDI co-polyimide (P84) dual-layer hollow fiber membranes, J. Membr. Sci., 287 (2007) 60-66.

[109] Y. Wang, S.H. Goh, T.S. Chung, P. Na, Polyamide-imide/polyetherimide dual-layer hollow fiber membranes for pervaporation dehydration of C1-C4 alcohols, J. Membr. Sci., 326 (2009) 222-233.

[110] Y. Li, T.S. Chung, Exploration of highly sulfonated polyethersulfone (SPES) as a membrane material with the aid of dual-layer hollow fiber fabrication technology for protein separation, J. Membr. Sci., 309 (2008) 45-55.

[111] T. He, M.H.V. Mulder, H. Strathmann, M. Wessling, Preparation of composite hollow fiber membranes: co-extrusion of hydrophilic coatings onto porous hydrophobic support structures, J. Membr. Sci., 207 (2002) 143-156.

[112] Z.S. Li, J.Z. Ren, A.G. Fane, D.F. Li, F.S. Wong, Influence of solvent on the structure and performance of cellulose acetate membranes, J. Membr. Sci., 279 (2006) 601-607.

[113] J. Kopecek, Souriraj.S, Structure of porous cellulose acetate membranes and a method for improving their performance in reverse osmosis, J. Appl. Polym. Sci., 13 (1969) 637-&.

[114] M.J. Han, D. Bhattacharyya, Thermal annealing effect on cellulose-acetate reverse-osmosis membrane-structure, Desalination, 101 (1995) 195-200.

[115] Y.S. Su, C.Y. Kuo, D.M. Wang, J.Y. Lai, A. Deratani, C. Pochat, D. Bouyer, Interplay of mass transfer, phase separation, and membrane morphology in vapor-induced phase separation, J. Membr. Sci., 338 (2009) 17-28.

[116] J.A. Vanthof, A.J. Reuvers, R.M. Boom, H.H.M. Rolevink, C.A. Smolders, Preparation of asymmetric gas separation membranes with high selectivity by a dual-bath coagulation method, J. Membr. Sci., 70 (1992) 17-30.

[117] C.M. Hansen, Hansen Solubility Parameter: A User's Handbook, CRC Press, 1999.

[118] T. Matsuura, Synthetic Membranes and Membrane Separation Processes, CRC Press, Boca Raton, 1994.

[119] S.P. Sun, K.Y. Wang, D. Rajarathnam, T.A. Hatton, T.S. Chung, Polyamide-imide nanofiltration hollow fiber membranes with elongation-induced nano-pore evolution, AIChE J., 56 (2010) 1481.

[120] N. Peng, T.S. Chung, K.Y. Li, The role of additives on dope rheology and membrane formation of defect-free Torlon (R) hollow fibers for gas separation, J. Membr. Sci., 343 (2009) 62-72.

[121] I. Pinnau, B.D. Freeman, Membrane Formation and Modification, American Chemical Society, Washington DC, 2000.

[122] D. Rana, T. Matsuura, Surface Modifications for Antifouling Membranes, Chem. Rev., 110 (2010) 2448-2471.

[123] Q. Yang, K.Y. Wang, T.S. Chung, Dual-Layer Hollow Fibers with Enhanced Flux As Novel Forward Osmosis Membranes for Water Production, Environ. Sci. Technol., 43 (2009) 2800-2805.

[124] W. Albrecht, B. Seifert, T. Weigel, M. Schossig, A. Hollander, T. Groth, R. Hilke, Amination of poly(ether imide) membranes using di- and multivalent amines, Macromol. Chem. Physic., 204 (2003) 510-521.

[125] C. Trimpert, G. Boese, W. Albrecht, K. Richau, T. Weigel, A. Lendlein, T. Groth, Poly(ether imide) membranes modified with poly(ethylene imine) as potential carriers for epidermal substitutes, Macromol. Biosci., 6 (2006) 274-284.

[126] C.Y. Ba, J. Langer, J. Economy, Chemical modification of P84 copolyimide membranes by polyethylenimine for nanofiltration, J. Membr. Sci., 327 (2009) 49-58.

[127] T.S. Chung, M.L. Chng, K.P. Pramoda, Y.C. Xiao, PAMAM dendrimer-induced cross-linking modification of polyimide membranes, Langmuir, 20 (2004) 2966-2969.

[128] L.D. Nghiem, A.I. Schafer, M. Elimelech, Pharmaceutical retention mechanisms by nanofiltration membranes, Environ. Sci. Technol., 39 (2005) 7698-7705.

[129] E. Steinle-Darling, E. Litwiller, M. Reinhard, Effects of Sorption on the Rejection of Trace Organic Contaminants During Nanofiltration, Environ. Sci. Technol., 44 (2010) 2592-2598.

[130] A.R.D. Verliefde, E.R. Cornelissen, S.G.J. Heijman, E.M.V. Hoek, G.L. Amy, B. Van Der Bruggen, J.C. Van Dijk, Influence of Solute-Membrane Affinity on Rejection of Uncharged Organic Solutes by Nanofiltration Membranes, Environ. Sci. Technol., 43 (2009) 2400-2406.

[131] L. Setiawan, R. Wang, K. Li, A.G. Fane, Fabrication of novel poly(amide-imide) forward osmosis hollow fiber membranes with a positively charged nanofiltration-like selective layer, J. Membr. Sci., 369 (2011) 196-205.

[132] Y.C. Chiang, Y.Z. Hsub, R.C. Ruaan, C.J. Chuang, K.L. Tung, Nanofiltration membranes synthesized from hyperbranched polyethyleneimine, J. Membr. Sci., 326 (2009) 19-26.

[133] P.B. Kosaraju, K.K. Sirkar, Interfacially polymerized thin film composite membranes on microporous polypropylene supports for solvent-resistant nanofiltration, J. Membr. Sci., 321 (2008) 155-161.

[134] R.M. Boom, I.M. Wienk, T. Vandenboomgaard, C.A. Smolders, Microstructures in phase inversion membranes 2. The role of a polymeric additive, J. Membr. Sci., 73 (1992) 277-292.

[135] K. Boussu, C. Vandecasteele, B. Van der Bruggen, Relation between membrane characteristics and performance in nanofiltration, J. Membr. Sci., 310 (2008) 51-65.

APPENDICES

Publications:

1. **S.P. Sun**, T.A. Hatton, S.Y. Chan, T.S. Chung*, Novel thin-film composite nanofiltration hollow fiber membrane for effective removal of emerging organic matters from water, *Journal of Membrane Science* (2012),

   doi:10.1016/j.memsci.2012.01.046

2. **S.P. Sun**, T.A. Hatton, T.S. Chung*, Hyperbranched polyethyleneimine induced cross-linking of polyamide-imide nanofiltration hollow fiber membranes for effective removal of ciprofloxacin, *Environmental Science & Technology*, 45 (2011) 4003

3. **S.P. Sun**, K.Y. Wang, N. Peng, T.A. Hatton, T.S. Chung*, Novel polyamide-imide/ cellulose acetate dual-layer hollow fiber membranes for nanofiltration, *Journal of Membrane Science*, 363 (2010) 232

4. **S.P. Sun**, K.Y. Wang, D. Rajarathnam, T.A. Hatton, T.S. Chung*, Polyamide-imide nanofiltration hollow fiber membranes with elongation-induced nano-pore evolution, *AIChE Jounal*. 56 (2010) 1481

Conferences:

1. Membrane Science and Technology (MST) 2011, Singapore, Oral presentation, 24-26 Aug 2011

2. AIChE Annual Meeting 2009, Nashville, USA, Oral presentation, 8-13 Nov 2009

3. SMA 10th Anniversary Symposium (SMA 2009), Singapore, Oral and poster presentation, 17-21 Jan 2009